MODELING HUMAN VEINS, VENOUS THROMBOSIS & THERAPEUTICS WITH ORGAN-ON-CHIPS

A Dissertation

by

NAVANEETH KRISHNA RAJEEVA PANDIAN

Submitted to the Graduate and Professional School of
Texas A&M University
in partial fulfillment of the requirements for the degree of

DOCTOR OF PHILOSOPHY

Chair of Committee,	Abhishek Jain
Committee Members,	Akhilesh K Gaharwar
	Gerard L Coté
	Victor Ugaz
Head of Department,	Michael J McShane

December 2021

Major Subject: Biomedical Engineering

ABSTRACT

Venous valves are anatomical structures in the veins, small and large, that help in the unidirectional flow of blood towards the heart. Unwanted clot (thrombus) formation at these valves and its subsequent complications is the third leading cause of cardiovascular deaths in the world. Our knowledge of this thrombus formation is limited due to our over reliance on murine models, which do not have venous valves. As human *in vivo* study of these valves is difficult due to its location there is a need for physiologically relevant in vitro models that can efficiently dissect the contribution of Virchow's triad – endothelial inflammation, blood flow dynamics and coagulable nature of blood, at the venous valves for thrombus formation. This dissertation focusses on the development of physiologically relevant *in silico* and *in vitro* models of veins containing venous valves.

An *in silico* model was used to analyze the unique flow patterns within physiological and pathological non-actuating micro venous valves (vein diameter less than 200 μm). I observed that an incompetent non-actuating micro venous valve may have a different mechanism of thrombus formation compared to valves at larger veins.

Deep vein thrombosis (DVT) that occurs at the valves of the deep (larger) veins and its consequences lead to around 100,000 deaths annually in the US alone. I used the organ-on-chip technology to create a Vein-Chip platform that integrated fully vascularized venous valves and its hemodynamic, as seen in vivo. The vascular endothelium of valves adapted to the locally disturbed microenvironment by expressing

a different phenotype from the other regions of the vein that had uniform flow. The platform is used to modulate the three factors of Virchow's triad to investigate the determinants of fibrin and platelet dynamics of DVT.

Healthy venous valves actuate to help unidirectional blood flow in the body. I extended the current model by including a 3D printed hydrogel valve that could actuate. The current model helps us understand how an actuating venous valve may keep the valves healthy and thrombus free.

Overall, the Vein-Chip offers a new preclinical approach to study venous pathophysiology and show effects of antithrombotic drug treatment.

DEDICATION

To my mother, father, and wife, whose support throughout this time period made this work possible.

ACKNOWLEDGEMENTS

There are many people I would like to thank for their support during my doctoral research. I would like to thank my supervisor Dr. Abhishek Jain for his expertise, guidance, advice. His support made this work possible.

I would like to thank my committee members Dr. Akhilesh K Gaharwar, Dr. Gerard L Coté, and Dr. Victor Ugaz for their constant support. I would like to also thank Dr John P Cooke for his support in this work.

The many people I worked with made this dissertation possible, and without their collaboration and enthusiasm, this work would not be. I thank Ms. J.A. Culpepper at Texas A&M University for managing phlebotomy of healthy individuals used in this thesis. I thank Dr. R. B. Mouneimne at the Texas A&M Image Analysis Laboratory for assisting with the confocal imaging. I thank Dr. S. Vitha at the Microscopy and Imaging Center at Texas A&M University for assisting with SEM imaging. I thank P. Gadangi for fabricating some of the Vein-Chips.

I would like to thank David Luna, Tanmay Mathur, Laura K. R. Tarazona, Dr. C. W. Peak, Dr. Brandon K. Walther, Aparna Murali, Kaivalya Deo, Kanwar Abhay Singh for their help, support and long thoughtful, and insightful dialogues during my doctoral training.

I would also like to thank my family - my wife, mom, and dad, for their unending love and support throughout my training.

CONTRIBUTORS AND FUNDING SOURCES

Contributors

This work was supervised by a thesis committee consisting of Dr. Abhishek Jain [advisor], Dr. Akhilesh K Gaharwar, and Dr. Gerard L Coté of Department of Biomedical Engineering [Home Department] and Dr. Victor Ugaz of the Department of Chemical Engineering [Outside Department].

Dr. Brandon K. Walther, and Dr. John P Cooke of Houston Methodist Research Institute, provided the PCR data of Chapter 3 (Figure 3.5 and 3.9). Rishi Suresh of Texas A&M Health Science Center, College of Medicine, fabricated and vascularized some of the Vein-Chip devices used in Chapter 3. Laura K. Rivera-Tarazona and Dr. Taylor H Ware of the department of Biomedical Engineering provided the 3D printed venous valves used in Chapter 4.

All other work conducted for the thesis was completed by the student independently.

Funding Sources

Graduate study was supported by a fellowship from Texas A&M University and the Texas A&M Engineering Experiment Station. Grant funding sources were the AggieChallenge of Texas A&M University, NIBIB Award R21EB025945, NSF CAREER Award 1944322 and Texas A&M University Presidents Excellence in Research Award (X-Grant) to Dr. Abhishek Jain.

NOMENCLATURE

BOECs	Blood Outgrowth Endothelial Cells
DVT	Deep Vein Thrombosis
CFD	Computational Fluid Dynamics
ECM	Extracellular matrix
FSI	Fluid Structure Interaction
HUVECs	Human Umbilical Vein Endothelial Cells
HSaVECs	Human Saphenous Vein Endothelial Cells
VWF	von Willebrand Factor
TNF-α	Tumor Necrosis Factor – α
PDMS	polydimethylsiloxane
DOAC	Direct Oral Anticoagulant
PBS	Phosphate Buffer Solution
ICAM-1	Inter Cellular Adhesion Molecule-1
eNOS	Endothelial Nitric Oxide Synthase
TF	Tissue Factor
GAPDH	Glyceraldehyde 3-phosphate dehydrogenase

TABLE OF CONTENTS

Page

LIST OF FIGURES

Page

LIST OF TABLES

Page

1. INTRODUCTION TO THROMBOSIS-ON-A-CHIP: PROSPECTIVE IMPACT OF MICROPHYSIOLOGICAL MODELS OF VASCULAR THROMBOSIS*

1.1. Abstract

The most common pathology of the blood-vessel organ system is thrombosis or undesirable clotting of the blood. Thrombosis is life threatening as more than 25% of such cases lead to sudden death from stroke and myocardial infarction. Even though the process of thrombosis has been extensively investigated with animal models, its exact pathobiology in different blood vessels is not yet fully understood and drug assessment remains unpredictable. This is primarily because the cause for thrombus formation is multifactorial and depends on the interplay of flow patterns within the blood vessel, the vessel wall or endothelium, extracellular matrix, parenchymal tissue, and the cellular and plasma components of the blood. Current *in vitro* and animal models do not mimic or dissect this organ-level complexity faithfully. However, microfluidic technology has recently been deployed to effectively recapitulate blood-endothelial-epithelial interactions in the onset of thrombosis in blood vessels. This technology is promising because it permits inclusion of primary human cells and blood obtained from patients, which is currently lacking in other in vitro models of thrombosis. In this review, we summarize the current state-of-the-art and practices in microfluidics and expected improvements in this field that will impact basic understanding of thrombosis, drug discovery and personalized medicine.

* Pandian, Navaneeth KR, Robert G. Mannino, Wilbur A. Lam, and Abhishek Jain. "Thrombosis-on-a-chip: Prospective impact of microphysiological models of vascular thrombosis." *Current Opinion in Biomedical Engineering* 5 (2018): 29-34.

1.2. Background

Under physiological conditions, the blood remains in a fluid state by maintaining a balance between the procoagulant and the anticoagulant factors present in the blood. When this balance is impaired, a shift towards anticoagulant factors leads to unexpected bleeding and blood loss whereas a shift towards procoagulant factors leads to thrombus formation that occludes blood vessels eventually becoming a cause of stroke [1]. Such undesirable clotting of blood is the most common pathology found in the vasculature. Pathologic clotting of blood, or thrombosis, in the vasculature has been studied extensively since the 18th century. In the earliest studies, the initiation of thrombus formation (thrombogenesis) was related to one of the following factors: hypercoagulability of blood, blood stasis and endothelial damage. However, Rudolf Virchow in 1856 was the first to make a profound observation that all these three factors together are critical to thrombogenesis. These factors that collaboratively contribute to thrombosis are known as the Virchow's triad [2]. Blood can become hypercoagulable due to the activation of blood cells (such as platelets) and release of clotting factors (such as thrombin) into plasma [3]. Stasis of blood flow may occur due to occlusion of the blood vessel resulting from plaque formation in arteries (atherosclerosis) or due to impairment of valves in the deep veins (deep vein thrombosis) [4]. Vascular activation occurs when the endothelium is exposed to circulating stimulants, making it procoagulant and pro-inflammatory [5]. Endothelial cell inflammation increases cell permeability contributing to thrombus formation by the interaction of platelets and

clotting factors with the exposed components of the vascular surface [6]. Since the discovery of Virchow's triad, its factors have been extensively investigated independently at molecular and cellular levels, but the mutual interplay of these factors (and others) has not been fully understood because it requires dissectible organ-level modeling of the physiology of thrombosis. Current methods that are used to investigate the multivariate factors that lead to thrombosis do not permit analysis of the organ-level prothrombotic responses with incremental level of complexity that underlies in several diseases. While several sophisticated animal models of thrombosis exist, and have contributed to our basic understanding of certain specific mechanisms, integrated models that can separate contributions of platelet-endothelial interactions versus tissue-tissue (e.g., epithelial-endothelial) interactions are still underdeveloped and significantly non-predictive. Most current *in vitro* assays of hemostasis and thrombosis on the other hand, do not incorporate vascular function. Several recent studies have enabled microfluidic flow chambers to include endothelial lumen within which whole blood can be perfused and platelet-endothelial interactions can be visualized with high resolution [7-10]. This development is promising as it opens opportunities to include the more complex organ-level interactions in the assessment of thrombosis as well as anticlotting drugs. There are further advantages of using such microphysiological systems (or organs-on-a-chip) due to their micro scale, for e.g. these devices require little amount of blood samples, tight control of dimensions, lower cost per device and easy fabrication and repeatability of large number of experiments [11]. Also, with organ-on-a-chip technology, assessment of thrombosis at a patient-specific level is possible by including specific vessel anatomy,

vascular endothelial cells and blood, all derived from the same patient. Here, we succinctly discuss current animal and *in vitro* methods applied in modeling arterial, venous and microvascular thrombosis, followed by an overview of utilization of microphysiological devices in assessing complex features of thrombosis and future directions that could improve status quo.

1.3. Current models of thrombosis: The gold standard

Current models used to investigate thrombosis include *in vivo* animal models ranging from zebra fish to nonhuman primate models, and *in vitro* models in the form of parallel plate flow chambers and cone-and-plate viscometers.

1.3.1. Animal models:

The most common animal model of thrombosis is the mouse. Numerous murine thrombosis models have been developed to study the arterial, venous, and microvascular thrombosis [12]. In these models, arterial thrombosis is generally induced using injury of the carotid arteries (for example, ferric chloride or Rose Bengal-plus-light), venous thrombosis is induced slowly by stasis or stenosis (both by ligation) or rapidly by an acute injury (using free-radicals) of the inferior vena cava, and microvascular thrombosis is induced by free-radical injury or laser injury of the mesenteric veins. A few other models also exist, like direct electric injury, anastomosis, ultrasound disruption or intraluminal collagen, which are less preferred due to the difficulty in obtaining repeatable results between labs. These diverse mouse models have contributed immensely over the last few decades in decoding several key mechanisms that govern thrombosis [12-16], as well as capturing the thrombus dynamics in human-relevant

conditions [17]. They have also been effective in studying the role of genetic variation and different clotting factors in thrombus formation. However, the physiological and genetic differences of these models with respect to humans limits them considerably [18, 19]. This is mostly true because several drug trials that succeeded in such animal models have failed in human clinical trials [20], thus contributing to high healthcare costs and stroke remaining to be the biggest cause of patient mortality. While small animal models (zebra fish, mice etc.) are preferred in thrombosis research mostly due to their easy availability and established genetic data [13], the large animal models (dogs, pigs, nonhuman primates etc.) offer increased physiological relevance to humans. However, large animal studies cannot be easily conducted in academic laboratories and impose several ethical restrictions thus making small animals or in vitro models the first choice to model thrombotic diseases.

1.3.2. *In vitro* models:

A commonly used *in vitro* thrombosis system, the parallel plate flow chamber is a hollow rectangular space with millimeter or centimeter scale dimensions, through which blood or its components can be transported to induce physiological wall shear stresses over purified proteins (such as, von Willebrand factor (VWF) or tissue factor), extracellular matrix (ECM like collagen, laminin or fibronectin) or cultured vascular endothelial cell monolayers [21]. The flow rates are often controlled using constant-flow pumps, although pressure and gravity are also used to transport blood. While these systems have been useful in studying the effects of shear and recirculating flow [22] on platelet function and coagulation [23], accurate blood vessel anatomy is not replicated in

these chambers. For example, these flow chambers have not included the complex vascular features like venous valves where abrupt shear stresses may contribute to the onset of deep vein thrombosis (DVT). The other commonly used *in vitro* system, the cone-and-plate viscometer, works by rotating a cone shaped insert above a stationary plate containing proteins or cultured vascular cells [24]. The rotational speed of the cones in these devices are controlled to generate shear stresses. These devices are bulky and need large amounts of blood, cultured cells and reagents for each experiment, making them low throughput. Also, the experiments in these devices are conducted over 2D monolayers of proteins or cells and therefore, they do not mimic the function of a 3D round vascular lumen and natural blood flow. These limitations have been countered by the recent development of microfluidic devices that can be designed to offer more reliable physiologically-relevant readouts of vascular thrombosis.

1.4. Microfluidic models of thrombosis: State-of-the-art

Microfluidic devices are typically hollow rectangular channels of micrometer scale dimensions that can be designed using standard microfabrication methods (such as, soft lithography [10], through which whole blood can be perfused. A major advantage of the microfluidic devices is that they can be perfused at both high arterial wall shear rates (1000-5000 s^{-1}), as well as low venous wall shear rates (100-200 s^{-1}), thus incorporating the diversity in the composition and behavior of a thrombus that is dependent on the type of blood vessel [25]. In addition, different anatomical structures like atherosclerotic plaques, bifurcations etc. observed in blood vessels can be relatively easily included

while designing the flow path of these devices. It is also possible to introduce complex flow patterns (pulsatile motion, rapid accelerations and decelerations etc.) as they exist *in vivo*. Finally, a more recent development in microfluidics has been the incorporation of vascular cells in the process of thrombosis in various diseases [8, 26].

1.4.1. Arterial thrombosis:

A major arterial thrombotic disease is atherosclerosis, where rupture of plaques leads to release of inflammatory cytokines and rapid thrombus formation [27]. These plaques are largely formed at vessel branching points and large bends where disturbed or stagnating flow is present [28]. Formation of these plaques creates stenosed regions in the artery that further augments the disturbed flow which is already present in this region. Microfluidic channels can be easily designed to incorporate channel geometries (such as stenosis) and disturbed flow conditions relevant to atherosclerosis. For example, a plaque-like geometry was modeled in a microfluidic conduit showing thrombus mostly forms in specific post-stenosed region [29]. This phenomenon was further utilized to model an arterial vascular bed and assess clotting time in extracorporeal devices and patients [30]. Further advancement in microfluidics permitted endothelialization of a similar geometry which showed that cell-secreted VWF further exacerbates platelet recruitment and adhesion [31]. More recently, a 3D printed microfluidic channel containing an atherosclerotic plaque using computed tomography angiography data of patients has been demonstrated [32]. Taken together, these studies have surveyed geometry-dependent arterial thrombosis due to atherosclerosis but several advancements

can potentially be made to more faithfully mimic more complex biology of atherosclerosis. For example, pulsatile flow may be introduced in these devices to mimic arterial blood flow more closely. Secondly, extracellular matrix and residing smooth muscle cell signaling also influences plaque formation and thrombosis, which can potentially be included with organ-on-a-chip technology.

1.4.2. Venous thrombosis:

Human veins are macro-fluidic and are mostly of size 5 mm and above. Yet, downscaled microfluidic models of venous thrombosis (DVT) that match murine sizes could serve as a more efficient source to study shear-dependent mechanisms in DVT using very low volumes of human tissue and blood samples. Notably, the Virchow's triad is more dominant in the setting of venous thrombosis [33]. Also, venous thrombosis initiates near venous valves where abrupt and pulsatile flow conditions, and hypoxic endothelium contribute to the propagation of thrombus and its embolism [34]. Due to the scale difference and larger complexity, there have been relatively very few efforts to design microfluidic models of DVT. In one study, it was predicted in a microfluidic device that clot propagation from superficial veins to deep veins is regulated by fluid shear rate, which might explain the correlation between superficial thrombosis and the development of DVT [35]. Another study showed using murine blood that venous thrombi have lower platelet density compared to arterial thrombi because platelet aggregation and adhesion over ECM is dependent on the wall shear rates [36]. In future, microfluidic models of DVT containing endothelium and venous structures could

contribute to a better understanding of the unique thrombus pathology in veins and specific drug-tissue interactions.

1.4.3. Microvascular thrombosis:

Several diseases (like sickle cell disease, diabetes, cancer, and pulmonary injury) lead to fatal thrombosis in the microvascular arterioles and venules of various organs (lung, kidney, brain etc.). Modeling intravascular thrombosis can be very difficult because it is regulated by the several local mechanical and biological conditions of the blood flow, vessel wall, ECM and the epithelium. Nevertheless, microfluidic devices offer a huge opportunity to model this complexity due to their ability to use blood, tissue and vessel architecture derived from such patients to make *in vitro* models that are as close as possible to the *in vivo* disease microenvironment. Recent efforts to mimic vascular physiology in vitro leverage the microfluidic device technology that enables creation of arteriole-sized channels capable of endothelialization and blood perfusion [10, 37]. In one example, a microfluidic device with arteriole-sized channels was lined with endothelial cells and when blood from sickle cell disease (SCD) patients or blood spiked with a bacterial toxin that causes hemolytic uremic syndrome (HUS) were perfused, it revealed increase in occlusion and clot formation [8]. The same system also showed clots when endothelial cells were activated with an inflammatory cytokine TNF-α. More recently, a microfluidic device containing stimulated and fixed endothelial cells could result in thrombosis upon whole blood perfusion and was proposed to be used as a diagnostic device in clinical settings [7].

1.5. Microphysiological models of thrombosis: new directions

The process of thrombosis in diseases can be more complex than the interactions between the endothelium, extracellular matrix and the blood cells (Figure 1A-B). For example, in cancer, the tumor cells release inflammatory factors that result in endothelial activation and platelet activation, eventually leading to the onset of blood clots [38]. Similarly, in acute lung injury or pneumonia, the alveolar epithelium may secrete factors that lead to platelet recruitment and thrombosis [39]. Organ-on-a-chip technology could offer a platform in order to mimic this thrombotic microenvironment and dissect tissue-tissue and drug-tissue interactions for systematic analysis of thrombosis (Figure 1C). Recently, a model of lung thrombosis [26] showed 3 new features that support organ-level functional design: a) human primary alveolar and endothelial cells are co-cultured in adjacent microfluidic conduits, separated by thin layer of matrix, b) the endothelial cells cover all sides of one chamber to form a complete vascular tube, and c) when human whole blood is perfused at a designated shear stress through the stimulated vascular lumen of this device, the thrombus formed *in vitro* is identical to *in vivo* (Figure 1D-E). With this device, it was discovered that the alveolar epithelium is critical to thrombosis that is initiated by lipopolysaccharide (LPS).

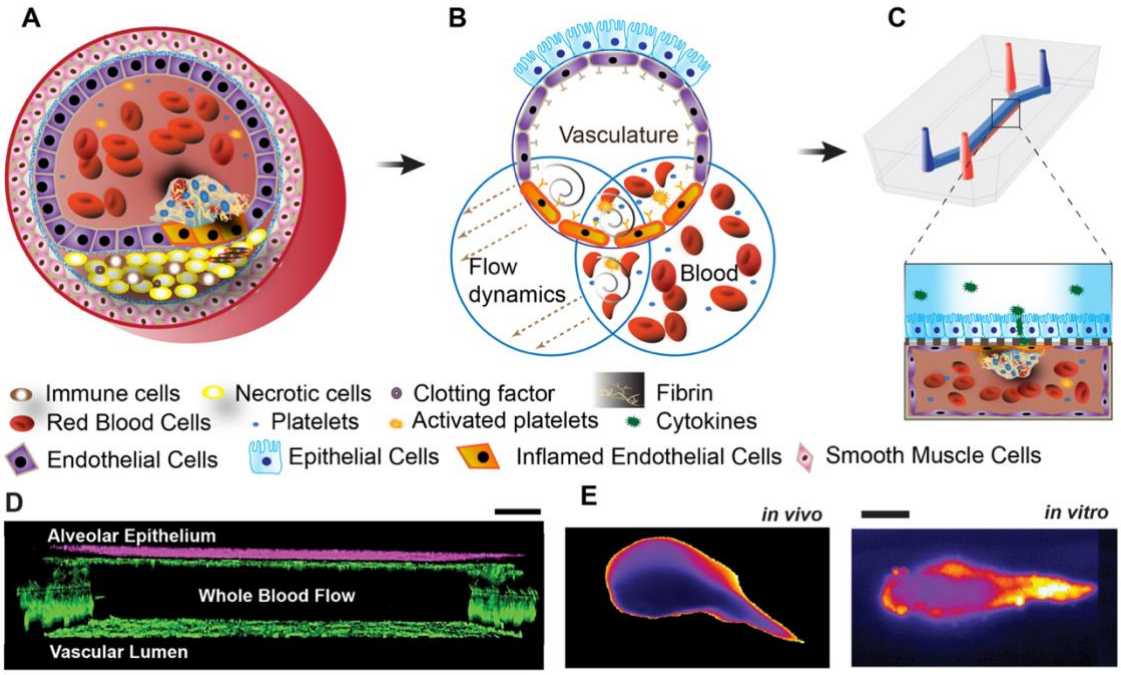

Figure 1-1: Organ-level complexity of thrombosis and microphysiological modelling.
A) A blood clot formed in vivo may contain contributions from endothelial cells, blood cells, extracellular matrix and parenchymal cells, along with released clotting factors and cytokines B) The three factors of Virchow's triad: inflamed or activated vascular endothelial cells (and activated epithelial cells), change in flow dynamics and blood rich in clotting factors, determine the dynamics of thrombosis. C) The organ-on-a-chip technology has been able to model the complex signaling in pulmonary thrombosis in vitro. D) Confocal micrograph of an alveoli-on-a-chip device showing co-culture of primary alveolar epithelial cells (purple) and endothelial lumen (green), with whole blood flow (not visible). E) Identical morphology of a thrombus formed in vivo (left) and inside the device (right). Bar: 10 μm.

Further, an endothelium-specific therapeutic effect of an antithrombotic compound was identified in the presence of alveolar epithelial endothelial-blood cell signaling, not easily possible with animal models. Finally, a critical mechanism of action of this compound was discovered and shown that it performs via the natural β-arrestin pathway of activated protein-C (APC) [40]. These recent developments in

microphysiological systems are highly promising and it may be expected that the blood vessels in these organ-chips may be designed to take complex shapes (branches, valves, stenosis etc.) through which blood may be transported under physiologically-relevant fluid dynamical states. A major opportunity offered by these systems is that the biological processes can be visualized using microscopy, measured using biosensors, and quantified using analytical algorithms and genomic screening. However, there are still some limitations in the current microfluidic designs that limit the extent to which human physiology can be reconstituted. For example, a fundamental limitation of most microfluidic devices is that they are made of rectangular channels with a high surface-to-volume ratio. While the rectangular shape is easy to fabricate and image on microscopes, the flow near the edges of the rectangular walls does not recapitulate the flow inside a cylindrical vascular tube. Therefore, the analysis of thrombus can only be done distant from the wall [7]. Another limitation is that even though soft-lithography is most widely used in developing the aforementioned microfluidic devices, there is high initial setup cost, low throughput and limited 3D capability as layered 2D designs have to be used for 3D designs [41]. Also, due to small and rigid channel sizes, it is difficult to create turbulence (high Reynolds number) that may be present in large and elastic blood vessels in pathophysiological conditions and therefore, their contributions to thrombotic occlusion cannot be easily assessed [42]. Finally, microfluidic devices may not mimic all the biological processes of vascular thrombosis and therefore, *in vivo* models may still be needed for some studies. Whole blood perfusion without significant anticoagulation in organ-on-a-chip can only be done for a short-term duration and therefore, it is

currently not possible to study long-term systemic thrombotic processes, that may also include vascular remodeling and embolism. With 3D-printing technology advancing fast in resolution and biocompatibility, it is an exciting option to fabricate microfluidic systems in future due to easy process automation, assembly-free 3D fabrication, and high throughput. Tissues and blood obtained from patients and induced pluripotent stem-cell (iPSC) technology could potentially personalize such systems and provide patient-specific readouts that can never be obtained from animal models or current hemostasis and thrombosis assessment devices. In summary, the prospects of such microphysiological models are promising. As progress is made in this direction, they are expected to mimic the complex pathophysiology of thrombosis at an organ-level and permit dissection of mechanism of action of various cells and tissues to the extent that it will ultimately predict therapeutic responses and toxicities to drugs, thus directly impacting the health outcomes of patients, as well as cost of treatment.

2. IN SILICO ANALYSES OF BLOOD FLOW AND OXYGEN TRANSPORT IN MICROSCALE HUMAN VEINS PREDICT IN VIVO FLUIDICS AND A NOVEL HYPOTHESIS OF THROMBOSIS

2.1. Abstract

Almost 90% of the venous valves in a human body are micro venous valves, which are found in veins with diameters less than 200 μm. The fluid dynamics of blood flow and transport through these micro venous valves and their contribution to thrombosis is not yet well understood or characterized due to difficulty in making direct measurements in murine models. Therefore, leveraging an *in silico* modelling approach both in 2D and 3D, the unique flow patterns within physiological or pathological non-actuating micro venous valve are predicted. The model successfully recreates the typical non-Newtonian vortical flow within the valve cusps seen in preclinical experimental models and in clinic. The analysis further reveals variation in the vortex strengths in the venous lumen as well as within valves due to temporal changes in blood flow. The addition of oxygen transport phenomena to the fluid model shows that cusp oxygen is typically low from the main lumen, and it is regulated by the variations in the systemic venous flow. Overall, the *in silico* analysis leads to a clinically-relevant hypothesis that micro venous valves may not create a hypoxic environment needed for endothelial inflammation, which is one of the main causes of thrombosis. But incompetent micro venous valves are still locations for complex fluid dynamics of blood leading to low shear regions in the valve cusps that may contribute to thrombosis through other pathways.

2.2. Introduction

Venous valves are essential mechanical components of blood vessels and responsible for maintaining the efficient circulation of blood in the human body [43, 44]. Unique shape of the venous valves maintains the unidirectional flow of blood from tissues and distant body parts towards the heart. Such valves are observed in the deep veins, superficial veins, and micro veins as small as 40 μm diameter [45]. Flow through venous valves in the deep veins have been rigorously studied [46-54], as they are the prime locations to develop unwanted clots, a fatal condition known as deep vein thrombosis (DVT), which can lead to serious cardiovascular complications such as pulmonary thromboembolism [34, 55, 56]. But the fluid dynamics of blood in the micro venous valves, which constitute about ~94% of the total venous valves in the body (found in vessels with diameter less than 300 μm), have not yet been extensively characterized [57]. Venous valves in the deep veins have been suggested to develop DVT mainly through two mechanisms i.e., the hypoxic inflammation of the valve endothelium or the deposition of procoagulant factors such as tissue factor laden microparticles that are shed by various cells [58]. But it is not known whether these mechanisms are also responsible for thrombus formation in micro venous valves. Limitations in studying in thrombus formation in micro venous valves are because of the lack of relevant in vitro models and difficulty in conducting in vivo studies due to the location of these micro venous valves in the human body [59]. Since fluid mechanical analysis of small veins is extremely difficult in murine models, *in silico* and more

advanced *in vitro* models of the micro venous valves may help us understand if these valves are also locations of thrombus formation similar to the venous valves in deep veins, which have a larger diameter. Use of computational modelling to study the flow of whole blood through micro venous valves can help us understand the unique and complex fluid flow dynamics of blood in these valves. The results of such analysis can also be the basis for future development of in vitro models of micro venous valves.

In the present study, we use computational fluid dynamic simulations to show the effects of non-Newtonian blood flow in a 2D model of a pathological micro venous valve. We then analyze the effects of transient flow and resulting fluid profiles within the venous valves. We also validate the fluid mechanics predicted in a 2D system with a significantly more computationally expensive 3D model of the micro venous valve to suggest strategies for future modeling of such phenomena. Finally, we superimpose an oxygen transport model over fluid mechanics to analyze hypoxia in a micro venous valve, a determinant of endothelial dysfunction and thrombosis.

2.3. Methods

2.3.1. Fluid mechanics of blood

In order to conduct the computational fluid dynamic simulation of blood flow through the micro venous valves, we solved the conservation of mass, conservation of momentum, and conservation of energy equations (Equation 1,2,3) for an incompressible fluid flow, using the commercially available CFD software package Fluent (Ansys v20R1) based on a finite volume scheme.

$$\nabla \cdot \bar{\boldsymbol{V}} = \mathbf{0} \qquad \text{Equation 1.0}$$

$$\rho \frac{\partial \overline{\boldsymbol{V}}}{\partial t} + \rho \overline{\boldsymbol{V}} \cdot \nabla \overline{\boldsymbol{V}} = -\nabla p + \nabla \cdot [\mu(\nabla \overline{\boldsymbol{V}} + (\nabla \overline{\boldsymbol{V}})^T)] + \rho \overline{\boldsymbol{F}} \quad \text{Equation 2.0}$$

$$\rho \left[\frac{\partial}{\partial t} \left(e + \frac{1}{2} \overline{\boldsymbol{V}} \cdot \overline{\boldsymbol{V}} \right) + \nabla \cdot \left(\overline{\boldsymbol{V}} \left(e + \frac{1}{2} \overline{\boldsymbol{V}} \cdot \overline{\boldsymbol{V}} \right) \right) \right] =$$

$$\nabla \cdot \left[-p \overline{\boldsymbol{V}} + \left(\left(\mu(\nabla \overline{\boldsymbol{V}} + (\nabla \overline{\boldsymbol{V}})^T) \right) \cdot \overline{\boldsymbol{V}} \right) \right] + \overline{\boldsymbol{V}} \cdot \rho \overline{\boldsymbol{F}} \quad \text{Equation 3.0}$$

Blood in the fluid domain was modelled as a non-Newtonian fluid with constant density of 1060 kg m-3 and viscosity following the three different viscosity models given below [60-62].

Newtonian model:

$$\mu = 0.0035 \, Pa \cdot s \quad \text{Equation 4.0}$$

Casson Model (non-Newtonian model):

$$\mu = [(\eta^2 J_2)^{0.25} + 2^{-0.5} \tau^{0.5}]^2 (J_2)^{-0.5} \quad \text{Equation 5.0}$$

$$\text{where, } |\dot{\gamma}| = 2(J_2)^{0.5}$$

$$\tau = 0.1(0.625H)^3$$

$$\eta = \eta_0 (1 - H)^{-2.5}$$

$$\eta_0 = 0.0012 \, Pa \cdot s \text{ and } H = 0.3$$

Generalised power law Model (non-Newtonian model):

$$\mu = \lambda(\dot{\gamma}) |\dot{\gamma}|^{[n(\dot{\gamma})-1]} \quad \text{Equation 6.0}$$

$$\text{where, } \lambda(\dot{\gamma}) = \mu_\infty + \Delta \mu \cdot e^{\left[-\left(1 + \frac{|\dot{\gamma}|}{a}\right) e^{\left(\frac{-b}{|\dot{\gamma}|}\right)} \right]} \quad \text{Equation 6.1}$$

$$n(\dot{\gamma}) = n_{\infty} - \Delta\, n \cdot e^{\left[-\left(1+\frac{|\dot{\gamma}|}{c}\right)e^{\left(\frac{-d}{|\dot{\gamma}|}\right)}\right]} \qquad \text{Equation 6.2}$$

$$\mu_{\infty} = 0.0035, n_{\infty} = 1, \Delta\,\mu = 0.25, \Delta\, n = 0.45,$$

$$a = 50, b = 3, c = 50\ and\ d = 4$$

where μ is the viscosity, $\dot{\gamma}$ is the shear rate, $\lambda(\dot{\gamma})$ is the consistency index (dependent on the shear rate), and $n(\dot{\gamma})$ is the flow behaviour index (dependent on the shear rate). μ_{∞} and n_{∞} are the viscosity and flow behavior indices for infinite shear rate. a, b, c and d are constants.

The inlet boundary condition for the simulation is a "velocity" corresponding to the desired wall shear stress and the outlet boundary condition is a "pressure" outlet condition set to gauge pressure of zero.

The resulting vortex in the micro venous valves were characterized by the vorticity and the swirling strength the vortex. The direction of rotation of the vortex was given by the sign of the vorticity (a positive valve is a counterclockwise rotating vortex, and a negative value is a clockwise rotating vortex), which was calculated from the non-diagonal terms of the velocity gradient tensor. The swirling strength of the vortices were also calculated from the velocity gradient tensor, where the swirling strength was the imaginary part of the complex eigen value of the velocity gradient tensor [63].

In 2D velocity gradient tensor is given by $\nabla\overline{\boldsymbol{V}} = \begin{bmatrix} \frac{\partial u}{\partial x} & \frac{\partial u}{\partial y} \\ \frac{\partial v}{\partial x} & \frac{\partial v}{\partial y} \end{bmatrix}$,

where vorticity is given by $\omega_z = \left[\frac{\partial v}{\partial x} - \frac{\partial u}{\partial y}\right]$

The characteristic equation of $\nabla\overline{\boldsymbol{V}}$ is $\lambda^2 - (\mathrm{tr}(\nabla\overline{\boldsymbol{V}}))\lambda + |\nabla\overline{\boldsymbol{V}}| = 0$

And its solution (eigen values) is a complex number, $\lambda = \pm\sqrt{-|\nabla\overline{\boldsymbol{V}}|}$,

as $\mathrm{tr}(\nabla\overline{\boldsymbol{V}}) = \nabla \cdot \overline{\boldsymbol{V}} = \mathbf{0}$, for an incompressible flow.

In 3D velocity gradient tensor is given by $\nabla\overline{\boldsymbol{V}} = \begin{bmatrix} \frac{\partial u}{\partial x} & \frac{\partial u}{\partial y} & \frac{\partial u}{\partial z} \\ \frac{\partial v}{\partial x} & \frac{\partial v}{\partial y} & \frac{\partial v}{\partial z} \\ \frac{\partial w}{\partial x} & \frac{\partial w}{\partial y} & \frac{\partial w}{\partial z} \end{bmatrix}$,

where vorticity is given by $\omega_z = \left[\frac{\partial v}{\partial x} - \frac{\partial u}{\partial y}\right]$

The characteristic equation of $\nabla\overline{\boldsymbol{V}}$ is

$$-\lambda^3 + (\mathrm{tr}(\nabla\overline{\boldsymbol{V}}))\lambda^2 - \frac{1}{2}[\mathrm{tr}(\nabla\overline{\boldsymbol{V}})^2 - \mathrm{tr}(\nabla\overline{\boldsymbol{V}}^2)]\lambda + |\nabla\overline{\boldsymbol{V}}| = 0$$

Which will reduce to $-\lambda^3 + \frac{1}{2}\mathrm{tr}(\nabla\overline{\boldsymbol{V}}^2)\lambda + |\nabla\overline{\boldsymbol{V}}| = 0$ for an incompressible flow and two of the roots of the above cubic equation will be complex conjugates.

2.3.2. Transport of oxygen

For the mass transport problem, we solved the combined effects of diffusion and convection of the dissolved chemical species, in this case oxygen. We first solved the conservation of mass, conservation of momentum, and conservation of energy equations (Equation 1,2,3) in the fluid domain using the commercially available solver Comsol Multiphysics (v5.2), based on a finite element scheme. We obtained the convective flow of whole blood in the micro venous valves when the fluid flow problem was solved. We

then, solved the combined effects of convective mass transport with diffusive mass transport to obtain the mass transport of oxygen.

$$\bar{\mathbf{N}} = -\mathrm{D}\nabla\bar{\mathbf{c}} + \bar{\mathbf{c}}\bar{\boldsymbol{V}} \qquad \text{Equation 7.0}$$

$$\frac{\partial \bar{\mathbf{c}}}{\partial \mathbf{t}} + \nabla \cdot \bar{\mathbf{N}} = \bar{\mathbf{R}} \qquad \text{Equation 8.0}$$

Where, $\bar{\mathbf{N}}$, D, $\bar{\mathbf{c}}$ and $\bar{\mathbf{R}}$ are the flux, coefficient of diffusion, concentration, and reaction respectively. Also, $\bar{\boldsymbol{V}}$ is the velocity field evaluated from the flow analysis by solving Equations 1.0,2.0 and 3.0. For the mass transfer problem, we provided an influx boundary condition at the inlet and a reaction (absorption) at the walls of the venous valves and veins.

2.4. Results

2.4.1. Blood flow predictions in microscopic veins with comparative analysis of common constitutive equations of viscosity

We were inspired to mimic the design of a typical microscopic vein consisting of a venous valve of 200 um diameter [45]. Since small veins are not imaged *in vivo* with clarity, we analyzed the Doppler-ultrasound images of venous valves in the large superficial and deep veins available in literature and scaled down their geometry to design the micro venous valves [64, 65]. The designed valve was a bi-cuspid valve in which the valve leaflets emanated from the walls of the micro vein. The geometric similarity of the micro venous valves with the large venous valves were achieved by following the procedure illustrated in our previous work[66] in which the ratios of a) micro vein diameter to the maximum valve cusp depth (0.8-1.2); b) micro vein diameter to the maximum width of the valve bulb (1.0 - 1.5); and c) micro vein diameter

to the distance between the venous valve leaf tip and valve bulb reemergence (1.4) are matched.

The computational mesh of 2D micro vein consisting three valves that were equally spaced from each other (each valve was 5 mm apart) in a 2 cm long micro vein was built (Figure 1A). Blood is a highly complex fluid and several constitutive equations of viscosity have been proposed in literature to model its non-Newtonian behavior [60]. Therefore, we began by comparing three commonly applied models of blood viscosity – Newtonian model, Casson model, and generalized power law (GPL, equation 4-6) [61, 62, 67], and determined relative differences of the predicted velocity profiles, dynamic viscosity distribution and wall shear stress distribution in the venous valves. The distribution of apparent viscosity for shear strain sweep shows that while the viscosity of the Newtonian model remains constant, the viscosity of blood reduces at higher values of shear strain for the non-Newtonian models which predict the shear thinning nature of blood accurately (Figure 1B). Next, we simulated blood flow through the micro valves by selecting an inlet volume flowrate of 1 μl/min, which corresponds to a typical venous shear stress of 1.1 dynes/cm^2 [54, 66]. Velocity streamlines of the blood flow simulation showed maximum velocity at the gap widths that were the regions with smallest cross sections (Figure 1C). Interestingly, while the Newtonian model and non-Newtonian GPL model predicted the formation of a contra rotating twin vortex system in the valve cusp, the Casson model only predicted the formation of a single vortex in the valve cusp. To understand the variation in the prediction of the formation of a twin vortex system using different viscosity models, we also plotted the heat maps of dynamic viscosity in the

venous valves for different models. The dynamic viscosity of whole blood in the venous valves and its cusps showed a relatively sharp increase at the venous valve cusps for the non-Newtonian models (Figure 1D). The increased viscosity of blood at the venous valve cusps might be leading to the differences in the formation of the vortices in the venous valve cusps. In order to confirm the increase in viscosity of the blood at the venous valves may be due to the low shear, we plotted the wall shear stress in the walls of the venous valves, which showed that the cusps of the venous valves were locations of low shear (Figure 1E). These results reveal that while the Casson model doesn't result in a twin vortex system observed clinically and in micro-physiological systems [66, 68], all the models still exhibit that the shear thinning blood becomes highly viscous at the venous valves due to low wall shear stress present at the valve cusps. The difference in prediction of the secondary vortex formation between the Casson model and the generalized power law model is possibly due to the Casson model's prediction of much higher viscosity of blood at lower shear strain relative to the other (Figure 1B). Overall, these in silico experiments suggest that the non-Newtonian generalized power law (GPL) predictions are more suited to model blood blow in veins relative to Newtonian or Casson constitutive equations.

2.4.2. Blood flow predictions under transient venous flow

We next set out to apply our computations to explore the effects of transient flow on the formation and strength of the vortices at the venous valve cusps, since it is typically observed *in vivo* [44]. Non-Newtonian blood (generalized power law) flow through the micro venous valves were simulated under different transient inlet velocity

conditions to observe the changes in the flow pattern near the venous valves. Since the blood flow near a venous valve is governed by the actuation of surrounding muscles and opening and closing of upstream venous valves, we assumed an approximately similar sinusoidal inlet velocity profile whose magnitude varied with time [46, 69]. We chose a time period of four seconds for our inlet velocity profile similar to a full opening and closing cycle of *in vivo* venous valves [70]. We applied the magnitude of the inlet velocity profile such that total volume discharge over two seconds corresponded to the steady volume discharge for Reynold's number (Re) 0.04, which is typically observed[71] in *in vivo* micro veins (Figure 2A). The primary vortex formed at the venous valve cusps was characterized by calculating its swirling strength and vorticity over time (see METHODS). We found that the primary vortex formed at the venous valve cusps has a transient variation in its power as measured through the swirling strength (Figure 2B). Magnitude of the vortex swirling strength was comparable in forward and backward flow indicating that the vortex sizes remained the same even when the flow direction was reversed. By assessing vorticity, which is a metric for rotation and its direction, we found that the vortex direction was only reversed when the systemic flow direction changed from forward flow to backward flow (Figure 2C). Velocity streamlines at maximum forward flow and backward flow (at time points one second and three second respectively) showed a well-defined formation of a primary and secondary vortex in the venous valve cusps (Figure 2D). Further, the reversal of the direction of rotation of the vortices as we move from forward flow to the backward flow was seen (Figure 2E), which was observed experimentally in our prior work [66].

Further, the wall shear stress in the walls of the venous valves showed that the cusps of the venous valves remained a low shear region during the transient flow (Figure 2F-G). These results show that the vortex size/strength does not change significantly even when the systemic flow direction is changed under low Reynold's number. So, we next explored how a larger transient volume discharge (Re 10.00) of blood would affect the characteristics of the vortex system at the venous valve cusps (Figure 3A). Interestingly, swirling strength of the primary vortex with Re 10.00 does not have the same magnitude under forward and backward flow as we saw in low Reynolds number flow previously (Figure 3B). But this difference in the magnitude of swirling strength does not particularly result in a change of direction of the fluid rotation (Figure 3C). This is possibly because a change in direction of the systemic flow in the vein changes the direction of rotation, but the size of the vortex is constrained by the valve geometry in the backward flow, which we were able to visualize by the streamline and vector plots of the forward and backward flow (Figure 3D-E). Plotting the wall shear stress in the walls of the venous valves showed that the cusps of the venous valves remained a low shear region even at high Reynold's number flow (Figure 3F-G). These results show that the vortex size/strength changes significantly when the systemic flow direction is changed under high Reynold's number. Overall, this study suggests that changes in the systemic flow positively affects the vortex formation at the venous valve cusps and since venous valves are regions of shear gradients and low shear, these regions may serve as a conduit for accumulation of thrombotic factors, which may contribute to thrombosis.

2.4.3. Analysis of 3 dimensional computational modeling of micro venous blood flow

Micro veins have small diameters and thus wall effects can potentially influence the flow. Therefore, we wanted to perform a sensitivity test to our 2D analysis and perform a few critical simulations in a 3D model that is significantly computationally expensive but reduces the assumptions on boundary conditions made in 2D models. So, we conducted an *in silico* experiment with a 3D geometry of the micro vein containing venous valves to observe the extent to which the resulting flow profile and vortex characteristics may differ from 2D analyses. As extensive studies have also been conducted on microfluidic systems to model and study micro vasculature [7, 26, 30, 72], we designed our 3D model with a rectangular cross section of width of 200 μm (same as the 2D model) and a height of 75 μm (Figure 4A). Also, use of a rectangular cross section for 3D geometry helped us discretize the fluid domain with hexahedral elements, which would be extremely difficult and computationally time-consuming with a circular geometry (Figure 4A). Though the 3D analysis also showed the formation of the primary and secondary vortices (Figure 4B-D) under steady state (Re 0.04), the position and swirling strength of these vortices were distinct from the ones predicted by the 2D analysis. The center of the primary vortex in the 3D analysis was inside the venous valve cusp (Figure 4B-C) whereas the center of the primary vortex in the 2D analysis was just outside the venous valve cusp (Figure 1C, 2D). The swirling strength of the vortex was reduced under the 3D analysis (0.18 s^{-1}) compared to the 2D analysis (2.69 s^{-1}, Figure 2B). Also, our results showed that even though the vortex strength reduced in the 3D analysis the maximum velocity at the gap width of the 3D analysis had a higher velocity

(4.4 mm/s, Figure 4C) compared to the 2D analysis (3.2 mm/s, Figure 2D). This increase in maximum velocity is likely due to the effects of the top and bottom walls, which effectively reduced the total cross section at the valve gap width much more that the reduction in area in a 2D domain. Wall shear stress at the micro venous valve cusps of the 3D analysis (Figure 4E) were however, similar to the wall shear stress of the 2D analysis (Figure 2F and 3F), which was a low shear region.

We then plotted the variation of the swirling strength of the primary vortex to find the effects of the top and bottom walls on them (Figure 5A-B). The swirling strength of the primary vortex had a parabolic profile when moving from the bottom wall to the top wall of the microfluidic channel with the maximum swirling strength at the mid-section (~37.5 μm) for both Re 0.04 and 10.00. The transient analysis of sinusoidal velocity profiles (Re 0.04 and 10.00) showed the variation of the swirling strength to be similar to the variations shown in a 2D analysis, but with a lower magnitude (Figure 5C-D, Figure 2B-C, Figure 3B-C). These results suggest that it is possible that 3D modeling may better accommodate the wall effects of the microfluidic veins, and computational predictions of blood flow in small veins may require more expensive computational approaches.

2.4.4. Transport phenomena of oxygen in the microscopic veins and valves

Non-actuating venous valves are known to influence the fluid flow patterns that limits oxygen transport into the cusps fueling hypoxic inflammation of cusp endothelium. Hypoxic inflammation of the deep venous valves is one of the mechanisms that triggers thrombus formation, which ultimately leads to DVT formation. So, we

aspired to predict how changes of flow pattern in the micro venous valves due to changes in magnitude, direction, and the rate of change of velocity may regulate the transport and distribution of oxygen in the venous valves. To find the distribution of oxygen at the venous valves under different flow conditions, we superimposed the mass transport equations of diffusion and forced advection on the fluid flow domain (Equation 7.0-8.0 in Figure 6A). Once the contour plot and streamlines matched (Figure 6B-C), we simulated the mass transfer of oxygen at different flow rates corresponding to Re 0.04 and 10.00. We consider the inlet concentration and initial concentration of oxygen in the system to be 22.22 mols/m^3, which corresponds to 5% oxygenated blood that is observed in the veins [73]. The endothelium at the walls of the veins including the venous valves is assumed to absorb oxygen at a rate of $3.2e^{-8}$ mol/(m^2s) [74] and therefore, we kept that as a reaction wall boundary in our model. The bulk oxygen in the system is assumed to be transported by a combination convection and diffusion, where the coefficient of diffusion of oxygen was $1.62e^{-9}$ m^2/s [75]. Simulations of oxygen transport in the venous valve cusps revealed that the oxygen concentration at the venous valve cusps were higher at Re 10.00 compared to Re 0.04 (Figure 6D-E). Therefore, these *in silico* results showed that bulk transport of oxygen by convection plays a crucial role in the transport of oxygen to the valve cusps compared to diffusion. Oxygen concentration at the abyss of the venous valve cusps were tracked for transient flows and compared with the concentration at steady flow (Figure 6F-G). These results showed an interesting trend where the transient flow profile at Re 0.04 has lower oxygen concentration at the abyss compared to the steady flow at Re 0.04. This may be because the oxygen transport at the

valves is dominated by advection and the transient sine wave at Re 0.04 has near stasis systemic flow for a considerable interval of time (Figure 2A & B). But this observation was reversed for Re = 10.00. At Re = 10.00, the transient flow had the higher oxygen content at the valve cusp abyss for most of the time period (77%) compared to the steady flow (dotted vertical lines in Figure 6G). This result appears consistent as the transient profile has velocities higher than the steady flow at Re 10.00 and the transient flow does not have a near stasis systemic flow for a considerable interval of time (Figure 2A & C). Importantly, these *in silico* results for oxygen transport suggest that the cusp of a non-actuating micro venous valve do not become hypoxic even under steady systemic flow and thus prevent the hypoxic inflammation of the valve endothelium at the cusps and consequently prevent thrombus formation. This computational study provides a basis for experimental validation of this hypothesis.

2.5. Discussion and Conclusion

In the current study, we introduced a pathological model of a micro venous valve and the complex fluid flow patterns associated with the non-Newtonian blood flow through them. We showed that the shear thinning blood tend to become highly viscous and stagnant at the low shear regions of venous valve cusps. This stagnation region is generally formed in the region below the primary vortex fromed at the mouth of the venous valve cusps. Though the strength of the primary vortex varies in a transient flow, the stagnation region was still present in the venous valve cusps. Also, our study reveals that the stagnant flow inside the micro venous valves are not enough to create hypoxic inflammation that can lead to endothelial inflammation. We only see a drop from 2.22

mol/m^3 (5% weight per volume in blood) of oxygen in the vein to 2.17 (4.9 % weight per volume in bloo) mol/m^3 of oxygen in the venous valve cusps under Re = 0.04 transient flow. The oxygen content in the cusps are above pathological hypoxic levels which is less than 1% oxygen (weight per volume in blood). The oxygen tranport into the cusps are improved by an increase in the systemic flow of blood in the veins. Therefore, even in pathological state of thrombosis, the underying vascular inflammation may not be regulated by hypoxia but by the abrupt and vortical shear forces. This is a novel hypothesis that can be experimentally validated by contemporary *in vitro* models, such as a vein-chip [66]. Finally, we showed that the 3D models may predict a different location of fluid vortices within the cusps relative to the 2D models due to the wall effects, and therefore may be required when more accurate predictions are needed.

We have modelled the pathological state of a micro venous valve where the stiffening of the valve leaflets lead to non-actuation of the venous valves. But in a healthy micro venous vlaves the leaflets of the venous valves actuate and they open and close with time. This healthy actuation of a venous valve and the fluid dynamics of blood related to actuation are not captured in our present model. Simulation of an actuating venous valve would need a more complex fluid structure interaction (FSI) model where the fluid flow of blood affects the opening of the valve and the opening of the valve inturn affects the fluid dynamics of blood in the region till an equilibrium is reached. These simulatons in 3D need large structural deformation of the valve leaflets and subsequent change of fluid flow domain in each iteration. Though our models do not incorporate this complex fluid structure interaction, the transient analysis is still able to predict results that are

approximations of actual flow. But a more complex FSI model can be designed that would be an improvement to the current approach.

In summary, our computational study provides a prediction about the fluid dynamics of blood in a micro venous valve and its implications on valve heath, and thrombus formation, which can be a foundation for more efficient preclinical experimental approaches.

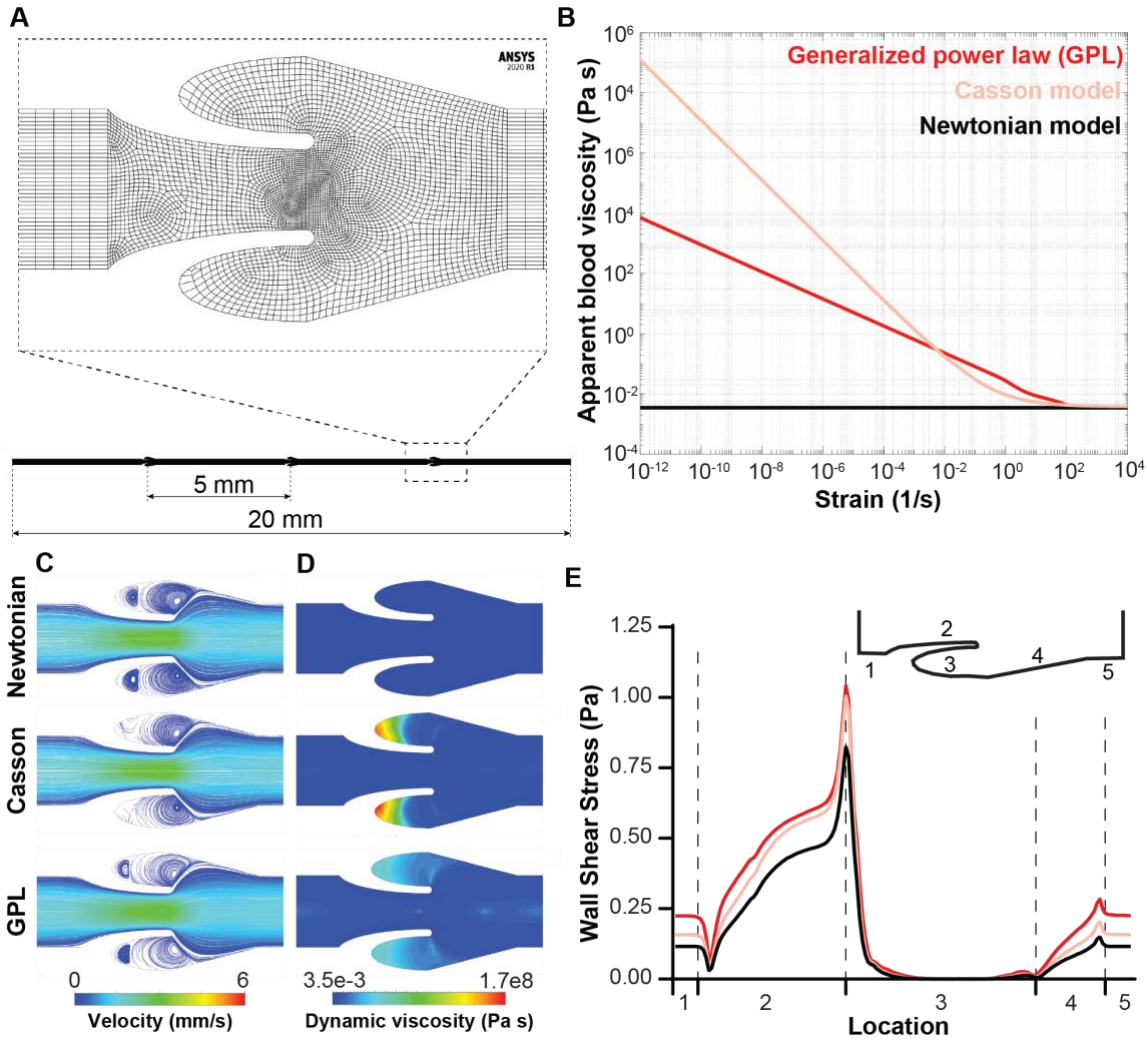

Figure 2-1: Modelling blood flow in venous valves.
(A) A straight micro vein of 20 mm length with three micro venous valves (5 mm apart) was designed and discretized. (B) Variation of viscosity of blood with wall shear rate sweep for different blood viscosity models – Newtonian model (black), Casson model (pink), and generalized power law (red). (C) Contour plot showing velocity streamlines of whole blood flow in venous valve using different viscosity models. (D) Contour plot showing the distribution of dynamic viscosity of whole blood in venous valve when using different viscosity models. (E) Graph comparing the wall shear stress distribution in the venous valve walls when different blood viscosity models are used - Newtonian model (black), Casson model (pink), and generalized power law (red).

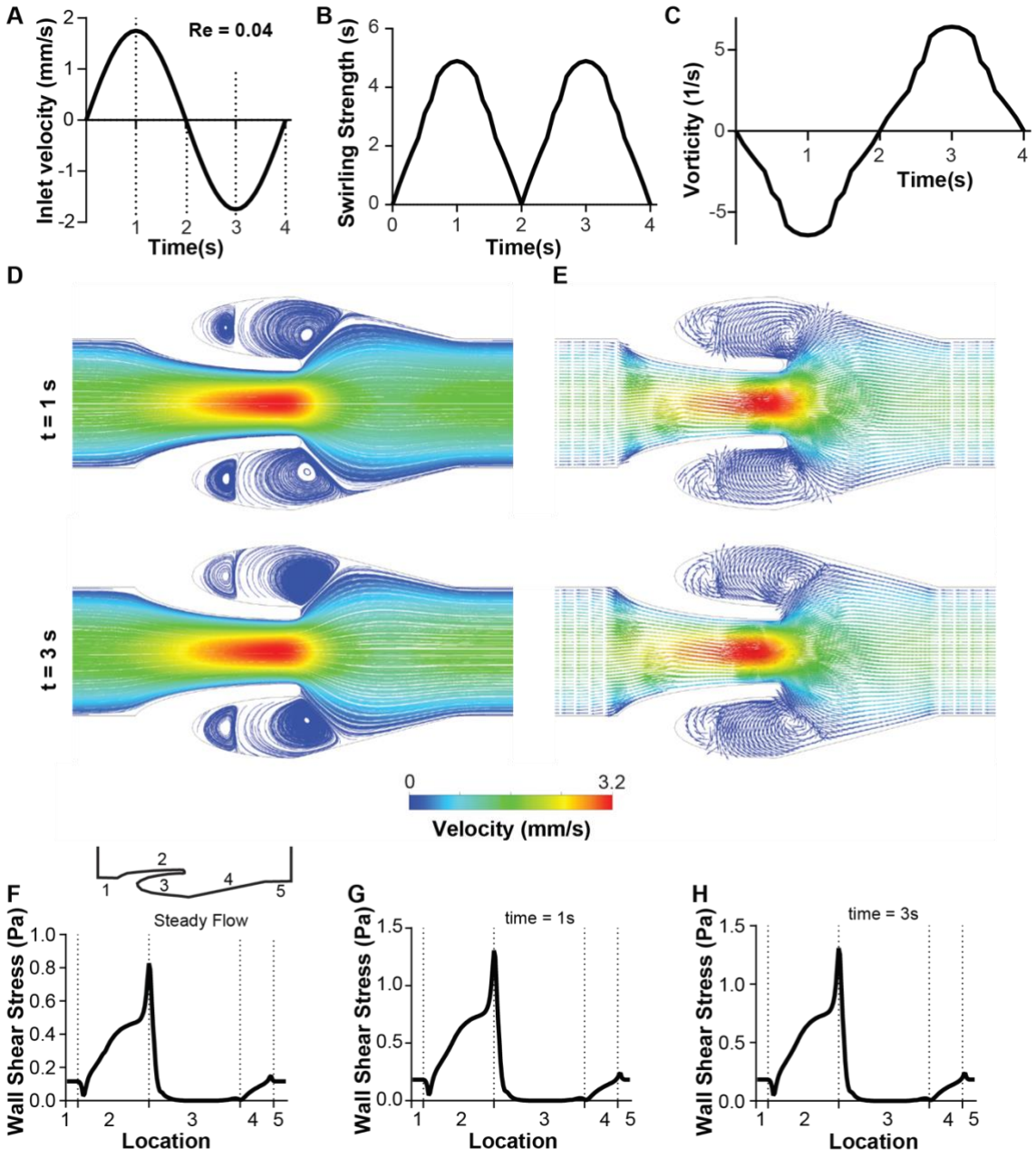

Figure 2-2: Transient analysis of blood flow through the venous valves under low Reynold's numbers (Re 0.04).

(A) Graph showing the transient inlet sinusoidal velocity profile. (B) Graph showing the transient variation of swirling strength of the primary vortex. (C) Graph showing the transient variation of vorticity of the primary vortex. (D) Contour plot showing velocity streamlines of whole blood flow in the venous valves at maximum forward and maximum backward velocity (time points t = 1s, and 3s respectively). (E) Vector plot showing velocity vectors of whole blood flow in the venous valve at maximum forward and maximum backward velocity (time points t = 1s, and 3s respectively). Graphs

comparing the variation the wall shear stress distribution in the venous valve walls under (F) steady flow, (G) max forward velocity (t = 1s), and (I) max backward velocity (t = 3s).

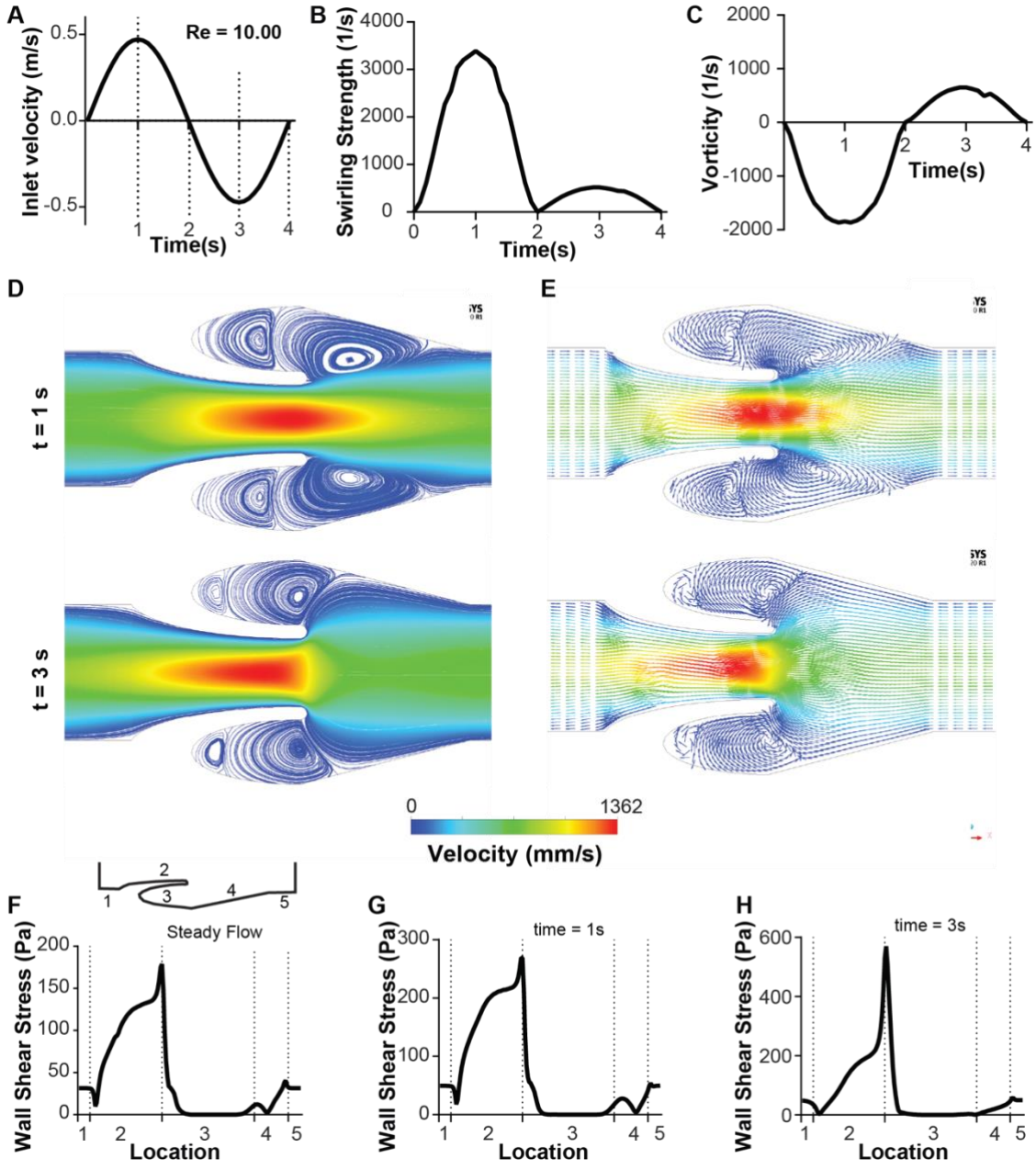

Figure 2-3: Transient analysis of blood flow through the venous valves under high Reynold's numbers (Re 10.00).

(A) Graph showing the transient inlet sinusoidal velocity profile. (B) Graph showing the transient variation of swirling strength of the primary vortex. (C) Graph showing the transient variation of vorticity of the primary vortex. (D) Contour plot showing velocity

streamlines of whole blood flow in the venous valves at maximum forward and maximum backward velocity (time points t = 1s, and 3s respectively). (E) Vector plot showing velocity vectors of whole blood flow in the venous valve at maximum forward and maximum backward velocity (time points t = 1s, and 3s respectively). Graphs comparing the variation the wall shear stress distribution in the venous valve walls under (F) steady flow, (G) max forward velocity (t = 1s), and (I) max backward velocity (t = 3s).

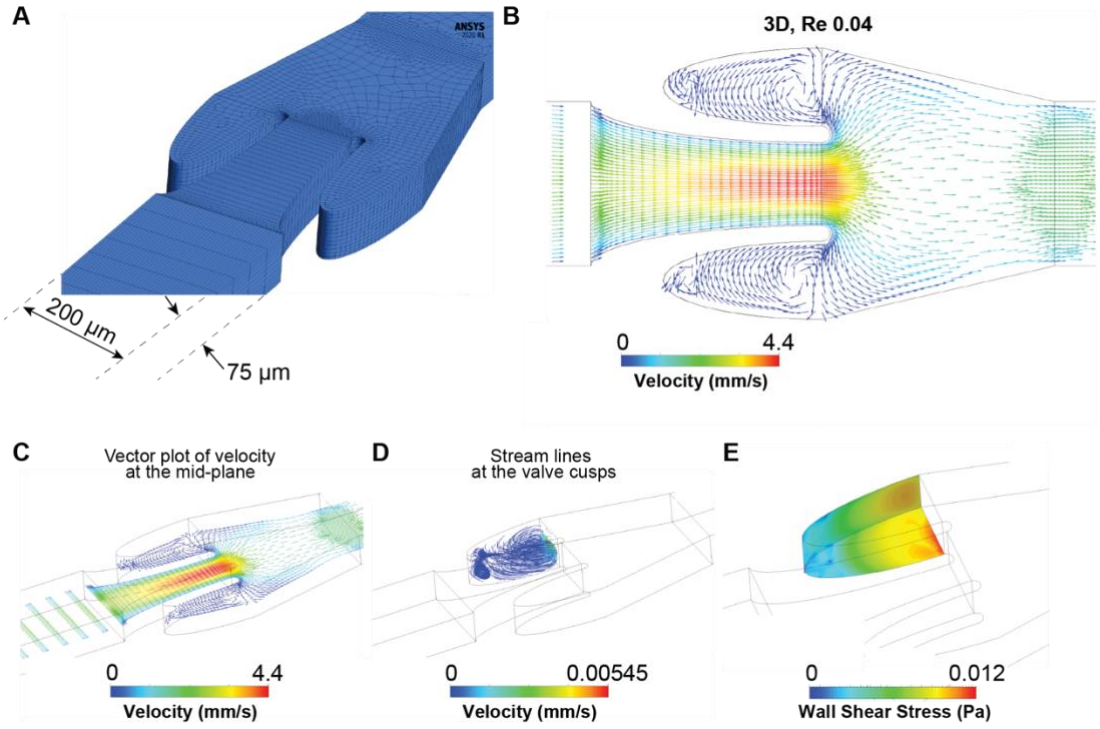

Figure 2-4: Blood flow simulation in 3D venous valves.
(A) The discretized domain of a 3D micro venous valve. Vector plot of the velocity profile at the midplane of the 3D venous valves (Re 0.04), (B) orthogonal view and (C) isometric view. (D) Contour plot of the primary and secondary vortices formed at the 3D venous valve cusps. (E) Contour plot of the wall shear stress distribution.

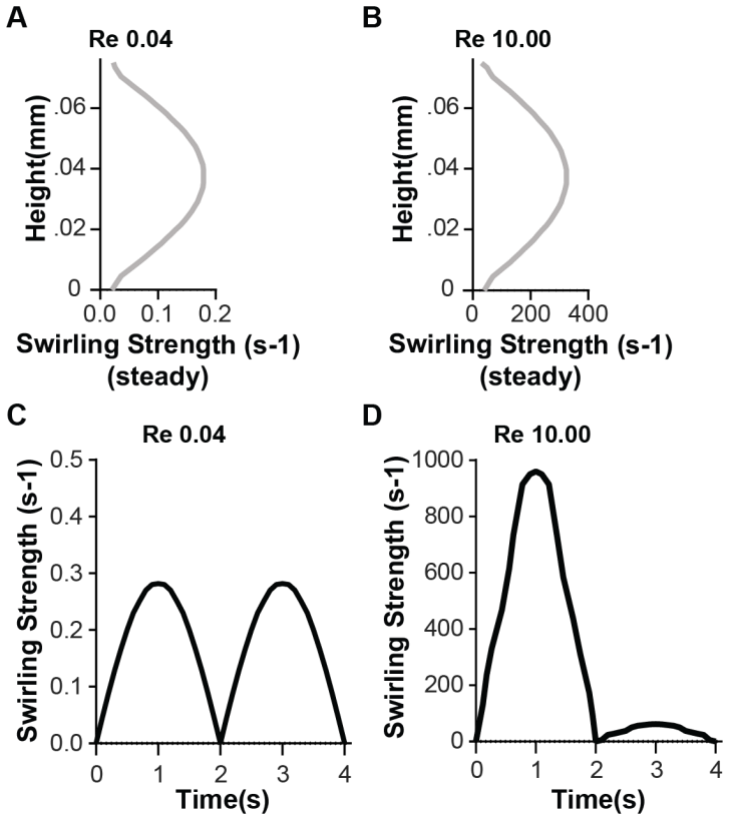

Figure 2-5: 3D vortex characterization at venous valves.
Graph showing the variation of swirling strength of the primary vortex along the height of the 3D venous valve at (A) Re = 0.04 and (B) Re = 10.00 (red). Graph showing the transient variation of swirling strength of the primary vortex at the 3D venous valve at (C) Re = 0.04 and (D) Re = 10.00.

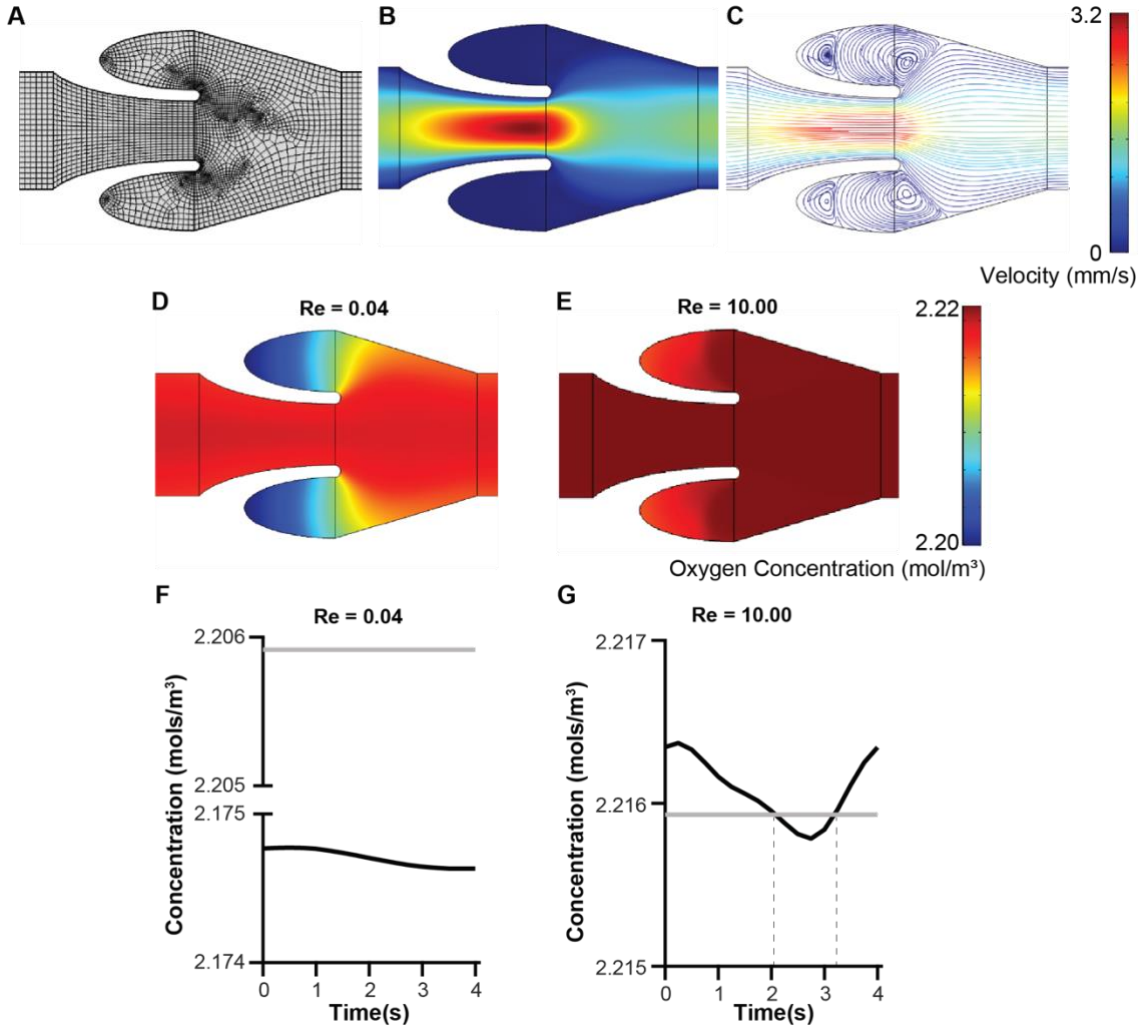

Figure 2-6: Mass transport of oxygen in the venous valves.
(A) Discretized fluid domain in Comsol Multiphysics for simulation of mass transfer. (B) Velocity contour and (C) streamline plot of whole blood flow in the venous valves. Contour plot of the distribution of oxygen concentration under different steady flow condition (D) Re = 0.04 and (E) Re = 10.00. (F) Graph showing the transient variation of oxygen concentration at the venous valve cusps for different inlet flow profiles.

3. MICROENGINEERED HUMAN VEIN-CHIP RECREATES VENOUS VALVE ARCHITECTURE AND ITS CONTRIBUTION TO THROMBOSIS*

3.1. Abstract

Deep vein thrombosis (DVT) and its consequences are lethal, but current models cannot completely dissect its determinants – endothelium, flow and blood constituents – together called Virchow's triad. Most models for studying DVT forego assessment of venous valves that serve as the primary sites of DVT formation. Therefore, our knowledge of DVT formed at the venous cusps has remained obscure due to lack of experimental models. Here, organ-on-chip methodology is leveraged to create a Vein-Chip platform integrating fully vascularized venous valves and its hemodynamic, as seen *in vivo*. These Vein-Chips reveal that vascular endothelium of valve cusps adapts to the locally disturbed microenvironment by expressing a different phenotype from the regions of uniform flow. This spatial adaptation of endothelial function recreated on this *in vitro* Vein-Chip platform is shown to protect the vein from thrombosis from disturbed flow in valves, but interestingly, cytokine stimulation reverses the effect and switches the valve endothelium to becoming prothrombotic. The platform eventually modulates the three factors of Virchow's triad and provides a systematic approach to investigate the determinants of fibrin and platelet dynamics of DVT. Therefore, this Vein-Chip offers a new preclinical approach to study venous pathophysiology and show effects of antithrombotic drug treatment.

---

* Rajeeva Pandian, Navaneeth Krishna, Brandon K. Walther, Rishi Suresh, John P. Cooke, and Abhishek Jain. "Microengineered Human Vein-Chip Recreates Venous Valve Architecture and Its Contribution to Thrombosis." *Small* 16, no. 49 (2020): 2003401.

3.2. Introduction

Severe clotting of blood in the deep veins, called Deep Vein Thrombosis (DVT), followed by pulmonary embolism (PE), together known as venous thromboembolism (VTE), is a major debilitating and fatal condition[15]. In the United States itself, about 100,000 patients die of VTE annually[14]. It has been known for over a century that DVT is primarily triggered at the sites of venous valve cusps (pockets) by endothelial inflammation, stasis of blood at the cusps and/or hypercoagulable blood – the three factors that form the Virchow's triad. Inclusion of venous valves in preclinical models of thrombosis is important, because they facilitate unidirectional flow of blood from the lower extremities to the heart. It is known that in venous thrombosis, valve function becomes impaired leading to reduced flow and local hypoxia, which exacerbates endothelial activation, adhesion, and ultimately, DVT[34]. But despite this knowledge, most research and treatments of DVT have focused on the blood coagulation system alone. In contrast to arterial thrombosis, the mechanisms of which have been intensively studied, DVT remains underexplored. This lack of emphasis on integrative research in DVT can partly be attributed to the extensive reliance on animal models which have not been able to include the flow dynamics near the venous valves [76-80]. Though these models have decoded several key mechanisms that govern DVT, their lack of valve architecture limits them considerably in revealing the precise role of Virchow factors, endothelium and hemodynamics. There have also been *in vitro* models of DVT using parallel flow and stepped flow chambers[81]. A commonly used *in vitro* thrombosis system, the parallel plate flow chamber is a hollow rectangular space through which

blood or its components can be perfused to induce physiological wall shear stresses over purified proteins (such as, von Willebrand factor or tissue factor), extracellular matrix (collagen, laminin or fibronectin) or endothelial cell monolayers [21]. While these systems have been useful in studying the effects of shear and recirculating flow [22] on platelet function and coagulation [23], venous valve anatomy is not replicated in these chambers. There are recent studies that have shown the incorporation of vascular cells in microfluidic devices to model thrombosis in various diseases [8, 26, 82]. However, very few microfluidic models of veins exist, none of which include venous valve architecture and endothelium together [35, 36]. Recent studies have demonstrated microfluidic models of venous thrombosis consisting of an expansion with an undercut or moving valves, but none of these models include endothelial function [83, 84].

Here, we introduce a vein-on-a-chip (Vein-Chip) that is a microfluidic model of a vein containing valve architecture, where living endothelial tissue and whole blood flow provide the incorporation and dissection of the Virchow's triad. For example, with the inclusion of the venous valve architecture, our Vein-Chip could recapitulate the fluid mechanical microenvironment of the veins as observed via several models and *in vivo*, respectively. Further, with the inclusion of the vascular endothelial function, we systematically reveal its regional adaptation to flow and contribution to venous thrombosis. Finally, we determine how the anatomy of venous valves could also affect DVT formation. These predictions of venous pathophysiology from our model show that this device can be used to investigate the regulators of the disease and targeted therapies against thrombosis.

3.3. Results

3.3.1. Design and microfabrication of Vein-Chip

We initially sought to determine the anatomy of a typical human vein and venous valve that provide geometric similarity for a microfluidic Vein-chip. Therefore, we analyzed Doppler-ultrasound images available in literature[64], and translated the geometry of the vein (Figure 3-1A). The venous valve consisted of two leaflets that emanated from the walls of the channel on either side. Geometric similarity of the Vein-Chip with the in vivo venous valves were achieved by conserving the ratios of a) maximum venous valve cusp depth to the diameter of the vein (1.0); b) maximum width of the venous valve bulb to the diameter of the vein (1.2); and c) distance between the venous valve leaf tip and valve bulb reemergence to the vein diameter (1.4) (Figure 1B). Our values are typical to physiological range [64, 65]. The other two important anatomical features of the designed valves were (iv) valve cusp leaflet, and (v) gap width (distance between the tips of two leaflets) (Figure 3-1B). The width and height of the venous lumen (channel) were selected to be 200 μm and 75 μm respectively, equal to a hydraulic diameter of ~120 microns. The tip of each leaflet had a thickness of 20 μm. We designed a valve configuration that had a gap width of 100 μm, which was 50% of the channel width (Figure 3-1C). Before we fabricated the devices, to confirm if our venous valve design is representative of the physical microenvironmental conditions *in vivo*, we determined if simulation of blood flow through these devices could recapitulate critical aspects of fluid dynamics at the valves. Numerical models of pathological venous

valves have shown formation of two counter-rotating vortices inside the venous valve cusps [68, 85]. Computational fluid dynamic (CFD) analysis of the whole blood flow (modelled as non-Newtonian fluid with a generalized power law for viscosity based on prior work [30, 67], see Experimental Section) in the designed microfluidic venous valves were carried out, which revealed that our configuration developed two contra rotating vortices (a twin vortex system) at the venous valve cusps [68] (marked i and ii in Figure 3-1D). Further, blood had maximum velocity near the valve opening and minimum velocity at the cusps, which created steep velocity gradients near the venous valves (Figure 3-1D, Figure 3-2A and 3-2B, Table 1). Since the purpose of this *in vitro* vein was to model thrombosis, these data predict that Vein-Chip consists of a fluid mechanical environment (twin vortex system with a near stasis of blood in the secondary vortex of cusps) near the valves that is expected to promote thrombosis [34]. Next, we set out to fabricate the Vein-Chip and experimentally validated the fluid dynamics of whole blood flow against computational data. Three venous valves were placed equidistant from each other in a Vein-Chip device such that the flow disturbances caused by one valve did not affect the flow dynamics in the downstream valve (Figure 3-1C). The design aimed to mimic a typical section of a vein consisting of multiple valves and was also useful in multiplexing experimental observations. In this setup, the Vein-Chips were 20 mm long, and the valves were separated by 5 mm. We made each device using standardized procedures of soft lithography of PDMS (see Experimental Section)[86]. These devices were bonded with PDMS coated glass slides to obtain a sealed system (Figure 3-1E). The Vein-Chips were then plasma treated to prevent fouling and

anticoagulated whole blood was perfused through them at 1 µl min^{-1}, corresponding to a typical venous luminal shear stress of 2 dynes cm^{-2} (Figure 3-2C) [25].

Expectedly, upon blood perfusion, we observed formation of the primary vortex in the venous valves of the Vein-Chip as predicted in the CFD analysis (Figure 3-1F). We observed the RBCs in the primary vortex to move in a circular path and direction as predicted by the CFD simulation, with nearly the same velocity (Figure 3-1G). The blood in the secondary vortex region had very low velocity possibly due to rouleaux formation by red blood cells that is typical when shear is very low [68] (Figure 3-3). Overall, our whole blood flow experiments through the Vein-Chip showed that these devices were able to recreate the circulation in fluid flow of human vein cusps.

3.3.2. Endothelial lumen formation and analysis of Vein-Chip

The endothelial cells within the venous valves have been suggested to significantly regulate vascular inflammation, blood cell adhesion and thrombosis [56, 87]. Since endothelial activation is also one of the three factors of Virchow's triad predicted to be a cause of venous thrombosis, we set out to line all the walls of the Vein-Chip with primary human endothelial cells which would eventually allow a better understanding of how endothelial-derived factors contribute in the pathogenesis of thrombosis in the venous valves. Similar to prior vascular organ-on-chips albeit consisting straight channels[7, 26], we first coated the Vein-Chip with extracellular matrix proteins (collagen-fibronectin, see section 3.5), and then cultured human umbilical vein endothelial cells (HUVECs) under perfusion over the underlying matrix. Imaging of the chip within the incubator revealed that a confluent lumen of endothelium

forms on the device, including the valve cusps, within 12-18 hours (Figure 3-4, Figure 3-5A). The cell growth dynamics in these devices also showed that when HUVECs were seeded, they were only present in the non-cusp regions initially; but with time, cells started to enter and proliferate in the cusps and became confluent at nearly 18 hours of perfusion (Figure 2B). We repeatedly found a nearly consistent distribution of junction membranes, cytoskeleton, as well as nuclei across the device including the venous cusps suggesting that our procedure to endothelialize these complex microfluidic geometries is robust (Figure 2C). Further, when we perfused recalcified citrated whole blood through the Vein-Chip consisting intact endothelium at venous shear stress, we did not see any blood cell adhesion to the endothelial surface, illustrating that the endothelium was able to protect the blood cells from contacting the underlying matrix. This is typically observed in vascular organ-chips when endothelium is untreated [32]. Indeed, we saw platelet adhesion and fibrin in devices that were comprised only of ECM proteins (Figure 2D).

More interestingly, even though our Vein-Chip included valves, where blood flow formed vortices and regions of stasis, the endothelium still prevented flowing blood from cell adhesion and thrombosis in the cusps (Figure 2E-F). This observation suggested that rotating flow and stasis are not enough to initiate thrombus formation at the cusps in the presence of endothelial cells. We speculated that the endothelial cells in the cusps adapted during the culture period and downregulated the expression of procoagulant factors to inhibit cell activation and adhesion. This spatial heterogeneity in endothelial cell function in an organ-chip has not been characterized in prior studies with

bioengineered devices. In support of this hypothesis, in our Vein-Chip, we observed that the expression of von Willebrand Factor (VWF) was less in the venous valve cusps compared to the straight portions of the chip (Figure 2G-H) corresponding to what has been shown *in vivo* [55, 56, 87]. To further characterize the cell adaptation to the cusp microenvironment, we extracted RNA from the endothelial cells and measured gene expression levels of antithrombotic proteins endothelial nitric oxide synthase (eNOS), and thrombomodulin (TMBD), and the thrombotic proteins intracellular adhesion molecule-1 (ICAM-1), VWF and tissue factor (TF), specifically within the cusps as well as the venous lumen of the device. We observed that eNOS and TMBD were upregulated whereas ICAM-1, VWF and TF were downregulated within the endothelial cells of the cusps compared to the venous lumen (Figure 2I), suggesting cusp endothelium has adapted to become less adhesive and inhibit coagulation responses. These data strengthen our finding that the endothelial cells within our Vein-Chip mimic some of the heterogeneity of vascular function in different regions of human veins. Therefore, endothelialized Vein-Chips are novel organ-on-chips which provide insights into vascular endothelial function in its regulation of venous pathology.

3.3.3. Dissecting Virchow's triad with Vein-Chip: flow and stasis

We next set out to model human DVT with the Vein-Chip. Specifically, we sought to leverage our platform to dissect the factors of Virchow's triad sequentially (hemodynamics, endothelial state, and blood chemistry) and investigate their individual and collaborative contributions in the onset and propagation of DVT through our platform. Stasis of blood flow within the vein cusps, associated with immobility

(bedridden state) or limited mobility (wheelchair bound), is a serious risk factor for DVT [88]. But, in bedridden (supine posture) state calf muscles are compressed compared to other positions (sitting or standing), which leads to contraction of deep veins and higher velocity of blood through them [89, 90]. Although the exact pathophysiological venous shear stresses are not known in literature, clinical observations suggest higher wall shear stress within the vein in supine position. Therefore, we were inspired to first leverage our platform to investigate if challenging the Vein-Chip to higher systemic shear would modulate thrombosis. We experimentally perfused blood through the matrix-coated Vein-Chips at physiological and supraphysiological shear. We found that at the supraphysiological shear stress (Table 1), the fibrin formation in the venous lumen decreased (Figure 3-6A-B) whereas the platelet adhesion increased (Figure 3-6C) possibly due to higher shear activating more platelets [91], and making fibrin monomers and oligomers unstable, leading to its reduced deposition [92]. Interestingly, fibrin formation in the cusps increased at supraphysiological shear (Figure 3-6D). The platelet adhesion in the cusps also increased (Figure 3-6E), which was mainly due to the formation of platelet plugs at the mouth of the cusps (Figure 3-6A), as was observed in another venous thrombosis model [83]. Computational simulations of fibrinogen transport due to coupled convection and diffusion at the venous valves predicted an increased influx of fibrinogen into the cusps at supraphysiological flow rate (Figure 3-7), thus supporting more thrombus formation within the cusps.

Next, we also speculated that the shape of the venous valve cusps may determine hemodynamics and therefore, DVT, since valve gap widths and valve openings can

change hemodynamics within the valve, as observed clinically [49, 93, 94]. Specifically, in addition to the veins with 50% gap widths, we further analyzed veins with 75% and 25% gap width (150 µm and 50 µm width respectively; Figure 3-8A). First, CFD analysis of blood flow through these different configurations showed that the formation of twin contra rotating vortices occurs in all the three configurations (Figure 3-8B,). Further, the rate at which gap velocity changed with respect to change in inlet velocity was linear and increased with a decrease in gap width (Figure 3-8C). This suggested that if the gap width is small, it may facilitate thrombosis, because rate of change of hemodynamic flow is high. To test this, we fabricated the different configurations of Vein-Chips and perfused blood through these devices that contained endothelium. We found that the devices had more fibrin rich thrombi at the cusp as we moved from 75% to 25% gap width configuration (Figure 3-8D-E). The increased thrombus formation in cusps may be related to the increased blood velocity at the gap widths as this leads to an increased concentration of coagulation factors in the cusps when the gap width velocity increases. Taken together, these results suggest that hemodynamics, either varied through systemic flow or valve geometry may regulate venous function and DVT. Therefore, this platform could become a tool to investigate unique hemodynamic states in the vein and their contributions in DVT.

3.3.4. Dissecting Virchow's triad with Vein-Chip: endothelial activation

Several studies suggest that increased cytokine levels in blood leads to endothelial activation, barrier disruption, and increased thrombosis *in vivo* [95, 96]. Therefore, we stimulated the confluent endothelialized Vein-Chips with an inflammatory

cytokine TNF-α, a widely used cytokine to model the effect of endothelial activation on thrombosis *in vitro*[97]. We observed that prior treatment with TNF-α dose-dependently increased thrombus formation when the device was perfused with whole blood in a calcium-containing buffer (Figure 3-9A). The morphology of the thrombi formed over the endothelium were distinct from the thrombi that formed on underlying collagen, suggesting active participation of endothelial cells in regulating thrombosis (Figure 3-9A). Recalcified blood was perfused through the devices for at least 15 min and the thrombi formation was imaged and quantified over time (Figure 3-9B). The measurement at the end of 15 min was used as an endpoint to compare groups. Whereas fibrin formation was conspicuous at the cusps relative to untreated controls, platelet adhesion was similar to the untreated channel cusps, suggesting lack of platelet recruitment or activation in venous thrombosis formed under these conditions and supporting the dogma that venous clots are fibrin rich and platelet deficient (Figure 3-9C-F). Further, scanning electron micrographs of thrombi formed in the venous valve cusps reinforced that the thrombi were rich in fibrin and red blood cells, and devoid of platelets (Figure 3-9G). In most devices, we also saw leukocytes in the thrombi formed at the venous valves [98] (Figure 3-10). Interestingly, when we measured the endothelial surface VWF expression, in contrast to untreated controls, we now saw that the VWF at both the cusps and the venous lumen increased to nearly the same level upon stimulation (Figure 3-9H-I), corresponding to the increased fibrin formation at the cusps in addition to the disturbed flow [81]. Prior studies have shown that TNF-α induces changes in endothelial cell functions, such as upregulation of tissue factor, resulting in endothelial

procoagulant activity [97, 99]. To validate this aspect, we proceeded to characterize the gene expression of TF and TMBD within the venous valve cusps to verify their contribution in valve thrombus formation. We observed upregulation of TF and downregulation of TMBD within the cusps of TNF-α treated device cusps compared to the non-treated devices (Figure 3-9J), suggesting that the cusp endothelium has become procoagulant at the cusp upon TNF-α stimulation. This suggested that stimulation of endothelium resulted in a prothrombotic microenvironment, and the disturbed flow at the valves further contributed to increased thrombosis at the cusps in the presence of a cytokine. Therefore, these results together demonstrated that thrombus formation within Vein-Chip is differentially regulated by endothelial cells at the site of venous valves, and this model may provide a systematic evaluation of state of endothelium in venous thrombosis.

3.3.5. Dissecting Virchow's triad with Vein-Chip: blood chemistry

The current gold standard treatment of DVT is anticoagulation [100]. However, because of the diversity of patients and multiplicity of environmental factors, treatment with anticoagulants may be insufficient to prevent venous thromboembolism, or conversely may provoke bleeding [101, 102]. Unfortunately, methods to monitor the adequacy of anticoagulation are imperfect. Therefore, we sought to provide a proof-of-concept that Vein-Chip may become a modeling system to investigate anticoagulation therapy in DVT. First, we treated the blood with heparin ($0.25 – 0.5$ IU ml^{-1}) - an intravenously administered drug that inactivates coagulation factors [103] and perfused the treated blood through TNF-α treated endothelialized Vein-Chips. Heparin treatment

significantly reduced thrombi formation in a dose-dependent manner (Figure 3-11A-B). However, while we saw a reduction in fibrin even at a lower dose of heparin within the Vein-Chip, reduction of fibrin in the cusps required a higher dosage of the anticoagulant (Figure 3-11C). These data revealed that venous cusps require higher heparin anticoagulation than the systemic heparin anticoagulation to completely prevent the formation of the local thrombi. Next, we also investigated the anticoagulation effect of two clinically-prescribed direct oral anticoagulants (DOAC; rivaroxaban or Xarelto, 100 – 500 ng ml^{-1}; apixaban or Eliquis, 50-500 ng ml^{-1}) since they are increasingly being prescribed to patients and are potent antithrombotic drugs that inhibit factor Xa [104, 105]. When added to blood samples and introduced in TNF-α treated Vein-Chips, fibrin rich clots were still seen in the cusps at their standard dosage (100 ng ml^{-1} of rivaroxaban and 50 ng ml^{-1} of apixaban) while there were unobservable thrombi in the venous lumen (Figure 3-12). Only when the dosage of the DOACs was increased to 500 ng ml^{-1} (both rivaroxaban or apixaban) was thrombus formation abrogated at the cusps (Figure 3-11C). In contrast, when we investigated the effects of an antiplatelet agent (tirofiban or Aggrastat, 500 ng ml^{-1}) in these Vein-Chips, we observed no reduction of thrombus in the venous valve cusps, since platelets entering the cusps were few (Figure 3-11C, Figure 3-10). Taken together, these data indicated that our device might provide insights into choice of therapeutics and dosing, especially when vein cusps need to be treated.

3.4. Discussion

The current approach to study the pathobiology of DVT and to test new therapeutics is to employ one of several different mouse models [78]. While these

diverse models have together contributed to our current understanding of DVT, these models don't always mimic thrombogenesis within the valve cusps or study the stages of DVT once a thrombus has formed. The Vein-Chip device introduced in this work has many potential advantages over existing systems used to study vein physiology. One of the main advantages of this device is the inclusion of venous valve architecture which recapitulates the microenvironment observed in human venous valves. We observed that the unique structure of the venous valves leads to the formation of a twin vortex system *in vivo*. In contrast to our anatomically-inspired geometry, prior microfluidic studies often included steps, corners or rapid expansion/contractions in their model that are known to result in abrupt changes in geometry (diameter) and resulting blood flow profile not expected physiologically [44, 83]. These geometries can lead to non-physiological disturbed flow profiles that may artificially activate the endothelial cells. Further, due to non-physiological disturbed flow profiles and an unfavorable endothelial phenotype, these models may be less predictive of venous thrombosis relative to the vein-chip platform that conserves the geometric and dynamic similarity of the veins in vivo. Intriguingly, endothelial cells within this region appear to adapt to the vortical flow to protect against thrombosis under normal conditions. The cellular signaling mechanisms that facilitate this adaptation of venous endothelial phenotype are still unknown. Nevertheless, our Vein-Chip permits us to replicate this difference in phenotype of the endothelial cells at venous valve cusps of the Vein-Chip at functional, cellular and gene expression levels. Therefore, by including valves and endothelium, this system can now become a useful *in vitro* tool to investigate such mechanisms. In our

first presentation of the vein-chip as an experimental model, we applied the TNF-α treatment because it is a very common procedure to induce endothelial activation and prothrombotic state. This was done primarily so that we can characterize thrombus formation differentially between the main luminal part and the vein pockets of the vein-chip. Several prior studies, including our data presented here, have rigorously presented endothelial dysfunction, hyperpermeability, adhesiveness and prothrombotic state due to increase in tissue factor expression and decrease in thrombomodulin after the TNF-α treatment [97, 99]. In that context, we successfully show that our chip reproduces the state of endothelial activation and its consequences, but to a different extent comparing the vein lumen to its cusp section. Our effort here is not directed to explore the biological mechanisms of TNF-α induced thrombosis, or to characterize the multiple pro/anti-coagulant pathways that are expected to be involved in this process although our platform may serve as an opportunity to do so.

Another merit of this device is the ability it provides to perfuse whole blood and control its flow. It is well established that the clotting system is regulated by fluid dynamic mechanisms [106], and therefore to understand the relationship between hemodynamics and thrombosis independent of other regulators, the Vein-Chip provides the flexibility to introduce a wide range of shear rates. Here, our Vein-Chip shows that high shear promotes more fibrin-rich DVT, which may involve recruitment of platelets. These studies are very difficult to perform in mice as precise flow control in mice requires extensive surgery [87]. Furthermore, changes in venous circulation may result

in systemic maladaptation of organs and inflammatory responses that may confound the *in vivo* data.

By including venous valves, endothelium, and blood flow together, we observed regional effects of anticoagulant drugs with thrombus formation at the venous valves being more resistant to anticoagulation. This data may be useful in designing future preclinical therapeutic discovery approaches, as it appears that a systemic anticoagulant effect may not reflect an adequate effect at the venous valves. Thus, the transport phenomena of a drug, i.e. its distribution throughout different hemodynamic conditions in the venous circulation, may also be critical in its overall pharmacological effect. However, this modeling platform still has limitations that need to be overcome. Notably, because we still lack the full understanding of DVT, this model, like other models, represents a prediction of the human pathology which will be validated against clinical trials of DVT in future. In this first presentation, we have also balanced simplicity with complexity by not including rigorous analysis of blood immune cells and pericytes, or vein propulsion, that are likely to influence the pathogenesis and progression of DVT. For ease of manufacturing and practical use by us and other users, we created a pseudo-3D architecture of the vein, that is not fully cylindrical. But the final confluent lumen formed within the Vein-Chip has an ellipsoidal shape (Fig. 2C). Also, while a more circular architecture that mimics the human vein can be more advantageous, our experiments did not reveal significant additional thrombosis in corners, and we were able to substantiate several results with animal models or clinical observations, that we refer to throughout the manuscript. Also, all our experiments were conducted along with

relevant controls, and we inferred all our results against the controls that we used. Nevertheless, our platform can be expanded further to perform more specific investigations on 3D geometry of a vein and its relation to thrombosis in future. Our model does not incorporate venous valve pumping action or the oscillatory flow observed *in vivo*. This also limits the model although the static Vein-Chip mimics an immobilized patient predisposed to DVT, and in some cases DVT itself makes the valve dysfunctional. If needed however, the technology to include pumping action exists [107], and may be adapted to include venous pumping motion, when mechanisms driven by contractility needed to be explored with this system. Therefore, our approach provides a linear path to incrementally design and study several multifactorial mechanisms of the disease.

In summary, this human Vein-Chip methodology allowed us to dissect and recapitulate many features of venous thrombosis *in vitro* that have only previously been observed *in vivo*. For example, we observe the endothelium at the venous valve cusps to have an antithrombotic phenotype compared to venous lumen [55, 56, 87, 108]. We also observe stagnation of flow in the venous valves as observed in vivo venograms [68, 109]. A major opportunity of this modeling platform is that it can include iPSC-derived endothelial cells and blood from patients, offering personalized assessment of drug responses, as well as potential toxicities. This patient specificity combined by the opportunity to perform contemporary gene and molecular analyses of samples (for example, RNA-seq), may allow new mechanistic insights and identification of specific

patient groups and targets, for which drugs can be designed with higher precision in future.

3.5. Experimental Section

3.5.1. Blood samples and human subjects

Blood from healthy adult donors was collected upon informed consent in 3.2% sodium citrate tubes (BD Biosciences). All experiments were performed according to the policies of the US Office of Human Research Protections (OHRP) and approved by the Texas A&M University Institutional Review Board (IRB) (ID: IRB2016-0762D). Blood was used within four hours of withdrawal to prevent abnormal platelet functioning[110].

3.5.2. Numerical analysis

We solved the mass and momentum equations for an incompressible fluid flow, using the CFD software package FLUENT (ANSYS v19.2) based on a finite volume scheme. We considered the flow to be two-dimensional, steady, and incompressible. Blood was modelled as a non-Newtonian fluid with constant density of 1070 kg m^{-3} and viscosity following a generalized power law for viscosity [60],

$$\mu = \lambda(\dot{\gamma})|\dot{\gamma}|^{[n(\dot{\gamma})-1]} \quad \text{Equation 1.0}$$

$$\lambda(\dot{\gamma}) = \mu_{\infty} + \Delta\,\mu \cdot e^{\left[-\left(1+\frac{|\dot{\gamma}|}{a}\right)e^{\left(\frac{-b}{|\dot{\gamma}|}\right)}\right]} \quad \text{Equation 1.1}$$

$$n(\dot{\gamma}) = n_{\infty} - \Delta\,n \cdot e^{\left[-\left(1+\frac{|\dot{\gamma}|}{c}\right)e^{\left(\frac{-d}{|\dot{\gamma}|}\right)}\right]} \quad \text{Equation 1.2}$$

where μ is the viscosity, $\dot{\gamma}$ is the shear rate, $\lambda(\dot{\gamma})$ is the consistency index (dependent on the shear rate), and $n(\dot{\gamma})$ is the flow behaviour index (dependent on the shear rate). μ_{∞} and n_{∞} are the viscosity and flow behavior indices for infinite shear rate. a, b, c and d

are constants. The inlet boundary condition for the simulation is a "velocity" corresponding to the desired wall shear stress and the outlet boundary condition is a "pressure" outlet condition set to atmospheric gauge pressure of zero. The velocity of the vortex in the CFD analysis was calculated at different locations near the center of the vortex. This was done as we tracked single particle (RBCs) velocity along the vortex (velocity along the pathline) in the experimental model.

The mass transfer of dissolved fibrinogen in blood occurs in the Vein-Chip due to the convection by bulk fluid motion, and by the diffusion due to the concentration gradients. The mass transfer simulations were performed in a finite element software package COMSOL Multiphysics (v5.2) in 2D. The blood was assumed to contain 70,000 Mol m^{-3} fibrinogen [111]. The diffusivity of fibrinogen in the Vein-chip and the rate of reactivity (consumption) at the walls of the device per unit height while thrombi are formed were assumed to be $2x10^{-7}$ cm^2s^{-1} and 0.0015 Mol $ml^{-1}s^{-1}$, respectively.

3.5.3. Fabrication of Vein-Chip

Masks needed to pattern these designs using photolithography were obtained from CAD-Art services (Bandon, Orlando). The designs were subsequently patterned on Si (100) wafers (University Wafer Corp) at Aggie-Fab nanofabrication facility of Texas A&M University. The microfluidic channels were then prepared using soft lithography of polydimethylsiloxane (PDMS, Dow Corning). Each device had three independent parallel channels with each of them having three 25% open, 50% open or 75% open venous valves. Inlet and outlet holes for the devices were made with a 1.5 mm wide biopsy punch (Ted Pella). PDMS block containing the features was bonded to either a

PDMS coated glass slide (75 x 25 mm) or a block of PDMS or coverslips using a 100 Watt plasma cleaner (Thierry Zepto, Diener Electronic). Devices made on glass slides, PDMS block and coverslip are used for blood perfusion experiment, staining for proteins of interest at cusps and confocal imaging of lumen respectively. An open slip-tip syringe was connected to the devices through a curved dispensing tip (Qosina) which acted as a reservoir. The outlet was connected to a syringe pump (Harvard Apparatus, PHD Ultra) using a 20" tubing (Qosina).

3.5.4. Device functionalization and endothelialization

The Vein-Chips were treated with an oxygen plasma for 30 seconds at a power of 50 Watts and then filled with mixture of type-I rat-tail collagen (100 µg mL^{-1}, Corning) and fibronectin (50 µg mL^{-1}, Biosciences). The devices were incubated for an hour in a 5% CO2 incubator, followed by rinsing with phosphate buffer solution (PBS, Gibco) and endothelial growth media (EGM-2, PromoCell). 30 µL of HUVEC cell suspension (10^7 cells/ml) was seeded into the matrix coated channels and incubated upside down for two hours. HUVECs used were between passages P3 and P8. At the end of two hours a fresh suspension of 30 µL of HUVECs was again perfused through the channels and incubated for additional two hours to promote cell adhesion to all the sides of the device. Overnight perfusion of growth media was then carried out under flow (1 µL min^{-1}) to ensure continuous supply of nutrients to the cells, also leading to cell alignment along the flow direction. For studies that required vascular activation, the endothelialized channels were treated with growth media spiked with TNF-α (recombinant from E. coli, Sigma) to yield a concentration range of 5-100 ng mL^{-1} for 18 hours.

3.5.5. Cell fixation and immunohistochemistry

Vein-Chips were fixed with a 4% paraformaldehyde solution (Sigma) for 15 min and washed with endothelial growth media. The devices were then cut open at the interface of two PDMS blocks. The cut portion with an imprint of cells were permeabilized using 0.1% Triton X (Sigma-Aldrich) in BSA/DPBS for ten minutes at room temperature. To remove the non-specific binding, the channels were blocked using a 2% solution of BSA in DPBS for 30 m at room temperature. Mouse or rabbit antibodies against intercellular adhesion molecule-1 (ICAM-1, Invitrogen), von Willebrand Factor (VWF, Invitrogen) and vascular endothelial-cadherin (VE-cadherin, Invitrogen) were added to the channels and incubated for one hour. Then the channels were washed with 2% solution of BSA in DPBS (also the wash buffer) and perfused with secondary anti-rabbit or anti-mouse fluorescent antibodies (Invitrogen) which were incubated for 45 m at room temperature. This was again perfused with wash buffer and then Rhodamine Phalloidin (Invitrogen) was perfused to tag the cytoskeletal protein F-actin. After incubating this for 20 m, the channels were washed with wash buffer. Finally, Hoechst was perfused in the channel to stain for nuclei. After 10 minutes, devices were perfused with wash buffer before imaging under fluorescence microscope (Zeiss Axio Observer Z1 Inverted Microscope) or confocal microscope (Zeiss Stallion Digital Imaging Workstation at Image Analysis Lab, Veterinary Medicine and Biomedical Sciences at Texas A&M University).

3.5.6. RNA Isolation and Gene Expression

Blunt tip syringes were attached at inlet and outlet of the device and filled with Accutase (Promocell) solution at the inlet. The Accutase solution was perfused via syringe pump at 40 µl/min (high flow) for the first four minutes to collect cells from the lumen and then at 200 µl/min (low flow) for the next four minutes to collect the cells from the valve cusps. RNA was extracted using an ArturusTM PicoPureTM RNA Extraction Kit (Thermo Fisher Scientific), and qPCR was performed as per manufacturer instructions (QuantStudio 12K Flex, Applied Biosystems, Life Technologies). The polymerase chain reaction primer sequences are shown in **Table S2**. All gene expression results were reported as a fold change with respect to the denoted control and the housekeeping gene GAPDH.

3.5.7. Blood perfusion

Devices fabricated on PDMS coated glass slides were used for blood perfusion experiments. 500 µl of blood pre-incubated with FITC conjugated anti-human CD41 antibody (10 µl ml^{-1}, Invitrogen) and fluorescently labelled anti-fibrinogen (15 µl ml^{-1}, Invitrogen), was added to the inlet reservoir. Calcium chloride and magnesium chloride were added to the blood to arrive at a concentration of 10 mM $CaCl_2$ and 7.5 mM $MgCl_2$. Blood was then perfused through the Vein-Chip through a syringe pump at a designated flow rate.

3.5.8. Drugs

During anticoagulant dosage estimation studies, heparin lock flush (0.25 U/ml and 0.5 U/ml), rivaroxaban (Xeralto, 100 ng/ml and 500 ng/ml), apixaban (Eliquis, 100 ng/ml and 500 ng/ml) and tirofiban (Aggrastat, 500 ng/ml) were added to blood before the addition of calcium-containing buffer. Rivaroxaban and apixaban were dissolved in DMSO at 10 mg/ml and 5 mg/ml respectively to solubilize them before their addition to blood.

3.5.9. Image analysis

All the acquired images were exported as .ome.tiff uncompressed files and analysed in fiji imagej software. Each image was cropped to a size 1600 pixels X 800 pixels (width x height). A mask was drawn manually for each channel and corresponding venous valve cusps. Mean fluorescent intensity was calculated after subtracting the background noise. For analysing the cusps, only the cusp regions were selected using the polygon selections tool and the mean intensity was calculated.

3.5.10. Scanning electron microscopy

Trump's fixative (1.16 g of NaH_2PO_4, 0.27 g of NaOH, 10 ml of 40% formaldehyde and 2 ml of 50% glutaraldehyde in 88 ml of DI water) was perfused through the channels for 1 h at room temperature to fix the thrombi and cells. The microfluidic device was then disassembled, and the channels were rinsed with Trump's Buffer (1.16 g of NaH2PO4 and 0.27 g of NaOH in 98.57 ml of DI water). The channels were dehydrated in ethanol/water mixtures (ethanol content - 30%, 50%, 70%, 90%, 100%, 100%, 100%) serially for 30 minutes each. The samples were kept in a fume hood

overnight. The dry dehydrated samples were then sputter coated in gold and subsequently imaged in the scanning electron microscope (TESCA VEGA 3).

3.5.11. Statistical analysis

We employ non-parametric Mann-Whitney tests (two-group) and Kruskal-Wallis test (three or more groups). All data and error bars in the article are represented as mean and standard error of mean (SEM). All statistical analyses were performed using Prism 8.4 (GraphPad Software Inc.).

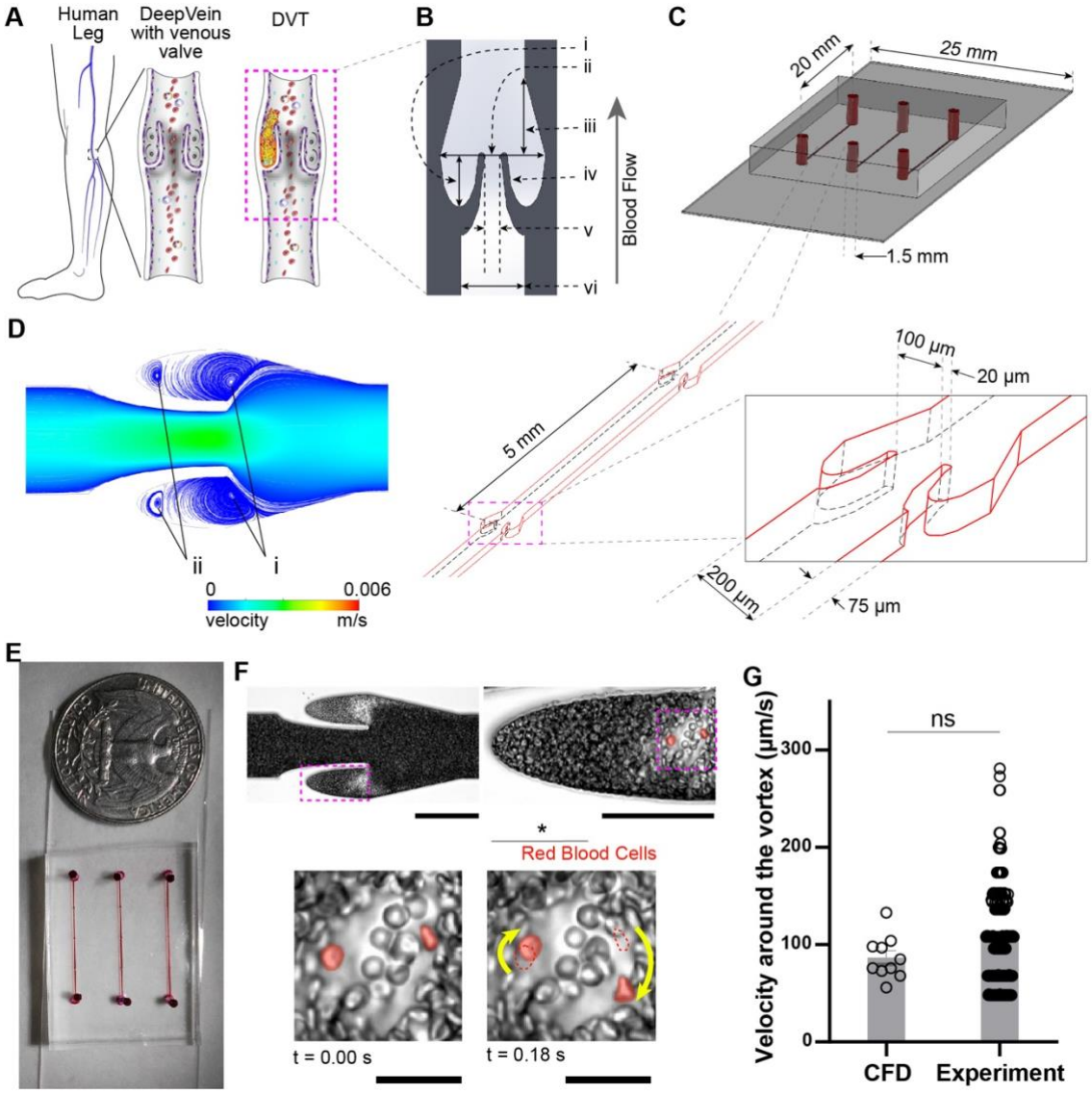

Figure 3-1: Design and analysis of Vein-Chip

(A) Illustration of a normal human vein vs vein with thrombus formation in its cusp. Engineering drawing of (B) a section of the Vein-Chip consisting venous valves with leaflet thickness 20 µm, (i) maximum valve depth (ii) maximum width of venous valve (iii) distance between the venous valve leaf tip and valve reemergence point (vi) valve leaflet, (v) gap width and (vi) channel width; and (C) microchip consisting of three Vein-Chip devices. Each device is 75 µm long and has three serially placed valves. The channel width, gap width and valve leaflet tip are 200 µm, 100 µm, and 20 µm respectively. (D) Contour plot showing velocity streamlines in 2D within a section of the Vein-Chip determined via computational fluid dynamics (CFD) analysis of whole blood. Twin vortices are formed – primary vortex (i) formed near the mouth of the cusp and secondary vortex (ii) formed at the abyss of the cusp. (E) Photograph of Vein-Chips on a

microchip used in experimentation (F) Brightfield microscopic snapshot showing whole blood perfusion (top left) and the formation of vortices within venous valves (top right and bottom). Red blood cells in the blood can be seen to follow a circular path in the primary vortex (red blood cells near vortex marked in red; bottom). Scale bar, 200 µm (top left), and 50 µm (top right and bottom). (G) Graph comparing velocity at the primary vortex measured with CFD vs the experiments. Student t-test.

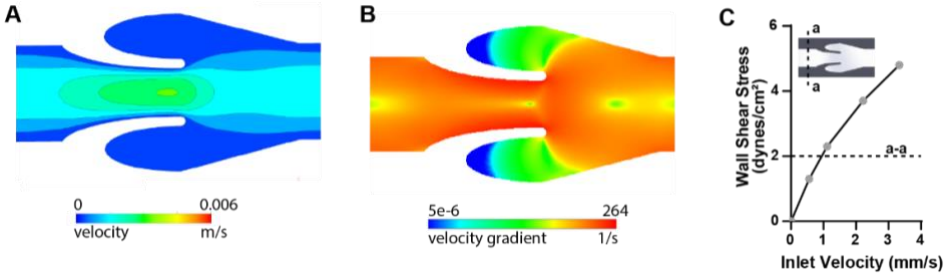

Figure 3-2: Computational fluid dynamics (CFD) analysis of whole blood flow in Vein-Chip.
Contour plots describing (A) velocity profile within a section of the Vein-Chip, revealing maximum velocity occurs at the gap width between the venous valve leaflets; (B) corresponding velocity gradients which are high in cusps. (C) Graph showing the relation between inlet flow velocity and wall shear stress in the venous lumen walls of Vein-Chip. Human veins are exposed to approximately 2 dynes/cm2 corresponding to an approximate flow rate of 1 µl/min (dotted line a-a).

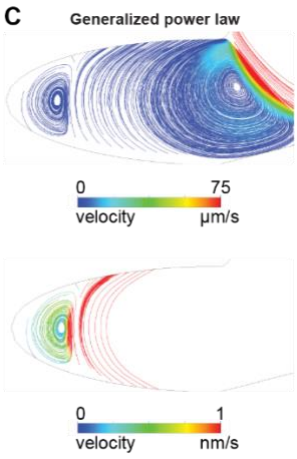

Figure 3-3: Vortex velocities
Velocity streamlines showing primary vortex and secondary vortex, at high magnifications, formed when generalized power law is used.

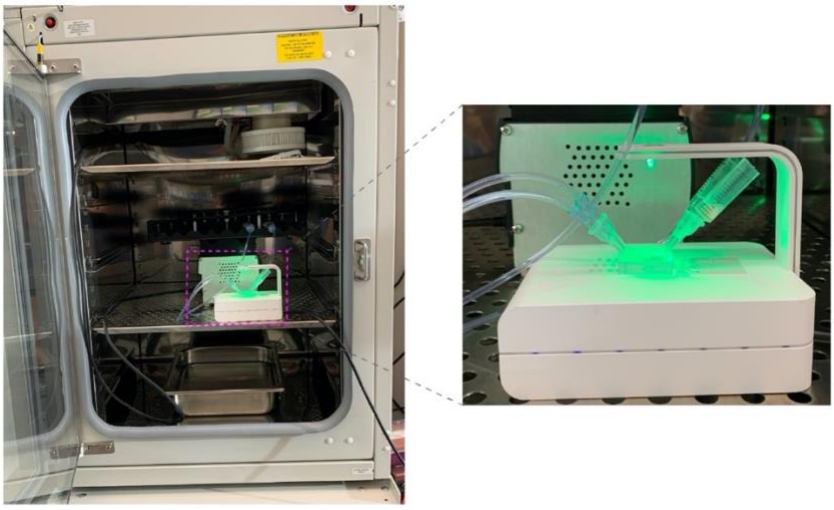

Figure 3-4: Vein-Chip under tissue culture.
A Vein-Chip within an incubator (left) mounted on a Cytosmart microscope for live-cell imaging (right).

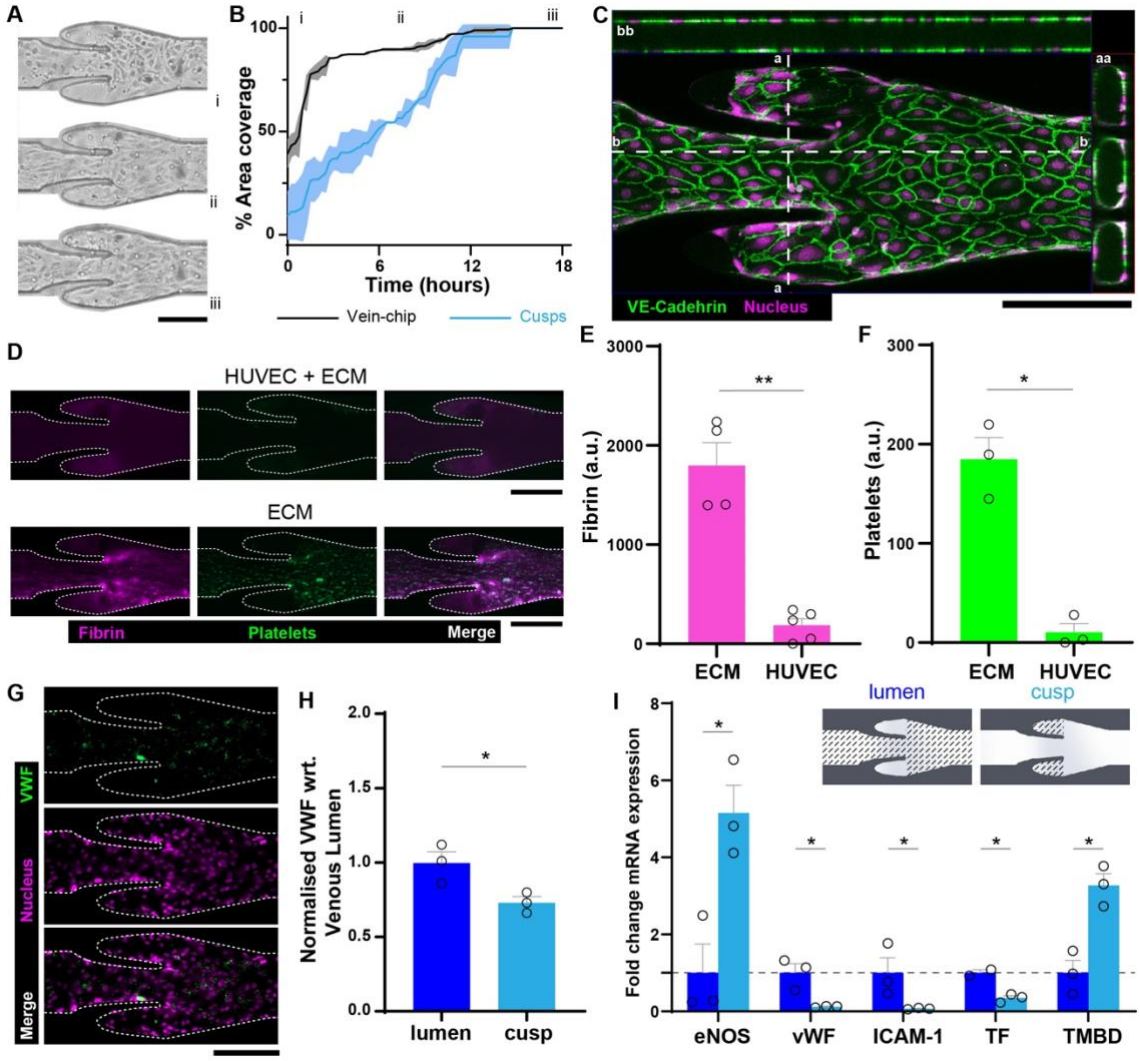

Figure 3-5: Endothelium lining and analysis of Vein-Chip
The dynamics of endothelial growth and lumen formation within Vein-Chip at (i) beginning of media perfusion after one hour of cell seeding, (ii) cells entering venous valve cusps and (iii) confluence at venous valves and non-valve regions; shown via (A) brightfield microscopy, and subsequent (B) quantification of area coverage comparing lumen vs cusp region. (C) Confocal microscopy of an endothelialized Vein-Chip showing 2D cross-sections of the 3D image. VE-cadherin (green), and nucleus (Hoechst, magenta). Fluorescence micrographs of Vein-Chips after perfusion of blood labelled with fibrin (magenta, left), platelets (green, center) and merged (right), when (D) the device was lined with endothelium over the ECM (top), and ECM alone (bottom). Graphs describing (E) fibrin, and (F) platelet adhesion within Vein-Chips lined with endothelium (HUVEC) or ECM. (G) Fluorescence micrographs showing immunostaining of von Willebrand Factor (VWF, green, top), nucleus (magenta, center), and merged (bottom) expressed by the endothelial cells within Vein-Chip. (H) VWF

expression in sections of the Vein-Chip normalized to the expression of VWF in the lumen. (I) Fold change in gene expression of anticoagulant and procoagulant proteins at the venous valve cusps compared to the venous lumen. Each data point corresponds to an independent experiment. Scale bars, 200 µm. Mann-Whitney test; *, p<0.05; **, p<0.01.

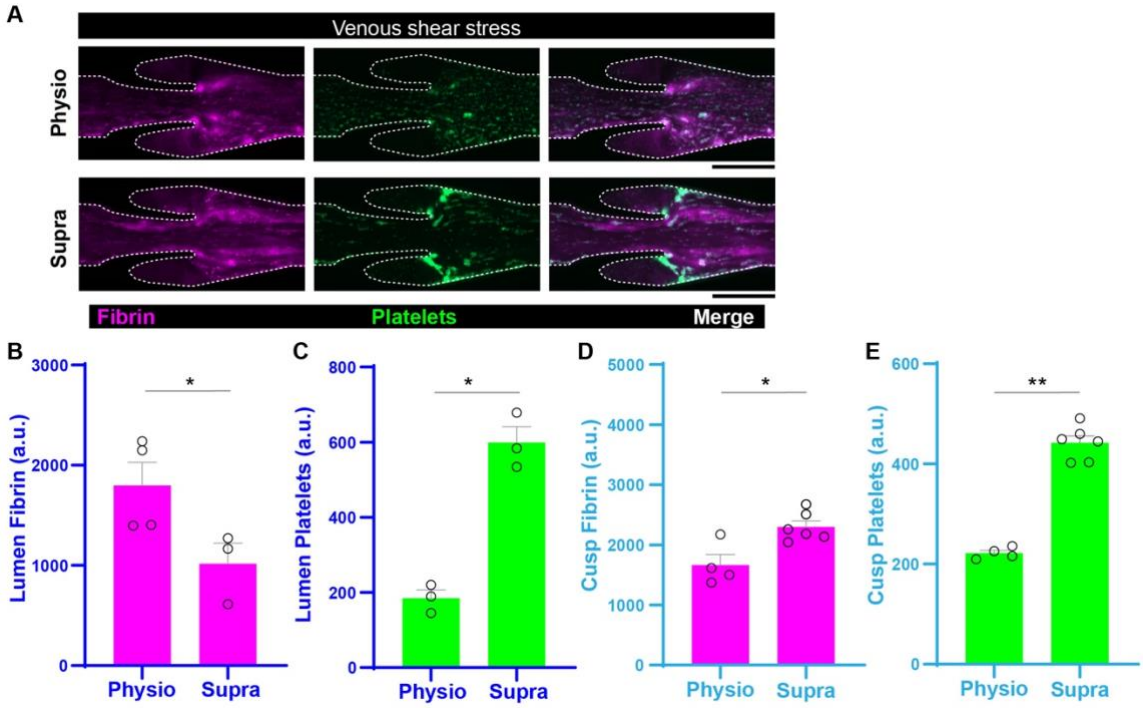

Figure 3-6: Dissecting Virchow's triad with Vein-Chip – flow and stasis. Fluorescence micrographs showing fibrin (magenta, left), platelets (green, center) and merge (right) in a section of a Vein-Chip lined with ECM, which was perfused with whole blood at (A) physiological shear (top), and pathological shear (~17.5 dynes/cm^2, bottom). Scale bar, 200 µm. Graphs showing assessment of (B) fibrin coverage in the venous lumen, (C) platelet adhesion in the venous lumen, (D) fibrin coverage in the cusp, and (E) platelet adhesion within the cusp, when the Vein-Chip was perfused with blood at physiological or pathological shear. Each data point corresponds to an independent experiment. Mann-Whitney test; *, p<0.05, **, p<0.01.

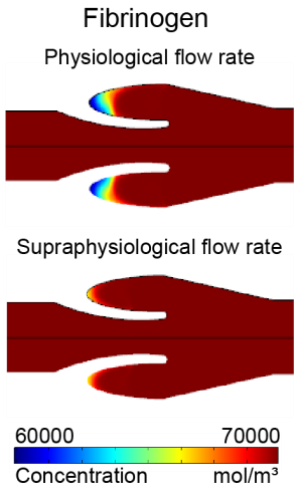

Figure 3-7: Transport of fibrinogen into vein cusps.
Contour plot showing computationally analyzed fibrinogen distribution in a section of a Vein-Chip perfused with blood at normal shear (top) or supraphysiological shear (bottom).

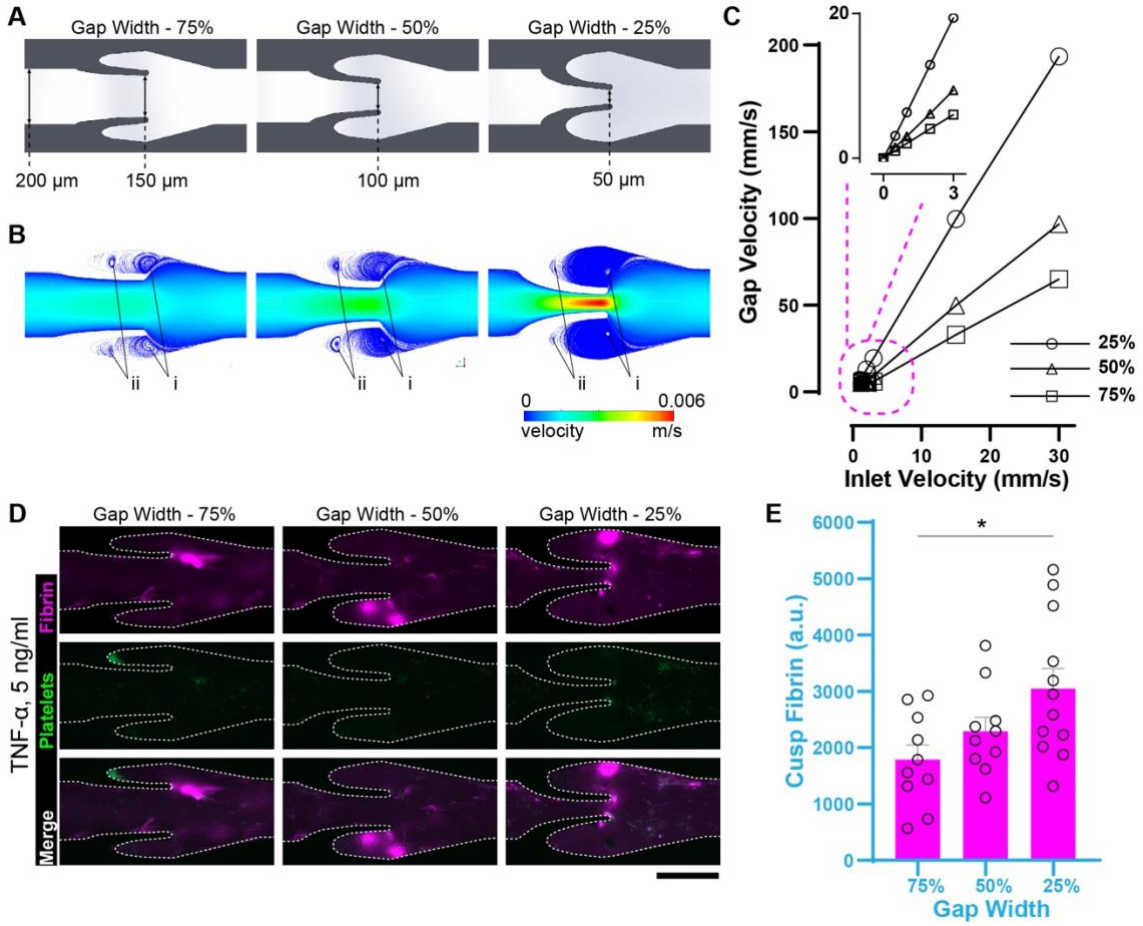

Figure 3-8: Dissecting role of venous cusp anatomy with Vein-Chip.
(A) Engineering drawing of sections of Vein-Chips consisting variable gap width of 75% (left), 50% (center), and 25% (right). (B) Contour maps showing velocity streamlines calculated from computational fluid dynamics (CFD) analysis of whole blood flow through the three configurations of Vein-Chips. (C). Graph comparing the relationship of gap velocity vs inlet velocity within different configurations of the Vein-Chips. (D) Fluorescence micrographs showing fibrin (magenta, top), platelets (green, center) and merge (bottom) in a section of an endothelialized Vein-Chip, which was perfused with whole blood within different configurations of the cusp anatomy. Scale bars, 200 µm. (E) Graph comparing fibrin at the venous cusps of different configurations. Each data point corresponds to an independent experiment. Kruskal-Wallis test; *, $p<0.05$.

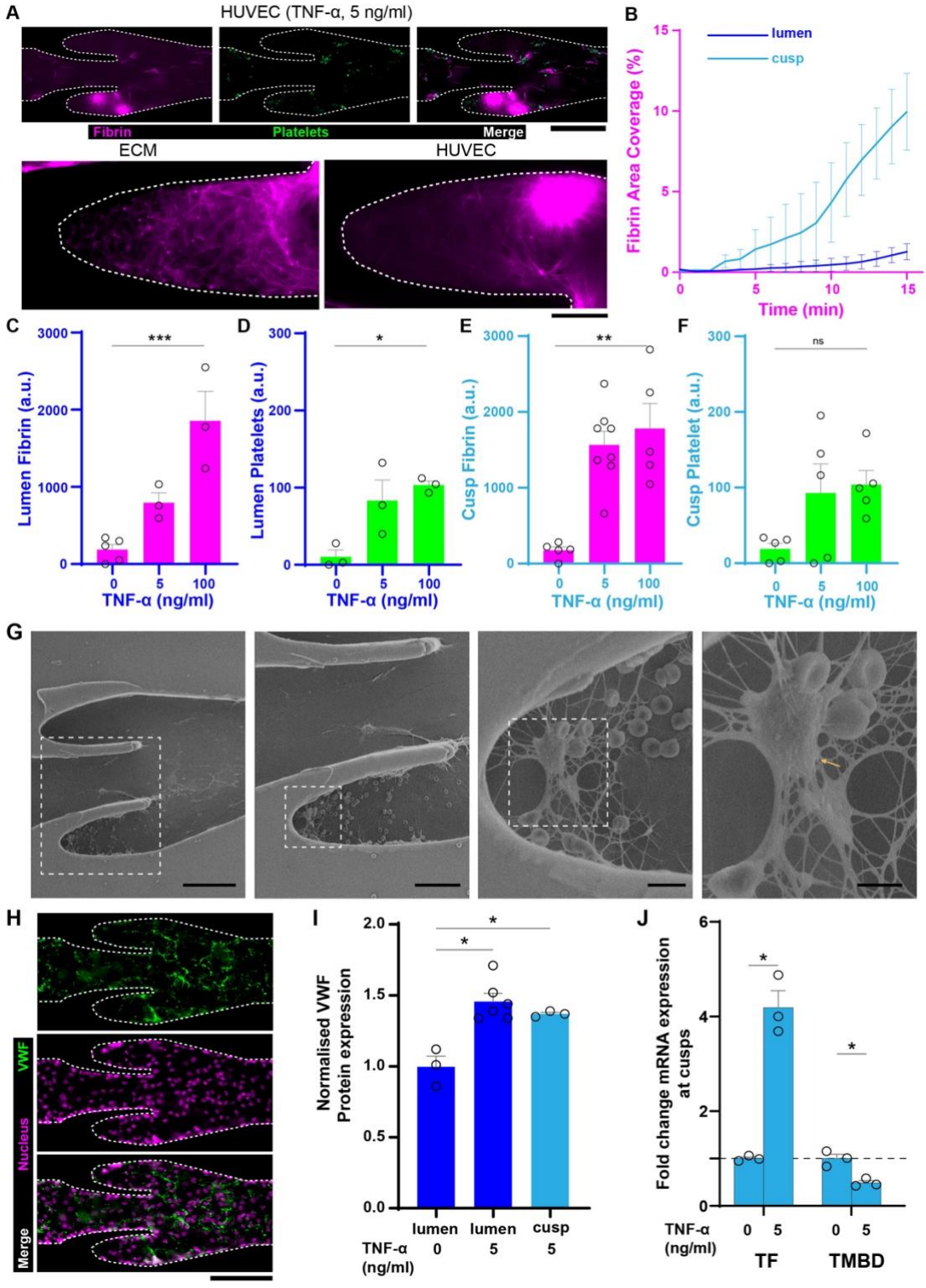

Figure 3-9: Dissecting Virchow's triad with Vein-Chip: endothelium.

After perfusion of blood within Vein-Chips lined with endothelium and treated with cytokine, TNF-α, fluorescence micrographs showing, (A) fibrin (magenta, top left), platelets (green, top center), merge (top right) in a venous section; and comparison of thrombi morphology on exposed ECM alone (bottom left) vs TNF-α treated endothelium (bottom right) in a venous cusp. Scale bar, 200 μm. (B) Fibrin area coverage over time in the lumen vs cusp region of the Vein-Chip. Graphs showing assessment of (C) fibrin coverage in the venous lumen, (D) platelet adhesion in the venous lumen, (E) fibrin coverage in the cusp, and (F) platelet adhesion within the cusp, when the Vein-Chip endothelium was treated with TNF-α at various doses. (G) Scanning electron micrographs of various sections (increasing magnification from left to right) of the Vein-Chips after thrombi have formed. Thrombi are rich in fibrin and red blood cells, devoid of platelets and contain leukocytes (marked). Scale bars from left to right, 100 μm, 50 μm, 10 μm and 5 μm. (H) VWF expression analysis between the lumen and the cusp of the Vein-Chip upon TNF-α treatment of the endothelium. (I) Immunofluorescent staining of VWF (green) when endothelium is treated with TNF-α. cell nuclei (magenta). (J) Fold change in gene expression of tissue factor (TF) and thrombomodulin (TMBD) at the venous valve cusps of TNF-α treated and non-treated cusps. Each data point corresponds to an independent experiment. Kruskal-Wallis test (C-F) and Mann-Whitney test (I); *, $p<0.05$, **, $p<0.01$, ***, $p<0.001$.

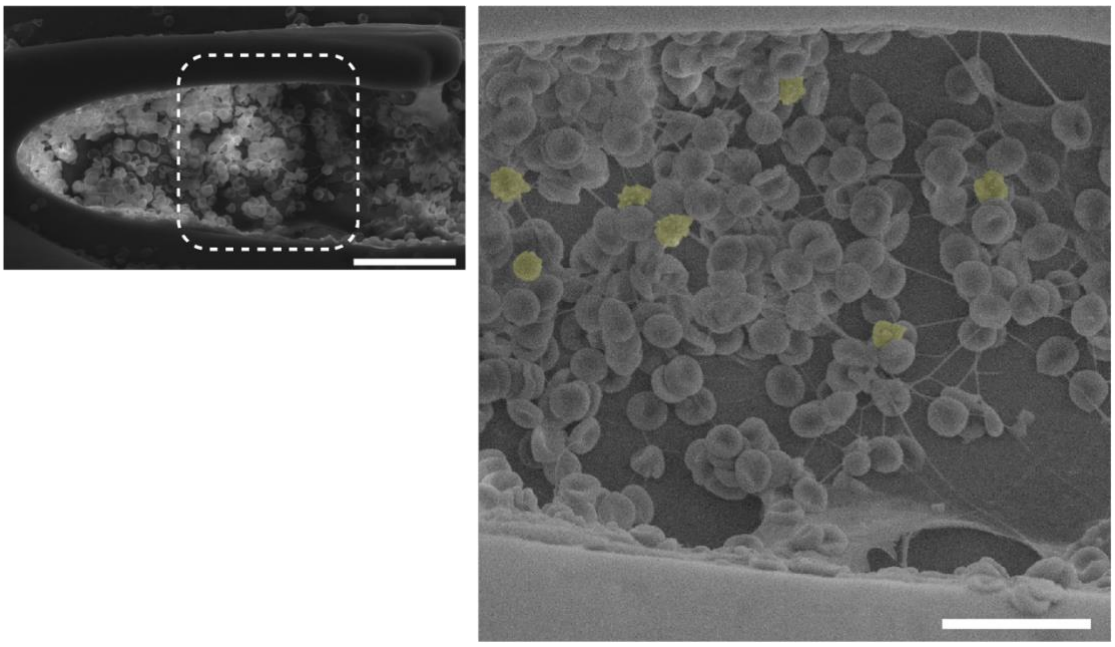

Figure 3-10: Scanning electron micrograph of a thrombus formed at the venous valve cusp of the Vein-Chip.
Image of a typical thrombus shows that it is rich in erythrocytes (red blood cells) and leukocytes (yellow). Scale bar, left,100 μm; right, 25 μm.

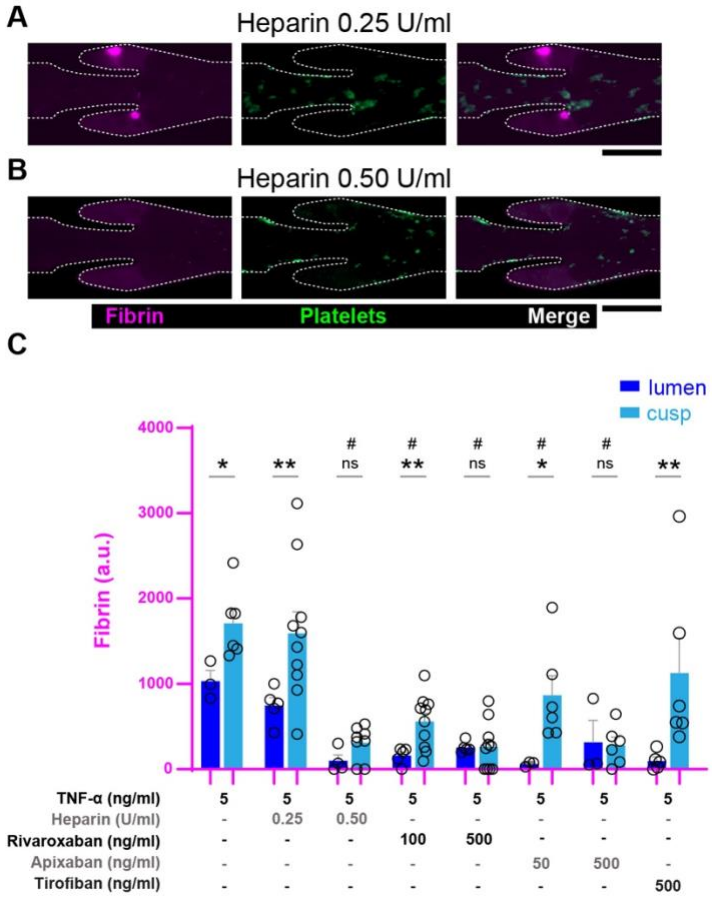

Figure 3-11: Dissecting Virchow's triad with Vein-Chip: blood.
Fluorescence micrographs showing fibrin (magenta, left), platelets (green, center) and merge (right) in a section of a Vein-Chip treated with TNF-α, which was perfused with whole blood containing heparin at a dosage of (**A**) 0.25 IU/mL, and (**B**) 0.5 IU/mL). (**C**) Graph showing fibrin formation within Vein-Chip lumen and cusps, when endothelium was treated with TNF-α and whole blood was perfused after addition of anticoagulants, heparin, apixaban, rivaroxaban and tirofiban. Each data point corresponds to an independent experiment. Mann-Whitney test; *, $p<0.05$, **, $p<0.01$, lumen vs cusps; #, $p < 0.05$, untreated vs treated cusps.

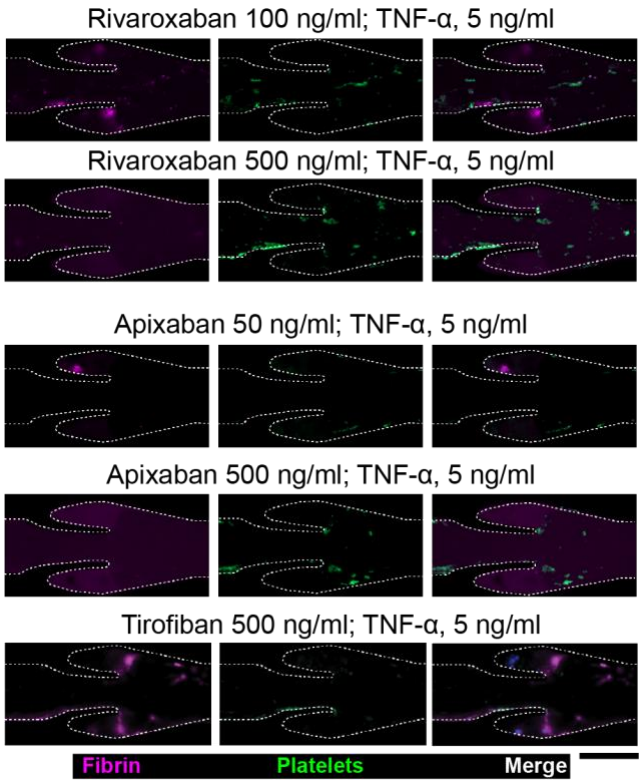

Figure 3-12: Analysis of anticoagulation in Vein-Chip.
Fluorescence micrographs showing the variations in fibrin (magenta) deposition and platelet (green) adhesion in Vein-Chips treated with different dosages of rivaroxaban (100 and 500 ng/ml, top), apixaban (100 and 500 ng/ml, bottom) and tirofiban (500 ng/ml). Scale bar, 200 μm.

Table 3-1: Wall shear rates and stresses at vein lumen, valve entrance, and valve cusps for different configurations.

Venous Valve Configuration	Wall Shear Rate (s^{-1})			Wall Shear Stress (dynes/cm^2)		
	Vein Lumen	Valve Entrance	Cusp	Vein Lumen	Valve Entrance	Cusp
75% Gap Width	35.17	121.10	8.25E-09	2.26	5.76	3.21E-05
50% Gap Width	35.17	257.24	1.20E-05	2.26	10.31	4.07E-04
25% Gap Width	35.17	777.04	8.57E-03	2.26	29.01	1.09E-04
50% Gap Width, Supraphysiological	497.20	3097.14	2.53E-04	17.62	86.67	2.17E-04

Table 3-2: List of PCR primer sequences used in mRNA expression analysis.

	Protein		Forward primer	Reverse primer
1	von Willebrand factor	VWF	5′-GCAGTGGA--GAACAGTGGTG-3′	5′-GTGGCAG--CGGGCAAAC-3′
2	Inter Cellular Adhesion Molecules-1	ICAM-1	5'-TATGGCAA--CGACTCCTTCT-3'	5'-CATTCAGC--GTCACCTTGG-3'
3	Tissue factor	TF	5'-CAGACAGC--CCGGTAGAGTGT-3'	5'-CCACAGCT--CCAATGATGTAGAA-3'
4	Endothelial nitric oxide synthase	eNOS	5′-GTGGCTGTC--TGCATGGACCT-3′	5′-CCACGATG--GTGACTTTGGCT-3′
5	Thrombomodulin	TMBD	5’-AAGAAGTGTCTG-GGCTGGGACGGACAGGAG -3’	5’- AGCAGTCGTGCTC--GACGCACTGGCTG CCAC -3’
6	glutaraldehyde 3-phosphate dehydrogenase	GAPDH	5′-CAAGGTCATC--CATGACAACTTTG-3′	5′-GGGCCAT--CCACAGTCTTCTG-3′

4. TOWARDS AN ACTUATING VENOUS VALVE IN VITRO MODEL

4.1. Abstract

Deep vein thrombosis (DVT) followed by pulmonary embolism (PE), together known as the venous thromboembolism (VTE) is the third leading cause of cardiovascular deaths in the world. This is mainly due to lack of understanding of the working of the venous valves in the veins, which are the primary locations for DVT formation. Current in vivo (especially murine models) and in vitro models are not able to reconstitute the exact human physiology of the human venous valves. We present an in vitro model of a large vein that consists of a polydimethylsiloxane (PDMS) casing and a 3D printed venous valve made of polyacrylamide hydrogel. We first design and develop the model of the venous valve structure that is 3D printable and functions similar to an in vivo venous valve. Next, we develop a strategy to fabricate the model where the 3D printed hydrogel is attached to the PDMS casing containing the channel that corresponds to the vein. Finally, we show the actuation of the developed venous valve model under different fluid dynamic forces. This new vein model offers a new preclinical platform to study venous physiology and pathophysiology that may help develop new therapeutic strategies to prevent DVT formation.

4.2. Introduction

Deep vein thrombosis (DVT) is the formation of unwanted clots at the venous valves of the deep veins [112]. DVT followed by pulmonary embolism, together known as venous thromboembolism (VTE) is a huge clinical burden [113]. About 1-2 persons

per 1000 people experience VTE annually [114]. Though venous valves are known to be the primary sites of DVT formation, DVT remains a serious clinical burden as our understanding of the functioning of the venous valves, and DVT formation is heavily dependent on animal models and invitro models that are not physiologically relevant to human physiology. Specifically, the murine models used to study the formation and growth of DVT do not contain venous valves [14, 77, 115, 116]. Also, most of the current in vitro models used to study venous valves or DVT do not contain either or both of endothelium and flexible venous valves [66, 83, 84, 117]. All aforementioned in vitro models and mouse models containing venous valves are of micron scale [87], whereas the human deep veins where DVT forms have diameter of the order of millimeters [118, 119].

Here, we introduce an in vitro model of a deep vein containing venous valve that contains a flexible venous valve that has an anatomical scale similar to human deep veins. We first design and develop a hydrogel construct that is 3D printable and able to actuate when the fluid flow direction is changed. Next, we integrate this 3D printed soft hydrogel into a channel made of polydimethylsiloxane (PDMS) that replicates the non-valve vein lumen. Finally, water is perfused in this deep vein model to visualize and characterize the dynamic actuation of the hydrogel venous valves.

4.3. Results

4.3.1. Design of an actuating venous valve

We begin by recreating the anatomy of a venous valve such that the designed valves have geometric similarity with the in vivo human venous valves as described in

our previous work [66]. The designed valve was given a leaflet thickness of 200 μm, which was limited by the size of the extrusion 3D printer nozzle diameter (160 μm) and polyacrylamide hydrogel used in this work (Figure 4-1A). We selected a square channel of height and width 2.4 mm that had a valve seating section, which could accommodate the designed venous valves. We then optimized the hydrogel composition to obtain an optimal combination of print fidelity, swelling ratio (under water/media), structural stability, and stiffness to deform under the applied hydrodynamic forces. We solved a fluid structure interaction (FSI) (ansys 2020, R1) problem to analyze the deformation of the valves under different flow conditions. FSI had a fluid domain and a structural domain (Figure 4-1B). Fluid domain included the straight vein region, venous valve opening (gap width) and venous valve cusps. The structural domain included the vein walls, venous valve walls and venous valve leaflets.

We first simulated the back flow condition that would result in the closing of the venous valves (Figure 4-1C). We then transferred the resulting pressure from the fluid solutions to the surfaces of the structural domain to solve for its deformation. We found that a backward flow of 50 μl/s was needed to close the venous valve structure when the hydrogel stiffness was 200 kPa (Figure 4-1D). 50 μl/s inlet velocity created a wall shear stress 2 Dynes/cm^2, which is typical wall shear stress found in deep veins containing venous valves that are prone to DVT formation. Intuitively the reversal of flow direction would result in the widening and opening up of the venous valves (not shown). The FSI simulations gave us confidence in the development of a hydrogel based venous valve that could actuate under hydrodynamic forces.

4.3.2. Fabrication of the vein containing actuating venous valves

Once we finalized the venous valve and the channel geometries, the next step was to 3D print the venous valve with polyacrylamide gel and integrate it to the PDMS vein channel. The valve geometries were first 3D printed, cured and stored in DI water (at least 10 minutes, Figure 4-2A). Storage of the polyacrylamide in DI water helps the washing off of the uncured polyacrylamide as well as the swelling of the venous valve to its final dimensions. In this work we have used a polyacrylamide gel formulation (see methods) that has less than 5% change in final volume after swelling. PDMS blocks containing the vein channels were fabricated from aluminum molds by soft lithography technique [120]. The PDMS channel walls were then embedded with a photo initiator (benzophenone) and coated with a polyacrylamide layer (Figure 4-2B). The printed valves in the DI water were removed, dried and applied with a layer of uncured polyacrylamide gel. This valve is then placed on the PDMS channel and cured under UV light to create a bond between the PDMS channel and the polyacrylamide venous valve (Figure 4-2C). Next, we created the closed vein channel by attaching a PDMS coated glass slide to the PDMS block containing the channel and the hydrogel valve (Figure 4-2D). Finally, we add another photo initiator in liquid form, incubate it and UV cure the whole vein model to form a non-leaky bond between the hydrogel and the bottom PDMS coated glass slide (Figure 4-2E). Thus, we were able to fabricate a vein model with valve region made of hydrophilic polyacrylamide hydrogel and a vein region that was made of hydrophobic PDMS (Figure 4-2F). Inherently this system is an example of an invitro model with localized variation in mechanical properties such as stiffness. Also, we

showed the ability to fabricate a large vein model that had similar length scales as that or in vivo veins.

4.3.3. Actuation of the fabricated venous valve

Once we fabricated the vein model (Figure 4-3A), we next actuated the venous valves in the with different flow rates. After the fabrication process the 3D printed venous valves were made to reach their equilibrium shape after prolonged (~12 hours) swelling in DI water (Figure 4-3B). We then perfused DI water at 10 ml/min in the forward direction, which showed the opening up of the venous valves (Figure 4-3C). Next, we perfused a volume of 150 μl of DI water at 10 ml/min in the backward direction, which closed the venous valve opening (Figure 4-3D). This simple perfusion experiment showed the stability of the fabricated vein model and its ability to recapitulate the opening and closing action of in vivo venous valves.

4.4. Discussion

We have shown the design and fabrication of an in vitro model of a vein with venous valves that can actuate. The dimensions of this model are comparable to in vivo human deep veins. We showed with this model that the soft hydrogel venous valves open and close when the flow directions are reversed.

As any other model system this system can also be improved and used to understand human physiology better. We can use this model to study the flow dynamics of blood under physiological and pathophysiological states, which the current venous valve models cannot provide. Increase in the recruitment of platelets and leukocytes at

the valve cites during actuation and non-actuation needs to be studied further using such systems.

Also, as the model is of physiological scale, one can endothelialize the model to study the effects of actuation related strain and oscillatory flow on the remodeling of the valve endothelium to stay healthy. This system can be used to understand if the mechanical stretching of the valve endothelium while actuation combined with the complex fluid flow at the venous valves would help valve endothelium to have an increased anti-thrombotic phenotype. Also, does actuation increase the inflammation of an already inflamed endothelium at the venous valve cusps needs to studied using this system.

Overall, this new vein model offers a new preclinical platform to study valve endothelial physiology and pathophysiology that may help develop new therapeutic strategies to prevent DVT formation.

4.5. Methods

4.5.1. Fluid Structure interaction modelling of venous valves

We solved the mass and momentum equations for an incompressible fluid flow, using the CFD software package Fluent (Ansys v20R1) based on a finite volume scheme. The fluid domain was extracted from the solid model used to fabricate the vein model in ansys spaceclaim modeling software. The fluid domain is three-dimensional, and the fluid is assumed to be incompressible, and the flow to be steady. The fluid properties were taken to be that of water, which is a Newtonian fluid. The inlet boundary condition for the simulation was a “velocity” boundary condition and the outlet

boundary condition was a “pressure” outlet condition set to atmospheric gauge pressure of zero. The walls of the fluid domain were grouped as “named selection” to transfer the pressure acting on them as structural pressure load into the structural simulation.

The structural deformation of the venous valves is studied using the finite element analysis software package Ansys Static Structural (Ansys v20R1). The valve region is given the mechanical properties of the polyacrylamide hydrogel (Young’s modulus – 200 kPa). The vein region is given the mechanical properties of PDMS (Young’s modulus – 3 mPa) [121]. The models modelled in SolidWorks 2020 (v28) was exported to Ansys Spaceclaim (from which the model was imported to Ansys Static Structural). We apply the pressure loads transferred from the fluid simulation to the inner walls of the channels and venous valve. The model is constrained with a fixed boundary condition at all outer walls of the model.

4.5.2. Fabrication of the vein model

Channels with sections to include 3D printed venous valves were casted on to PDMS (Dow Corning Sylgard 184) from aluminum molds. The casted PDMS channels were treated with 10% w/v benzophenone (milliporesigma) in acetone for 10 min. Excess photo initiator is removed from the PDMS channels and the channels are washed with acetone and dried with nitrogen. Next, we added an aqueous solution of acrylamide (8.0 % w/v, MBAA) and N,N’-Methylenebisacylamide (0.2 % w/v, MBAA), into the channel and incubated for five minutes before UV treating it for five minutes in a UV oven (name of oven). The excess uncured aqueous solution was pipetting out. The venous valves are then printed with Hyrell 3D printer with a hydrogel configuration of -

Acrylamide (10% w/v), N,N'-Methylenebisacylamide (0.6% w/v), Lap photo-initiator (lithium phenyl-2,4,6-trimethylbenzoylphosphinate, 0.2% w/v,), and Cellulose nanocrystals (22%w/v,). The printed valves are then washed/soaked DI water for at least 10 minutes. The valves were stores in the same DI water if they were being used on a later time. Before using the valves, they were taken out of the water and their surfaces were dried with kim wipes. Also, excess water trapped at the valve cusps were removed with the help of kim wipes. A polyacrylamide 'glue' was applied on the walls of the 3D printed venous valves as well as the PDMS channel walls before seating the venous valves at the appropriate location in the PDMS channels. Polyacrylamide 'glue' configuration - Acrylamide (10% w/v), N,N'-Methylenebisacylamide (0.6% w/v), Lap photo-initiator (lithium phenyl-2,4,6-trimethylbenzoylphosphinate, 0.2% w/v) and Cellulose nanocrystals (10%w/v). The venous valves placed in the PDMS channels are incubated in their location for five minutes. A glass slide is placed on top of the assembly and UV (365 nm) cured for 20 minutes in the UV oven under nitrogen atmosphere. Meanwhile, a glass slide coated with PDMS is plasma (13 minutes exposure, Thierry Zepto, Diener Plasma) treated. The polyacrylamide glue was applied to the fourth wall of the 3D print not attached to the PDMS walls. Next, the PDMS channel block containing the venous valves were bonded to the plasma treated glass slides containing PDMS (bonding time one hour with a weight if 1.5 kg). 400 ul of 2-hydroxy-2-methylpropiophenone (Thomas scientific) was added to the channels and incubated overnight (~12 hours). The photo initiator was removed, and nitrogen was blown through the channels gently with our affecting the venous valves. The device was

exposed to UV for three minutes and DI water was perfused through the channels. Sterile DI water was added and waited till further use.

4.5.3. Imaging of the vein

Devices were imaged using a (SteREO Discovery v 8, Carl Zeiss) microscope after fabrication. Images were processed and analyzed in ImageJ (NIH) and zen blue (Carl Zeiss) to quantify the opening and closing of the venous valves.

4.5.4. Actuation of the venous valves

A 60 ml syringe loaded on a syringe pump (Harvard Apparatus, PHD Ultra) was used to pump fluid into the vein devices. 2 mm outer diameter tubing (Qosina) with inner diameter 1 mm was used to connect the syringe to the vein model.

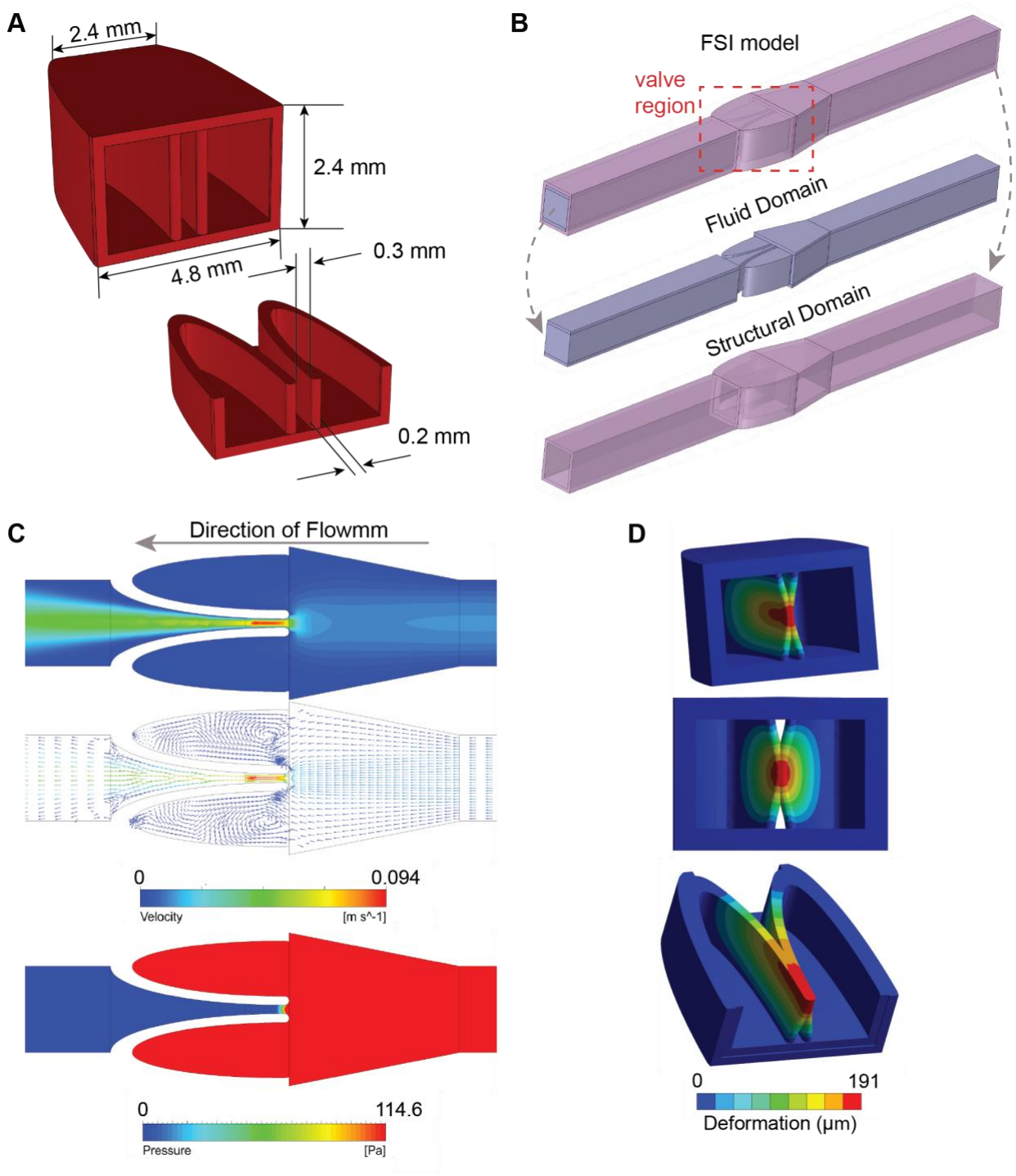

Figure 4-1: Design of an actuating venous valve
(A) Design of the venous valve to be 3D printed with polyacrylamide hydrogel. **(B)** Set up for the fluid structure interaction (FSI) problem with the fluid domain and the structural domain. **(C)** Plot of the velocity contour (top), plot of velocity vectors

(middle), and plot of pressure contour in the vein model when flow is in the backward direction. **(D)** Contour plot of the deformation of the venous valve deformation under the pressure load transferred from the fluid flow simulation

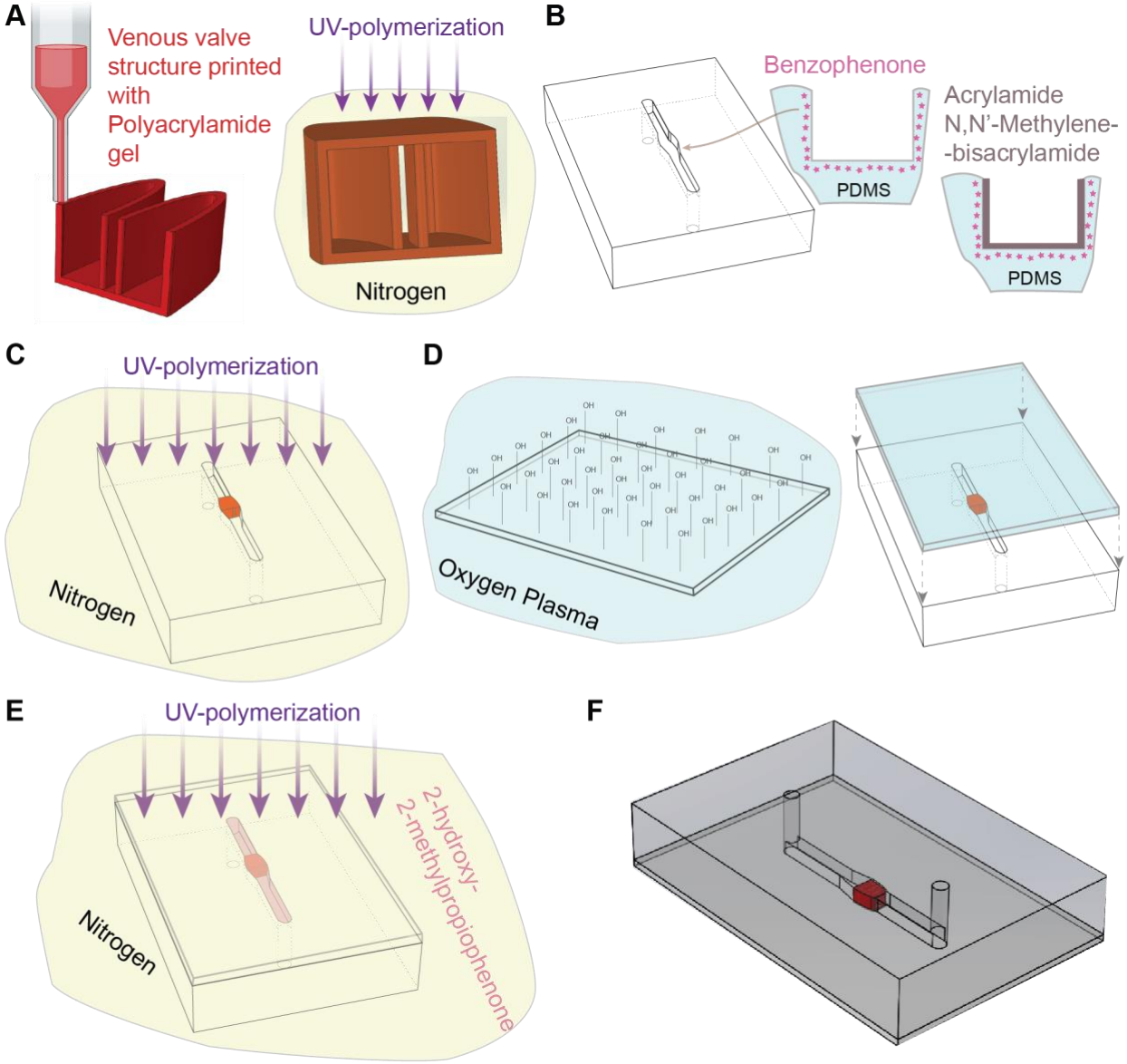

Figure 4-2: Fabrication of the vein model
(A) Extrusion 3D printing of the venous valve with polyacrylamide hydrogel. After curing the print under UV light, it is stored in DI water for long term storage. **(B)** Channels containing PDMS blocks casted from aluminum molds were surface treated with benzophenone and then coated with aqueous polyacrylamide. **(C)** The 3D printed valves were dried and its walls were applied with uncured polyacrylamide gel was placed on the channel and cured under UV. **(D)** Glass slides coated with PDMS is

plasma treated and bonded with the channels containing the venous valves to form a closed channel. **(E)** The closed channel is filled with a photo initiator (2-hydroxy-2-methylpropiophenone) and UV treated to bond the polyacrylamide hydrogel with the PDMS coated glass slide. (F) An illustration of a fabricated vein model.

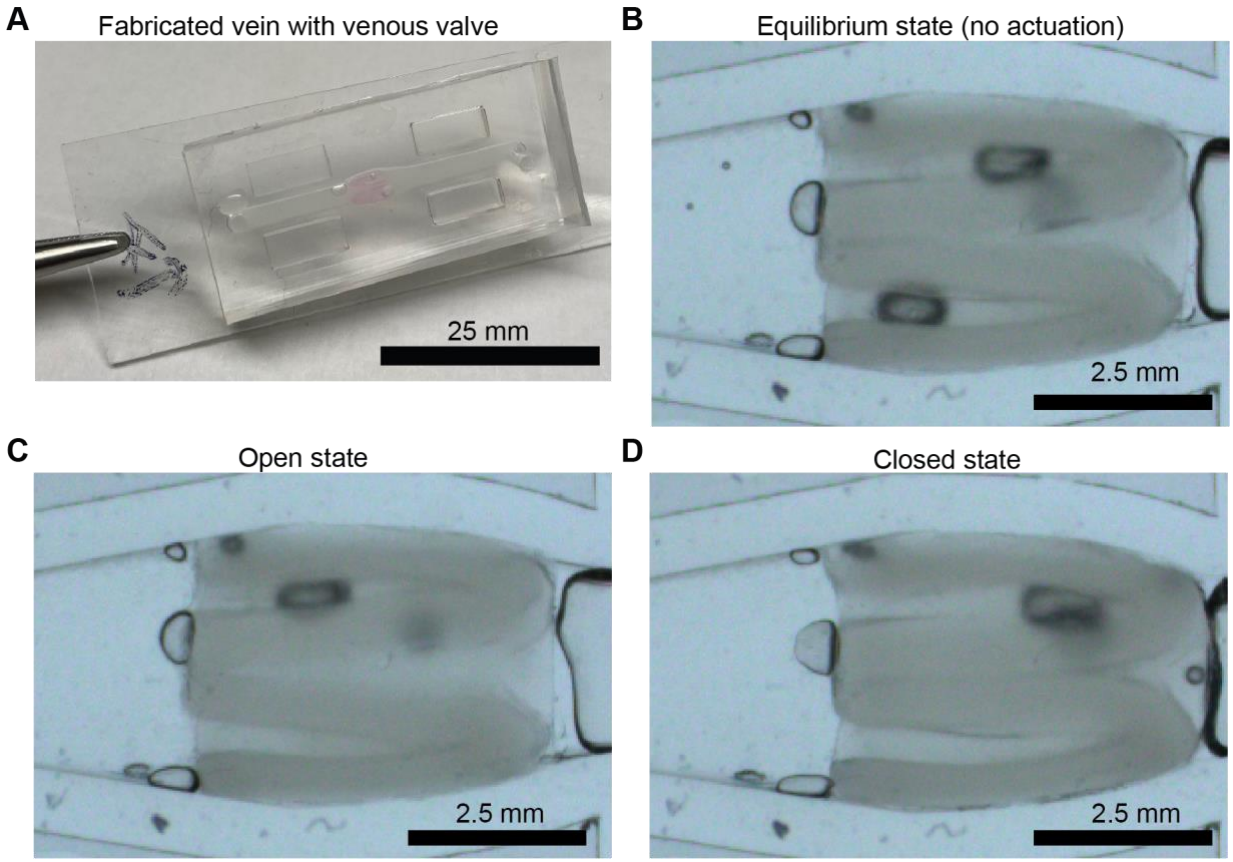

Figure 4-3: Actuation of the fabricated venous valve
(A) A fabricated vein device with a venous valve. **(B)** Equilibrium shape of the fabricated venous valve. **(C)** Fabricated venous valve in open position when fluid flow is in forward direction. **(D)** Fabricated venous valve in closed position when fluid flow is in backward direction.

5. FUTURE PERSPECTIVES

In this thesis we have introduced the first in vitro model of a vein that contains venous valves and living endothelial cells. We have successfully demonstrated the development of microfluidic and milli-fluidic models that were able to recapitulate the physiological and pathophysiological states of a human vein. The models showed that venous valve endothelium adapted to the complex flow patterns in the venous valve and had a distinct phenotype compared to vein endothelium. The models were also able to dissect the individual factors of Virchow's triad and show how variation in individual factors and combinations of factors would affect the DVT formation at the valve cusps.

But the models presented in this thesis have many limitations and shortcoming like any other *in vitro* model used to study human physiology or pathophysiology. Some of these shortcomings can be overcome in the future studies by introducing complexities into the model. Some of the factors that can be included in near future are discussed below.

5.1. Fluid flow

In order to simulate the pathological blood flow in an incompetent venous valve we have used steady flow of media and blood in the models described this thesis [122]. But this may not be true even with an incompetent valve where the valves get stiffer and ceases to actuate [123, 124]. Though the valves get incompetent, the tissue and muscles surrounding the veins may still be competent [125]. These tissues and muscles will actuate to impart blood an oscillatory flow while flowing into the venous valves. Thus,

we can perfuse blood with an oscillatory pattern in the current Vein-Chip models. These oscillatory flows will have implications on the phenotype of the valve endothelium, which will be different from the valve endothelium only exposed to steady vortex flow. Also, flow profiles derived from patients using venous compression devices can be input to the Vein-Chip to study the differences between the normal and compression device driven blood flow at the venous valves [44, 126].

5.2. Endothelial cells

All models described in this thesis have used the primary cells from human umbilical veins known as human umbilical vein endothelial cells (HUVECs). HUVECs are widely used in organ on chip technology [7, 31] as they are readily available commercially and are pooled from different donors. While cells pooled from different donors have the advantage of not having donor variability, they affect the fundamental concept of having organ on chip technology, which is to develop patient specific read outs. We can use patient specific endothelial cells derived from induced pluripotent stem cells (IPSCs) or late progenitor endothelial cells circulating in blood known as blood outgrowth endothelial cells (BOECs) [127, 128]. Another method is to use cells derived from saphenous veins of patients known as human saphenous vein endothelial cells (HSaVECs) [129]. Saphenous veins are large superficial veins in the human body that have venous valves [130]. Use of such patient derived endothelial cells will give us patient specific variability for propensity to develop DVT using Vein-Chips.

5.3. Sub-endothelial matrix

All models described in this thesis have used the basic extracellular matrix (ECM) proteins collagen and fibronectin to culture endothelial cells in the Vein-Chips. But in vivo ECM is very complex consisting of more that hundreds of different proteins [131, 132]. Development of such complex ECM similar to in vivo configuration is a difficult engineering task. Though the endothelial cells themselves remodel the ECM it would be beneficial to add sub-endothelial cells in the ECM of the Vein-Chips to remodel ECM that would be more similar to native ECM. We can include cells like smooth muscle cells and fibroblasts that are observed to be present in the native tissue surrounding the veins. Their cross talk with the endothelial cells can also change the endothelial cell behavior to stimulations, which can be further studied using the Vein-Chip platform

5.4. Blood

In this thesis we have used healthy donor blood to create DVT at the venous valve cusps of the Vein-Chip [66]. We have used the cytokine TNF-α to initiate valve endothelium inflammation and there by trigger the formation of DVT. But in certain diseases like cancer, blood becomes hypercoagulable due to release of clotting factors and inflammatory cytokines by tumor cells and the interactions between the tumor cells, and blood immune cells, or endothelial cells [133-136]. Also, cancer treatments such as hormonal therapy, chemotherapy, molecular targeted therapy, and anti-angiogenesis monoclonal antibodies are known to increase the coagulability of blood. Perfusion of

cancer patient blood through the Vein-Chip devices can throw light into the intricate dynamics at the venous valve cusps that lead to DVT formation in cancer patients.

5.5. Lymphatic valves

In this thesis we have introduced a Vein-Chip model that consists of venous valves. Another vascular system in the body that has similar anatomical feature is the lymphatic system [137]. Like venous valves, lymphatic valves also help in unidirectional flow of lymphatic fluid in the lymphatic system and both these valves undergo similar biological processes during developmental stage [138]. Incompetent lymphatic valves can lead to serious conditions such as lymphedema, but the cross talk of lymphatic endothelial cells and lymphatic smooth muscle cells in an incompetent lymphatic valve are not yet fully understood [139]. The microfluidic Vein-Chip model can be used to study lymphatic valves by using forming lumen with lymphatic endothelial cells and having lymphatic muscle cells in the extra cellular matrix in the system.

5.6. COVID related DVT

Coagulation activation and endothelial dysfunction are two severe complications in the corona virus disease 2019 (COVID-19) [140]. About 50% of the COVID-19 patients admitted to the ICU develop DVT even after initial administration of anti-coagulants like low molecular weight heparin (LMWH) [141]. The exact mechanisms of DVT formation in COVID-19 patients are not understood, which hinders the development of effective therapeutics. Levels of cytokines such as tumor necrosis factor-α (TNF-α), IL-1β, IL-6, IL-17A and IL-18 are observed to increase in patients with COVID-19 [142]. The effects of TNF-α on DVT formation at the venous valves were

shown by the vein-chip model developed in this thesis. Effect of other cytokines released during COVID-19 in the formation of DVT can also be studied using the Vein-Chip. Also, endothelial cells are known to have ACE-2 receptors, which help in maintaining a healthy vasculature. But ACE2 is the receptor through which the SARS-CoV-2 virus enter the lungs. So, Vein-Chip will be a good tool to see if the viruses themselves play a direct role in the DVT formation.

The model presented in this thesis can be extended to study various disease models in future by adding complexities gradually. These complex models can be further used for therapeutic discoveries and anticoagulant dosage estimation for DVT prevention.

REFERENCES

[1] R.W. Colman, Are hemostasis and thrombosis two sides of the same coin?, J Exp Med 203(3) (2006) 493-5. https://doi.org/10.1084/jem.20060217

[2] C.N. Bagot, R. Arya, Virchow and his triad: a question of attribution, Br J Haematol 143(2) (2008) 180-90. https://doi.org/10.1111/j.1365-2141.2008.07323.x

[3] S. Palta, R. Saroa, A. Palta, Overview of the coagulation system, Indian J Anaesth 58(5) (2014) 515-23. https://doi.org/10.4103/0019-5049.144643

[4] C.T. Esmon, Basic mechanisms and pathogenesis of venous thrombosis, Blood Rev 23(5) (2009) 225-9. https://doi.org/10.1016/j.blre.2009.07.002

[5] J. Zhang, A.F. Defelice, J.P. Hanig, T. Colatsky, Biomarkers of endothelial cell activation serve as potential surrogate markers for drug-induced vascular injury, Toxicol Pathol 38(6) (2010) 856-71. https://doi.org/10.1177/0192623310378866

[6] W.C. Aird, Vascular bed-specific thrombosis, J Thromb Haemost 5 Suppl 1 (2007) 283-91. https://doi.org/10.1111/j.1538-7836.2007.02515.x

[7] A. Jain, A.D. van der Meer, A.L. Papa, R. Barrile, A. Lai, B.L. Schlechter, M.A. Otieno, C.S. Louden, G.A. Hamilton, A.D. Michelson, A.L. Frelinger, 3rd, D.E. Ingber, Assessment of whole blood thrombosis in a microfluidic device lined by fixed human endothelium, Biomed Microdevices 18(4) (2016) 73. https://doi.org/10.1007/s10544-016-0095-6

[8] M. Tsai, A. Kita, J. Leach, R. Rounsevell, J.N. Huang, J. Moake, R.E. Ware, D.A. Fletcher, W.A. Lam, In vitro modeling of the microvascular occlusion and thrombosis that occur in hematologic diseases using microfluidic technology, J Clin Invest 122(1) (2012) 408-18. https://doi.org/10.1172/JCI58753

[9] R. Estrada, G.A. Giridharan, M.D. Nguyen, S.D. Prabhu, P. Sethu, Microfluidic endothelial cell culture model to replicate disturbed flow conditions seen in atherosclerosis susceptible regions, Biomicrofluidics 5(3) (2011) 32006-3200611. https://doi.org/10.1063/1.3608137

[10] R.G. Mannino, D.R. Myers, B. Ahn, Y. Wang, R. Margo, H. Gole, A.S. Lin, R.E. Guldberg, D.P. Giddens, L.H. Timmins, W.A. Lam, "Do-it-yourself in vitro vasculature that recapitulates in vivo geometries for investigating endothelial-blood cell interactions", Sci Rep 5 (2015) 12401. https://doi.org/10.1038/srep12401

[11] A.M. Streets, Y. Huang, Chip in a lab: Microfluidics for next generation life science research, Biomicrofluidics 7(1) (2013) 11302. https://doi.org/10.1063/1.4789751

[12] P. Jagadeeswaran, B.C. Cooley, P.L. Gross, N. Mackman, Animal Models of Thrombosis From Zebrafish to Nonhuman Primates: Use in the Elucidation of New Pathologic Pathways and the Development of Antithrombotic Drugs, Circ Res 118(9) (2016) 1363-79. https://doi.org/10.1161/CIRCRESAHA.115.306823

[13] G. Vilahur, T. Padro, L. Badimon, Atherosclerosis and thrombosis: insights from large animal models, J Biomed Biotechnol 2011 (2011) 907575. https://doi.org/10.1155/2011/907575

[14] H. Albadawi, A.A. Witting, Y. Pershad, A. Wallace, A.R. Fleck, P. Hoang, A. Khademhosseini, R. Oklu, Animal models of venous thrombosis, Cardiovascular Diagnosis and Therapy (2017). http://cdt.amegroups.com/article/view/16472

[15] T. Schonfelder, S. Jackel, P. Wenzel, Mouse models of deep vein thrombosis, Gefasschirurgie 22(Suppl 1) (2017) 28-33. https://doi.org/10.1007/s00772-016-0227-6
[16] D. Mege, S. Mezouar, F. Dignat-George, L. Panicot-Dubois, C. Dubois, Microparticles and cancer thrombosis in animal models, Thromb Res 140 Suppl 1 (2016) S21-6. https://doi.org/10.1016/S0049-3848(16)30094-9
[17] W. Wang, J.P. Lindsey, J. Chen, T.G. Diacovo, M.R. King, Analysis of early thrombus dynamics in a humanized mouse laser injury model, Biorheology 51(1) (2014) 3-14. https://doi.org/10.3233/BIR-130648
[18] J.C. Ciciliano, Y. Sakurai, D.R. Myers, M.E. Fay, B. Hechler, S. Meeks, R. Li, J.B. Dixon, L.A. Lyon, C. Gachet, W.A. Lam, Resolving the multifaceted mechanisms of the ferric chloride thrombosis model using an interdisciplinary microfluidic approach, Blood 126(6) (2015) 817-24. https://doi.org/10.1182/blood-2015-02-628594
[19] F.R. Kapourchali, G. Surendiran, L. Chen, E. Uitz, B. Bahadori, M.H. Moghadasian, Animal models of atherosclerosis, World J Clin Cases 2(5) (2014) 126-32. https://doi.org/10.12998/wjcc.v2.i5.126
[20] A. Akhtar, The flaws and human harms of animal experimentation, Camb Q Healthc Ethics 24(4) (2015) 407-19. https://doi.org/10.1017/S0963180115000079
[21] K. Rennier, J.Y. Ji, Effect of shear stress and substrate on endothelial DAPK expression, caspase activity, and apoptosis, BMC Res Notes 6 (2013) 10. https://doi.org/10.1186/1756-0500-6-10
[22] C.A. Skilbeck, P.G. Walker, T. David, G.B. Nash, Disturbed flow promotes deposition of leucocytes from flowing whole blood in a model of a damaged vessel wall, Br J Haematol 126(3) (2004) 418-27. https://doi.org/10.1111/j.1365-2141.2004.05057.x
[23] R. Van Kruchten, J.M. Cosemans, J.W. Heemskerk, Measurement of whole blood thrombus formation using parallel-plate flow chambers - a practical guide, Platelets 23(3) (2012) 229-42. https://doi.org/10.3109/09537104.2011.630848
[24] G. Girdhar, D. Bluestein, Biological effects of dynamic shear stress in cardiovascular pathologies and devices, Expert Rev Med Devices 5(2) (2008) 167-81. https://doi.org/10.1586/17434440.5.2.167
[25] S.L. Diamond, Systems Analysis of Thrombus Formation, Circ Res 118(9) (2016) 1348-62. https://doi.org/10.1161/CIRCRESAHA.115.306824
[26] A. Jain, R. Barrile, A.D. van der Meer, A. Mammoto, T. Mammoto, K. De Ceunynck, O. Aisiku, M.A. Otieno, C.S. Louden, G.A. Hamilton, R. Flaumenhaft, D.E. Ingber, Primary Human Lung Alveolus-on-a-chip Model of Intravascular Thrombosis for Assessment of Therapeutics, Clin Pharmacol Ther (2017). https://doi.org/10.1002/cpt.742
[27] P. Libby, Inflammation in atherosclerosis, Arterioscler Thromb Vasc Biol 32(9) (2012) 2045-51. https://doi.org/10.1161/ATVBAHA.108.179705
[28] J.J. Chiu, S. Chien, Effects of disturbed flow on vascular endothelium: pathophysiological basis and clinical perspectives, Physiol Rev 91(1) (2011) 327-87. https://doi.org/10.1152/physrev.00047.2009
[29] W.S. Nesbitt, E. Westein, F.J. Tovar-Lopez, E. Tolouei, A. Mitchell, J. Fu, J. Carberry, A. Fouras, S.P. Jackson, A shear gradient-dependent platelet aggregation

mechanism drives thrombus formation, Nat Med 15(6) (2009) 665-73. https://doi.org/10.1038/nm.1955
[30] A. Jain, A. Graveline, A. Waterhouse, A. Vernet, R. Flaumenhaft, D.E. Ingber, A shear gradient-activated microfluidic device for automated monitoring of whole blood haemostasis and platelet function, Nat Commun 7 (2016) 10176. https://doi.org/10.1038/ncomms10176
[31] E. Westein, A.D. van der Meer, M.J. Kuijpers, J.P. Frimat, A. van den Berg, J.W. Heemskerk, Atherosclerotic geometries exacerbate pathological thrombus formation poststenosis in a von Willebrand factor-dependent manner, Proc Natl Acad Sci U S A 110(4) (2013) 1357-62. https://doi.org/10.1073/pnas.1209905110
[32] P.F. Costa, H.J. Albers, J.E.A. Linssen, H.H.T. Middelkamp, L. van der Hout, R. Passier, A. van den Berg, J. Malda, A.D. van der Meer, Mimicking arterial thrombosis in a 3D-printed microfluidic in vitro vascular model based on computed tomography angiography data, Lab Chip (2017). https://doi.org/10.1039/c7lc00202e
[33] T.P. Rumbaut R.E., Chapter 6, Arterial, Venous, and Microvascular Hemostasis/Thrombosis. Available from: https://www.ncbi.nlm.nih.gov/books/NBK53453/, Platelet-Vessel Wall Interactions in Hemostasis and Thrombosis. (2010).
[34] E.G. Bovill, A. van der Vliet, Venous valvular stasis-associated hypoxia and thrombosis: what is the link?, Annu Rev Physiol 73 (2011) 527-45. https://doi.org/10.1146/annurev-physiol-012110-142305
[35] M.K. Runyon, C.J. Kastrup, B.L. Johnson-Kerner, T.G. Ha, R.F. Ismagilov, Effects of shear rate on propagation of blood clotting determined using microfluidics and numerical simulations, J Am Chem Soc 130(11) (2008) 3458-64. https://doi.org/10.1021/ja076301r
[36] K.B. Neeves, S.F. Maloney, K.P. Fong, A.A. Schmaier, M.L. Kahn, L.F. Brass, S.L. Diamond, Microfluidic focal thrombosis model for measuring murine platelet deposition and stability: PAR4 signaling enhances shear-resistance of platelet aggregates, J Thromb Haemost 6(12) (2008) 2193-201. https://doi.org/10.1111/j.1538-7836.2008.03188.x
[37] Y. Zheng, J. Chen, M. Craven, N.W. Choi, S. Totorica, A. Diaz-Santana, P. Kermani, B. Hempstead, C. Fischbach-Teschl, J.A. Lopez, A.D. Stroock, In vitro microvessels for the study of angiogenesis and thrombosis, Proc Natl Acad Sci U S A 109(24) (2012) 9342-7. https://doi.org/10.1073/pnas.1201240109
[38] G. Elyamany, A.M. Alzahrani, E. Bukhary, Cancer-associated thrombosis: an overview, Clin Med Insights Oncol 8 (2014) 129-37. https://doi.org/10.4137/CMO.S18991
[39] F. Violi, R. Cangemi, C. Calvieri, Pneumonia, thrombosis and vascular disease, J Thromb Haemost 12(9) (2014) 1391-400. https://doi.org/10.1111/jth.12646
[40] K.E.P. De Ceunynck, C.G. Peters, S.A. Chaudhry, A. Jain, S.J. Higgins, O. Aisiku, J. Fitch-Tewfik, C. Dockendorff, S. Parikh, D.E. Ingber, R.C. Flaumenhaft, A Chemical APC Mimetic Protects Endothelium from Thromboinflammatory Injury, Blood 128 (2016) 3835-3835.

[41] N. Bhattacharjee, A. Urrios, S. Kang, A. Folch, The upcoming 3D-printing revolution in microfluidics, Lab Chip 16(10) (2016) 1720-42. https://doi.org/10.1039/c6lc00163g
[42] S.M. Hastings, M.T. Griffin, D.N. Ku, Hemodynamic studies of platelet thrombosis using microfluidics, Platelets 28(5) (2017) 427-433. https://doi.org/10.1080/09537104.2017.1316483
[43] E. Bazigou, T. Makinen, Flow control in our vessels: vascular valves make sure there is no way back, Cell Mol Life Sci 70(6) (2013) 1055-66. https://doi.org/10.1007/s00018-012-1110-6
[44] F. Lurie, R.L. Kistner, B. Eklof, D. Kessler, Mechanism of venous valve closure and role of the valve in circulation: a new concept, J Vasc Surg 38(5) (2003) 955-61. https://doi.org/10.1016/S0741
[45] A. Caggiati, M. Phillips, A. Lametschwandtner, C. Allegra, Valves in small veins and venules, Eur J Vasc Endovasc Surg 32(4) (2006) 447-52. https://doi.org/10.1016/j.ejvs.2006.04.021
[46] Z. Hajati, F. Sadegh Moghanlou, M. Vajdi, S.E. Razavi, S. Matin, Fluid-structure interaction of blood flow around a vein valve, Bioimpacts 10(3) (2020) 169-175. https://doi.org/10.34172/bi.2020.21
[47] W.H. Tien, H.Y. Chen, Z.C. Berwick, J. Krieger, S. Chambers, D. Dabiri, G.S. Kassab, Role of sinus in prosthetic venous valve, Eur J Vasc Endovasc Surg 48(1) (2014) 98-104. https://doi.org/10.1016/j.ejvs.2014.03.041
[48] T. Ohashi, H. Liu, T. Yamaguchi, Computational Fluid Dynamic Simulation of the Flow through Venous Valve, in: T. Yamaguchi (Ed.), Clinical Application of Computational Mechanics to the Cardiovascular System, Springer Japan, Tokyo, 2000, pp. 186-18910.1007/978-4-431-67921-9_18.
[49] C.D. Buescher, B. Nachiappan, J.M. Brumbaugh, K.A. Hoo, H.F. Janssen, Experimental studies of the effects of abnormal venous valves on fluid flow, Biotechnol Prog 21(3) (2005) 938-45. https://doi.org/10.1021/bp049835u
[50] S. Calandrini, E. Aulisa, Fluid-structure interaction simulations of venous valves: A monolithic ALE method for large structural displacements, Int J Numer Method Biomed Eng 35(2) (2019) e3156. https://doi.org/10.1002/cnm.3156
[51] A.J. Narracott, J.M.T. Keijsers, C.A.D. Leguy, W. Huberts, F.N. van de Vosse, Fluid-structure interaction analysis of venous valve hemodynamics, in: P. Nithiarasu, E. Budyn (Eds.) 4th International Conference on Computational & Mathematical Biomedical Engineering (CMBE15), CMBE, Cachan, France, 2015.
[52] S.P. Downie, S.M. Raynor, D.N. Firmin, N.B. Wood, S.A. Thom, A.D. Hughes, K.H. Parker, J.H. Wolfe, X.Y. Xu, Effects of elastic compression stockings on wall shear stress in deep and superficial veins of the calf, Am J Physiol Heart Circ Physiol 294(5) (2008) H2112-20. https://doi.org/10.1152/ajpheart.01302.2007
[53] M. Ariane, D. Vigolo, A. Brill, F.G.B. Nash, M. Barigou, A. Alexiadis, Using Discrete Multi-Physics for studying the dynamics of emboli in flexible venous valves, Computers & Fluids 166 (2018) 57-63. https://doi.org/https://doi.org/10.1016/j.compfluid.2018.01.037

[54] Y. Wang, I. Pierce, P. Gatehouse, N. Wood, D. Firmin, X.Y. Xu, Analysis of flow and wall shear stress in the peroneal veins under external compression based on real-time MR images, Med Eng Phys 34(1) (2012) 17-27. https://doi.org/10.1016/j.medengphy.2011.06.012
[55] E.G. Brooks, W. Trotman, M.P. Wadsworth, D.J. Taatjes, M.F. Evans, F.P. Ittleman, P.W. Callas, C.T. Esmon, E.G. Bovill, Valves of the deep venous system: an overlooked risk factor, Blood 114(6) (2009) 1276-9. https://doi.org/10.1182/blood-2009-03-209981
[56] W.E. Trotman, D.J. Taatjes, P.W. Callas, E.G. Bovill, The endothelial microenvironment in the venous valvular sinus: thromboresistance trends and inter-individual variation, Histochem Cell Biol 135(2) (2011) 141-52. https://doi.org/10.1007/s00418-011-0783-5
[57] M.N. Phillips, G.T. Jones, A.M. van Rij, M. Zhang, Micro-venous valves in the superficial veins of the human lower limb, Clin Anat 17(1) (2004) 55-60. https://doi.org/10.1002/ca.10141
[58] D.A. Manly, J. Boles, N. Mackman, Role of tissue factor in venous thrombosis, Annu Rev Physiol 73 (2011) 515-25. https://doi.org/10.1146/annurev-physiol-042210-121137
[59] I.M. Braverman, A. Keh-Yen, Ultrastructure of the human dermal microcirculation. IV. Valve-containing collecting veins at the dermal-subcutaneous junction, J Invest Dermatol 81(5) (1983) 438-42. https://www.ncbi.nlm.nih.gov/pubmed/6631054
[60] B.M. Johnston, P.R. Johnston, S. Corney, D. Kilpatrick, Non-Newtonian blood flow in human right coronary arteries: transient simulations, J Biomech 39(6) (2006) 1116-28. https://doi.org/10.1016/j.jbiomech.2005.01.034
[61] Y.C. Fung, Biomechanics: Mechanical Properties of Living Tissues, New York, 1993. (Errata)
[62] P.D. Ballyk, D.A. Steinman, C.R. Ethier, Simulation of non-Newtonian blood flow in an end-to-side anastomosis, Biorheology 31(5) (1994) 565-86. https://doi.org/10.3233/bir-1994-31505
[63] C.H. Berdahl, D.S. Thompson, Eduction of swirling structure using the velocity gradient tensor, AIAA Journal 31(1) (1993) 97-103. https://doi.org/10.2514/3.11324
[64] M. Perrin, History of venous surgery (1), Phlebolymphology 18(3) (2011) 7. https://www.phlebolymphology.org/history-of-venous-surgery-1/
[65] R.L.K. Michael C. Dalsing, Deep Venous Incompetence and Valve Repair, in: J. Almeida (Ed.), Atlas of Endovascular Venous Surgery, Elsevier2019, https://doi.org/10.1016/B978-0-323-51139-1.00019-X.
[66] N.K. Rajeeva Pandian, B.K. Walther, R. Suresh, J.P. Cooke, A. Jain, Microengineered Human Vein-Chip Recreates Venous Valve Architecture and Its Contribution to Thrombosis, Small 16(49) (2020) e2003401. https://doi.org/10.1002/smll.202003401
[67] B.M. Johnston, P.R. Johnston, S. Corney, D. Kilpatrick, Non-Newtonian blood flow in human right coronary arteries: steady state simulations, J Biomech 37(5) (2004) 709-20. https://doi.org/10.1016/j.jbiomech.2003.09.016

[68] T. Karino, M. Motomiya, Flow through a venous valve and its implication for thrombus formation, Thromb Res 36(3) (1984) 245-57. https://www.ncbi.nlm.nih.gov/pubmed/6515603
[69] N.S. Wijeratne, K.A. Hoo, Numerical studies on the hemodynamics in the human vein and venous valve, 2008 American Control Conference, 2008, pp. 147-152.
[70] W.H. Tien, H.Y. Chen, Z.C. Berwick, J. Krieger, S. Chambers, D. Dabiri, G.S. Kassab, Characterization of a bioprosthetic bicuspid venous valve hemodynamics: implications for mechanism of valve dynamics, Eur J Vasc Endovasc Surg 48(4) (2014) 459-64. https://doi.org/10.1016/j.ejvs.2014.06.034
[71] G.W. Schmid-Schoenbein, Y.C. Fung, B.W. Zweifach, Vascular endothelium-leukocyte interaction; sticking shear force in venules, Circ Res 36(1) (1975) 173-84. https://doi.org/10.1161/01.res.36.1.173
[72] Y. Sakurai, E.T. Hardy, B. Ahn, R. Tran, M.E. Fay, J.C. Ciciliano, R.G. Mannino, D.R. Myers, Y. Qiu, M.A. Carden, W.H. Baldwin, S.L. Meeks, G.E. Gilbert, S.M. Jobe, W.A. Lam, A microengineered vascularized bleeding model that integrates the principal components of hemostasis, Nat Commun 9(1) (2018) 509. https://doi.org/10.1038/s41467-018-02990-x
[73] E. Ortiz-Prado, J.F. Dunn, J. Vasconez, D. Castillo, G. Viscor, Partial pressure of oxygen in the human body: a general review, Am J Blood Res 9(1) (2019) 1-14. https://www.ncbi.nlm.nih.gov/pubmed/30899601

https://www.ncbi.nlm.nih.gov/pmc/articles/PMC6420699/pdf/ajbr0009-0001.pdf
[74] H.E. Abaci, R. Truitt, E. Luong, G. Drazer, S. Gerecht, Adaptation to oxygen deprivation in cultures of human pluripotent stem cells, endothelial progenitor cells, and umbilical vein endothelial cells, Am J Physiol Cell Physiol 298(6) (2010) C1527-37. https://doi.org/10.1152/ajpcell.00484.2009
[75] T.K. Goldstick, V.T. Ciuryla, L. Zuckerman, Diffusion of oxygen in plasma and blood, Adv Exp Med Biol 75 (1976) 183-90. https://doi.org/10.1007/978-1-4684-3273-2_23
[76] J. Geddings, M.M. Aleman, A. Wolberg, M.L. von Bruhl, S. Massberg, N. Mackman, Strengths and weaknesses of a new mouse model of thrombosis induced by inferior vena cava stenosis: communication from the SSC of the ISTH, J Thromb Haemost 12(4) (2014) 571-3. https://doi.org/10.1111/jth.12510
[77] J.A. Diaz, A.T. Obi, D.D. Myers, Jr., S.K. Wrobleski, P.K. Henke, N. Mackman, T.W. Wakefield, Critical review of mouse models of venous thrombosis, Arterioscler Thromb Vasc Biol 32(3) (2012) 556-62. https://doi.org/10.1161/ATVBAHA.111.244608
[78] J.A. Diaz, P. Saha, B. Cooley, O.R. Palmer, S.P. Grover, N. Mackman, T.W. Wakefield, P.K. Henke, A. Smith, B.K. Lal, Choosing a Mouse Model of Venous Thrombosis, 39(3) (2019) 311-318. https://doi.org/doi:10.1161/ATVBAHA.118.311818
[79] B.C. Cooley, G. Schmeling, Murine model of large-vein electrolytic injury induction of thrombosis with slow resolution, Thromb Res 140 (2016) 149-52. https://doi.org/10.1016/j.thromres.2016.01.023

[80] J. Zhou, L. May, P. Liao, P.L. Gross, J.I. Weitz, Inferior vena cava ligation rapidly induces tissue factor expression and venous thrombosis in rats, Arterioscler Thromb Vasc Biol 29(6) (2009) 863-9. https://doi.org/10.1161/ATVBAHA.109.185678
[81] J.J. Chiu, C.N. Chen, P.L. Lee, C.T. Yang, H.S. Chuang, S. Chien, S. Usami, Analysis of the effect of disturbed flow on monocytic adhesion to endothelial cells, J Biomech 36(12) (2003) 1883-95. https://www.ncbi.nlm.nih.gov/pubmed/14614942

https://ac.els-cdn.com/S0021929003002100/1-s2.0-S0021929003002100-main.pdf?_tid=3ef0cde4-f996-4892-a547-18fe33373302&acdnat=1537135507_d9ab4c3a41f74df7e2c8651a854f3d49
[82] J. Nie, Q. Gao, Y. Wang, J. Zeng, H. Zhao, Y. Sun, J. Shen, H. Ramezani, Z. Fu, Z. Liu, M. Xiang, J. Fu, P. Zhao, W. Chen, Y. He, Vessel-on-a-chip with Hydrogel-based Microfluidics, Small 14(45) (2018) e1802368. https://doi.org/10.1002/smll.201802368
[83] M. Lehmann, R.M. Schoeman, P.J. Krohl, A.M. Wallbank, J.R. Samaniuk, M. Jandrot-Perrus, K.B. Neeves, Platelets Drive Thrombus Propagation in a Hematocrit and Glycoprotein VI-Dependent Manner in an In Vitro Venous Thrombosis Model, Arterioscler Thromb Vasc Biol (2018). https://doi.org/10.1161/ATVBAHA.118.310731
[84] X. Hu, Y. Li, J. Li, H. Chen, Effects of altered blood flow induced by the muscle pump on thrombosis in a microfluidic venous valve model, Lab Chip (2020). https://doi.org/10.1039/d0lc00287a
[85] E.V. Dydek, E.L. Chaikof, Simulated thrombin responses in venous valves, J Vasc Surg Venous Lymphat Disord 4(3) (2016) 329-35. https://doi.org/10.1016/j.jvsv.2015.09.005
[86] R.S. Kane, S. Takayama, E. Ostuni, D.E. Ingber, G.M. Whitesides, Patterning proteins and cells using soft lithography, Biomaterials 20(23-24) (1999) 2363-76. https://www.ncbi.nlm.nih.gov/pubmed/10614942

https://www.sciencedirect.com/science/article/pii/S0142961299001659?via%3Dihub
[87] J.D. Welsh, M.H. Hoofnagle, S. Bamezai, M. Oxendine, L. Lim, J.D. Hall, J. Yang, S. Schultz, J.D. Engel, T. Kume, G. Oliver, J.M. Jimenez, M.L. Kahn, Hemodynamic regulation of perivalvular endothelial gene expression prevents deep venous thrombosis, J Clin Invest 129(12) (2019) 5489-5500. https://doi.org/10.1172/JCI124791
[88] G. Arpaia, P.M. Bavera, D. Caputo, L. Mendozzi, R. Cavarretta, G.B. Agus, M. Milani, E. Ippolito, C. Cimminiello, Risk of deep venous thrombosis (DVT) in bedridden or wheelchair-bound multiple sclerosis patients: A prospective study, Thrombosis Research 125(4) (2010) 315-317. https://doi.org/https://doi.org/10.1016/j.thromres.2009.06.023
[89] H.P. Wright, S.B. Osborn, Effect of posture on venous velocity, measured with 24NaCl, Br Heart J 14(3) (1952) 325-30. https://doi.org/10.1136/hrt.14.3.325
[90] E.C. Ashby, N.S. Ashford, M.J. Campbell, Posture, blood velocity in common femoral vein, and prophylaxis of venous thromboembolism, The Lancet 345(8947) (1995) 419-421. https://doi.org/https://doi.org/10.1016/S0140-6736(95)90402-6
[91] H.J. Weiss, V.T. Turitto, H.R. Baumgartner, Role of shear rate and platelets in promoting fibrin formation on rabbit subendothelium. Studies utilizing patients with

quantitative and qualitative platelet defects, J Clin Invest 78(4) (1986) 1072-82. https://doi.org/10.1172/JCI112663
[92] K.B. Neeves, D.A. Illing, S.L. Diamond, Thrombin flux and wall shear rate regulate fibrin fiber deposition state during polymerization under flow, Biophys J 98(7) (2010) 1344-52. https://doi.org/10.1016/j.bpj.2009.12.4275
[93] L.T. Cotton, Varicose veins. Gross anatomy and development, Br J Surg 48 (1961) 589-98. https://doi.org/10.1002/bjs.18004821203
[94] R.T. Eberhardt, J.D. Raffetto, Chronic venous insufficiency, Circulation 130(4) (2014) 333-46. https://doi.org/10.1161/CIRCULATIONAHA.113.006898
[95] S.C. Christiansen, I.A. Næss, S.C. Cannegieter, J. Hammerstrøm, F.R. Rosendaal, P.H. Reitsma, Inflammatory Cytokines as Risk Factors for a First Venous Thrombosis: A Prospective Population-Based Study, PLOS Medicine 3(8) (2006) e334. https://doi.org/10.1371/journal.pmed.0030334
[96] B.R. Branchford, S.L. Carpenter, The Role of Inflammation in Venous Thromboembolism, Frontiers in Pediatrics 6(142) (2018) 1-7. https://doi.org/10.3389/fped.2018.00142
[97] D. Kirchhofer, T.B. Tschopp, P. Hadvary, H.R. Baumgartner, Endothelial cells stimulated with tumor necrosis factor-alpha express varying amounts of tissue factor resulting in inhomogenous fibrin deposition in a native blood flow system. Effects of thrombin inhibitors, J Clin Invest 93(5) (1994) 2073-83. https://doi.org/10.1172/JCI117202
[98] M.L. von Bruhl, K. Stark, A. Steinhart, S. Chandraratne, I. Konrad, M. Lorenz, A. Khandoga, A. Tirniceriu, R. Coletti, M. Kollnberger, R.A. Byrne, I. Laitinen, A. Walch, A. Brill, S. Pfeiler, D. Manukyan, S. Braun, P. Lange, J. Riegger, J. Ware, A. Eckart, S. Haidari, M. Rudelius, C. Schulz, K. Echtler, V. Brinkmann, M. Schwaiger, K.T. Preissner, D.D. Wagner, N. Mackman, B. Engelmann, S. Massberg, Monocytes, neutrophils, and platelets cooperate to initiate and propagate venous thrombosis in mice in vivo, J Exp Med 209(4) (2012) 819-35. https://doi.org/10.1084/jem.20112322
[99] D. Kirchhofer, K.S. Sakariassen, M. Clozel, T.B. Tschopp, P. Hadvary, Y. Nemerson, H.R. Baumgartner, Relationship between tissue factor expression and deposition of fibrin, platelets, and leukocytes on cultured endothelial cells under venous blood flow conditions, Blood 81(8) (1993) 2050-8. https://www.ncbi.nlm.nih.gov/pubmed/8097120
[100] M. Franchini, P.M. Mannucci, New anticoagulants for treatment of venous thromboembolism, European Journal of Internal Medicine 23(8) (2012) 692-695. https://doi.org/https://doi.org/10.1016/j.ejim.2012.10.001
[101] P. Prandoni, A.W. Lensing, A. Piccioli, E. Bernardi, P. Simioni, B. Girolami, A. Marchiori, P. Sabbion, M.H. Prins, F. Noventa, A. Girolami, Recurrent venous thromboembolism and bleeding complications during anticoagulant treatment in patients with cancer and venous thrombosis, Blood 100(10) (2002) 3484-8. https://doi.org/10.1182/blood-2002-01-0108
[102] L.J. Greenfield, M.C. Proctor, Recurrent thromboembolism in patients with vena cava filters, Journal of Vascular Surgery 33(3) (2001) 510-514. https://doi.org/https://doi.org/10.1067/mva.2001.111733

[103] M. Alquwaizani, L. Buckley, C. Adams, J. Fanikos, Anticoagulants: A Review of the Pharmacology, Dosing, and Complications, Curr Emerg Hosp Med Rep 1(2) (2013) 83-97. https://doi.org/10.1007/s40138-013-0014-6
[104] D. Hoppensteadt, D. Syed, M. Jezovnik, P. Poredos, S. Tetik, O. Iqbal, J.M. Walenga, J. Fareed, Circulating Levels of Rivaroxaban Provide Different Results in Different Clot Based and Amidolytic Assays. a Study on Patients Treated with Two Different Dosages of Rivaroxaban, Blood 124(21) (2014) 5084. http://www.bloodjournal.org/content/124/21/5084.abstract
[105] H. Shin, M.C. Cho, R.B. Kim, C.H. Kim, N.C. Choi, S.K. Kim, E.H. Koh, Laboratory measurement of apixaban using anti-factor Xa assays in acute ischemic stroke patients with non-valvular atrial fibrillation, J Thromb Thrombolysis 45(2) (2018) 250-256. https://doi.org/10.1007/s11239-017-1590-1
[106] A.L. Fogelson, K.B. Neeves, Fluid Mechanics of Blood Clot Formation, Annu Rev Fluid Mech 47 (2015) 377-403. https://doi.org/10.1146/annurev-fluid-010814-014513
[107] D. Huh, B.D. Matthews, A. Mammoto, M. Montoya-Zavala, H.Y. Hsin, D.E. Ingber, Reconstituting organ-level lung functions on a chip, Science 328(5986) (2010) 1662-8. https://doi.org/10.1126/science.1188302
[108] M.E. Shaydakov, J.A. Diaz, A.J. Comerota, F. Lurie, Targeted gene expression analysis of human deep veins, J Vasc Surg Venous Lymphat Disord (2020). https://doi.org/10.1016/j.jvsv.2020.08.025
[109] A.D. McLachlin, J.A. McLachlin, T.A. Jory, E.G. Rawling, Venous stasis in the lower extremities, Ann Surg 152 (1960) 678-85. https://www.ncbi.nlm.nih.gov/pubmed/13774059

https://www.ncbi.nlm.nih.gov/pmc/articles/PMC1613783/pdf/annsurg01295-0124.pdf
[110] M. Cattaneo, C.P. Hayward, K.A. Moffat, M.T. Pugliano, Y. Liu, A.D. Michelson, Results of a worldwide survey on the assessment of platelet function by light transmission aggregometry: a report from the platelet physiology subcommittee of the SSC of the ISTH, J Thromb Haemost 7(6) (2009) 1029. https://doi.org/10.1111/j.1538-7836.2009.03458.x
[111] L. Selmeci, M. Székely, P. Soós, L. Seres, N. Klinga, A. Geiger, G. Acsády, Human blood plasma advanced oxidation protein products (AOPP) correlates with fibrinogen levels, Free Radical Research 40(9) (2006) 952-958. https://doi.org/10.1080/10715760600818789
[112] P.C. Malone, P.S. Agutter, Deep venous thrombosis: The valve cusp hypoxia thesis and its incompatibility with modern orthodoxy, Med Hypotheses 86 (2016) 60-6. https://doi.org/10.1016/j.mehy.2015.12.002
[113] A. Ruppert, M. Lees, T. Steinle, Clinical burden of venous thromboembolism, Curr Med Res Opin 26(10) (2010) 2465-73. https://doi.org/10.1185/03007995.2010.516090
[114] L.J.J. Scheres, W.M. Lijfering, S.C. Cannegieter, Current and future burden of venous thrombosis: Not simply predictable, Res Pract Thromb Haemost 2(2) (2018) 199-208. https://doi.org/10.1002/rth2.12101

[115] J. Campos, A. Brill, By word of mouse: using animal models in venous thrombosis research, Platelets 31(4) (2020) 447-454. https://doi.org/10.1080/09537104.2019.1678117
[116] A. Schwein, L. Magnus, N. Chakfé, J. Bismuth, Critical Review of Large Animal Models for Central Deep Venous Thrombosis, European Journal of Vascular and Endovascular Surgery 60(2) (2020) 243-252. https://doi.org/https://doi.org/10.1016/j.ejvs.2020.03.051
[117] J. In, J. Ryu, H. Yu, D. Kang, T. Kim, J. Kim, Microfluidic valvular chips and a numerical lymphatic vessel model for the study of lymph transport characteristics, Lab on a Chip 21(11) (2021) 2283-2293. https://doi.org/10.1039/D1LC00022E
[118] P. Arbeille, R. Provost, K. Zuj, N. Vincent, Measurements of jugular, portal, femoral, and calf vein cross-sectional area for the assessment of venous blood redistribution with long duration spaceflight (Vessel Imaging Experiment), European Journal of Applied Physiology 115(10) (2015) 2099-2106. https://doi.org/10.1007/s00421-015-3189-6
[119] H. Ohmori, Y. Kanaoka, M. Yamasaki, H. Takesue, R. Sumimoto, Prevalence and Characteristic Features of Deep Venous Thrombosis in Patients with Severe Motor and Intellectual Disabilities, Ann Vasc Dis 11(3) (2018) 281-285. https://doi.org/10.3400/avd.oa.18-00028
[120] D.A. Chang-Yen, R.K. Eich, B.K. Gale, A Monolithic PDMS Waveguide System Fabricated Using Soft-Lithography Techniques, J. Lightwave Technol. 23(6) (2005) 2088. http://jlt.osa.org/abstract.cfm?URI=jlt-23-6-2088
[121] B.K. Walther, N.K. Rajeeva Pandian, K.A. Gold, E.S. Kiliç, V. Sama, J. Gu, A.K. Gaharwar, A. Guiseppi-Elie, J.P. Cooke, A. Jain, Mechanotransduction-on-chip: vessel-chip model of endothelial YAP mechanobiology reveals matrix stiffness impedes shear response, Lab on a Chip 21(9) (2021) 1738-1751. https://doi.org/10.1039/D0LC01283A
[122] G.H. Mostbeck, G. Strasser, J. Liskutin, Venous Hemodynamics and Normal Doppler Findings in the Venous System, in: G.H. Mostbeck (Ed.), Duplex and Color Doppler Imaging of the Venous System, Springer Berlin Heidelberg, Berlin, Heidelberg, 2004, pp. 35-4510.1007/978-3-642-18589-2_3.
[123] D.P. Vekilov, K.J. Grande-Allen, Mechanical Properties of Diseased Veins, Methodist Debakey Cardiovasc J 14(3) (2018) 182-187. https://doi.org/10.14797/mdcj-14-3-182
[124] Z. Schofield, H.A. Baksamawi, J. Campos, A. Alexiadis, G.B. Nash, A. Brill, D. Vigolo, The role of valve stiffness in the insurgence of deep vein thrombosis, Commun Mater 1(1) (2020) 65. https://doi.org/10.1038/s43246-020-00066-2
[125] E. Soifer, D. Weiss, G. Marom, S. Einav, The effect of pathologic venous valve on neighboring valves: fluid-structure interactions modeling, Med Biol Eng Comput 55(6) (2017) 991-999. https://doi.org/10.1007/s11517-016-1575-9
[126] W. Lee, J.H. Seo, H.B. Kim, S.H. Chung, S.H. Lee, K.G. Kim, H.G. Kang, Investigation of Blood Flow During Intermittent Pneumatic Compression and Proposal of a New Compression Protocol, Clin Appl Thromb Hemost 24(2) (2018) 338-347. https://doi.org/10.1177/1076029616683044

[127] T. Mathur, K.A. Singh, N.K. R. Pandian, S.-H. Tsai, T.W. Hein, A.K. Gaharwar, J.M. Flanagan, A. Jain, Organ-on-chips made of blood: endothelial progenitor cells from blood reconstitute vascular thromboinflammation in vessel-chips, Lab on a Chip 19(15) (2019) 2500-2511. https://doi.org/10.1039/C9LC00469F
[128] S. Sances, R. Ho, G. Vatine, D. West, A. Laperle, A. Meyer, M. Godoy, P.S. Kay, B. Mandefro, S. Hatata, C. Hinojosa, N. Wen, D. Sareen, G.A. Hamilton, C.N. Svendsen, Human iPSC-Derived Endothelial Cells and Microengineered Organ-Chip Enhance Neuronal Development, Stem Cell Reports 10(4) (2018) 1222-1236. https://doi.org/10.1016/j.stemcr.2018.02.012
[129] T. Girão-Silva, M.H. Fonseca-Alaniz, J.C. Ribeiro-Silva, J. Lee, N.P. Patil, L.A. Dallan, A.B. Baker, M.C. Harmsen, J.E. Krieger, A.A. Miyakawa, High stretch induces endothelial dysfunction accompanied by oxidative stress and actin remodeling in human saphenous vein endothelial cells, Scientific Reports 11(1) (2021) 13493. https://doi.org/10.1038/s41598-021-93081-3
[130] T. Nakahara, M. Yamada, Y. Yokoyama, Y. Yamada, K. Narita, N. Imanishi, M. Yamazaki, H. Shimizu, J. Narula, M. Jinzaki, Saphenous vein valve assessment utilizing upright CT to potentially improve graft assessment for bypass surgery, Scientific Reports 11(1) (2021) 11602. https://doi.org/10.1038/s41598-021-90998-7
[131] C. Frantz, K.M. Stewart, V.M. Weaver, The extracellular matrix at a glance, J Cell Sci 123(Pt 24) (2010) 4195-200. https://doi.org/10.1242/jcs.023820
[132] S. Kim, M. Uroz, J.L. Bays, C.S. Chen, Harnessing Mechanobiology for Tissue Engineering, Dev Cell 56(2) (2021) 180-191. https://doi.org/10.1016/j.devcel.2020.12.017
[133] N.J. Nasser, J. Fox, A. Agbarya, Potential Mechanisms of Cancer-Related Hypercoagulability, Cancers (Basel) 12(3) (2020). https://doi.org/10.3390/cancers12030566
[134] G.J. Caine, P.S. Stonelake, G.Y. Lip, S.T. Kehoe, The hypercoagulable state of malignancy: pathogenesis and current debate, Neoplasia 4(6) (2002) 465-73. https://doi.org/10.1038/sj.neo.7900263
[135] N.B. Abdol Razak, G. Jones, M. Bhandari, M.C. Berndt, P. Metharom, Cancer-Associated Thrombosis: An Overview of Mechanisms, Risk Factors, and Treatment, Cancers (Basel) 10(10) (2018). https://doi.org/10.3390/cancers10100380
[136] K. Date, C. Ettelaie, A. Maraveyas, Tissue factor-bearing microparticles and inflammation: a potential mechanism for the development of venous thromboembolism in cancer, J Thromb Haemost 15(12) (2017) 2289-2299. https://doi.org/10.1111/jth.13871
[137] J.P. Scallan, S.D. Zawieja, J.A. Castorena-Gonzalez, M.J. Davis, Lymphatic pumping: mechanics, mechanisms and malfunction, J Physiol 594(20) (2016) 5749-5768. https://doi.org/10.1113/JP272088
[138] E. Bazigou, O.T. Lyons, A. Smith, G.E. Venn, C. Cope, N.A. Brown, T. Makinen, Genes regulating lymphangiogenesis control venous valve formation and maintenance in mice, J Clin Invest 121(8) (2011) 2984-92. https://doi.org/10.1172/JCI58050

[139] D. Iyer, M. Jannaway, Y. Yang, P.S. J, Lymphatic Valves and Lymph Flow in Cancer-Related Lymphedema, Cancers (Basel) 12(8) (2020). https://doi.org/10.3390/cancers12082297
[140] C. Lodigiani, G. Iapichino, L. Carenzo, M. Cecconi, P. Ferrazzi, T. Sebastian, N. Kucher, J.-D. Studt, C. Sacco, A. Bertuzzi, M.T. Sandri, S. Barco, Venous and arterial thromboembolic complications in COVID-19 patients admitted to an academic hospital in Milan, Italy, Thrombosis Research 191 (2020) 9-14. https://doi.org/https://doi.org/10.1016/j.thromres.2020.04.024
[141] S. Chen, D. Zhang, T. Zheng, Y. Yu, J. Jiang, DVT incidence and risk factors in critically ill patients with COVID-19, Journal of Thrombosis and Thrombolysis 51(1) (2021) 33-39. https://doi.org/10.1007/s11239-020-02181-w
[142] F. Raucci, A.A. Mansour, G.M. Casillo, A. Saviano, F. Caso, R. Scarpa, N. Mascolo, A.J. Iqbal, F. Maione, Interleukin-17A (IL-17A), a key molecule of innate and adaptive immunity, and its potential involvement in COVID-19-related thrombotic and vascular mechanisms, Autoimmun Rev 19(7) (2020) 102572. https://doi.org/10.1016/j.autrev.2020.102572